SISSA ISAS

SCUOLA INTERNAZIONALE SUPERIORE DI STUDI AVANZATI
INTERNATIONAL SCHOOL FOR ADVANCED STUDIES

Towards Single Cell Genomics and Proteomics: New Methods in Nanoscale Surface Biochemistry

Thesis submitted for the degree of
Doctor of Philosophiae

Candidate

Fouzia Bano

Supervisors

Prof Giacinto Scoles

and

Dr. Loredana Casalis

October 2009

Declaration

I declare that this thesis submitted for Doctor of Philosophiae degree at Scuola Internazionale Superiore di Studi Avanzati (SISSA) represents my own research work in collaboration with co-authors described in each chapter and has not been handed to any other University for any reward.

To my mom and dad

Abstract

The development of DNA arrays, which allows for the parallel screening of thousands of genes in a single experiment, has promoted researchers to have a global view of biological systems. On the other hand, the need to increase the size of protein arrays to study protein expression on a large scale, not only reflects the drive towards a more integrated view of complex cellular networks, but also motivates researchers to develop innovative devices with novel functionalities and high performance. Recently, important technological inventions have been made in both array technologies but there is still a growing need of new methods, in protein arrays especially with respect to the immobilization of proteins with controlled orientations, and high sensitivity detection methods, in order to produce effective and efficient devices.

A novel approach, based on the combination of nanografting and DNA-Directed Immobilization (DDI), has been applied in this thesis for the development of multiple protein arrays at the nano-scale using Atomic Force Microscopy (AFM) relative height measurement as a detection tool. Nanografting, a well-known nano-lithography technique based on AFM that has unique capabilities for controlling density and conformation of patterned bio-molecules at the nanometer scale, was used as a fabrication tool. DDI, which has high efficiency of adsorption, reversibility and site-selectivity, enabled the highly parallel immobilization of multiple proteins on the generated DNA patterns using semisynthetic DNA-protein conjugates.

Before we engaged into the protein immobilization and detection work, an optimization of DNA patterns was carried out. Using nanografting, well ordered thiolated single stranded DNA (ssDNA) patterns were fabricated within self assembled monolayer (SAM) of non specific adsorption resistant thiols on gold surfaces. Nano-structures of variable packing densities of ssDNA molecules were obtained by varying the nanografting parameters, in particular the density of scanning lines. A detailed description of our study on the optimization of hybridization efficiency of ssDNA nano-structures is given in the first part of this thesis. In this study, the improvement in molecular order of highly-dense nanografted ssDNA patches with respect to spontaneously assembled DNA monolayers has been found to be a key feature to explain why the hybridization efficiency of dense nanografted

monolayers was found to be much larger than in SAMs of equal or even inferior density. Moreover, using AFM relative height and compressibility measurements, we demonstrated that hybridization of ssDNA nano-structures is sensitive to the position (upper or lower) of half-sequence target strands on the ssDNA probe molecules.

After optimizing the DNA fabrication process, immobilization of proteins on ssDNA nano-structures was carried out by a combined nanografting/DDI approach. The biochemical functionality of immobilized multiple proteins features was demonstrated by specific binding measurements with the corresponding antibodies even when dissolved in complex mixtures of human serum. This study suggests that immobilized proteins are not only biological active but also preserve their functionality in the presence of complex biological mixtures.

To further demonstrate the applicability of our approach, patterns of multienzyme complexes for miniaturized enzyme-based biosensors were created. In this work, both AFM relative height and friction measurements were used as detection tools. Significant changes in the friction signal indicated the activation of enzyme complexes at very low concentration of analyte.

The combination of nanografting with DDI, allowing for the easy, highly selective and precise arrangement of bio-molecules, has been found in this thesis to be an excellent tool for generating complex patterns of biomolecules with a very wide range of applications in nano-biotechnology.

Acknowledgment

My infinite gratitude goes to my supervisor; Professor Giacinto Scoles for his immense and generous guidance and interest in all the things that happened during my research work. His enormous encouragement along with criticism will always contribute to the nicest memory of my PhD course here in Trieste. My sincere gratitude goes to my advisor; Dr. Loredana Casalis for unlimited enthusiasm, encouragement, discussion and all the help she provided when things were not on the right track in SENIL (lab of glorious minds! I should add). I should not skip to mention about her genuine help during thesis writing and delicious dinners at her place on special occasions.

I want to express my profound gratitude to Dr. Ljiljana Fruk and Professor Christof Niemeyer for their kind collaboration with SENIL and helpful discussions.

I would like to express my deepest thanks to Barbara Sanavio for sharing her knowledge in biochemistry and helping me to learn “nice” words in Italian. My huge appreciation goes to Dr. Denis Scaini for his collaboration and help on reading and correcting a part of this work. I am also thankful to him for allowing me to use his microphone and for encouraging me in unpleasant situations in the lab. I am thankful to Dr. Matteo Castronovo for his help in understanding the fundamentals of AFM and nanografting process, fruitful discussions, and kindly inviting me to visit him in Philadelphia at Temple University.

Many thanks go to all the other members of SENIL (Francesca Toma, Mauro Melli and Pietro Parisse) and close collaborators. I am also thankful to all members of the bio-crystallography lab for letting me use their materials and instruments. I would like to thank all past and present visiting students who contributed and provided their excellent skills which helped me to enhance the depth of the subject. I am deeply grateful to Elham Mirmomtaz and Martina Dell’ Angela for their huge contribution in optimizing DNA grafting process.

I would like to thank -Barbara, Denis, Francesca, Mauro and Pietro who are not only my colleagues but for being very good friends. I want to thank them all for the coffees, afternoon ice-cream breaks and pizza dinners after lab work. Life would have been hard in Trieste without all my friends from all over the world; old friends back at home, and diploma buddies. I am grateful to all for sending amusing messages and chats. Many thanks go to Sumera Abrar for long phone calls and helping to forget

about unsuccessful experiments, Asha Nair for pleasant company at home and Subhra Mandal for entertaining with cheerful talks, movies and delicious food.

My enormous gratitude goes to Professor Arshad Bhatti who introduced me to the beautiful world of physics and successfully convinced me to apply for condensed matter diploma course at ICTP, prior to my PhD studies. I am also thankful to him for his abundant and genuine guidance at every stage of my career.

Most of all, I am immensely grateful to my dad, mom, uncles and aunts, for their endless love, support and guidance, and to my lovely brothers, Azeem and Ali, for making me laugh over the phone calls with funny jokes and talks.

Abbreviation list

AFM	atomic force microscopy
SAM	self-assembled monolayer
RNA	ribonucleic acid
mRNA	messenger ribonucleic acid
ssDNA	single stranded deoxyribonucleic acid
dsDNA	double stranded deoxyribonucleic acid
cDNA	complementary deoxyribonucleic acid
DDI	DNA directed immobilization
PCR	polymerase chain reaction
GST	glutathione *S*-transferase
NP	nanoparticles
TOEG	top oligo-ethylene-glycol
NAM	nanografted assembled monolayer
SNOM	scanning near-field optical microscopy
PBS	phosphate buffered saline
STV	streptavidin
IgG	immunoglobulin G
HRP	horseradish peroxidase
GOx	glucose oxidase
4CN	4-Chloro-1-Naphthol
B4CHD	Benzo-4-Chloro Cycloexadienone
NG	nanografting
H_2O_2	hydrogen peroxide

Contents

Chapter 3

Chapter 4

Chapter 5

Chapter 1

General Introduction

1.1 Nanoscale Protein Arrays: Motivations and State of the Art

The completion of the human genome served to drive the development of innovative tools, thereby allowing us to obtain a large amount of valuable information for understanding complex cellular processes. One of the most powerful analytical tools to study the genetic context of cells is DNA/RNA microarrays. These are micro-structured devices which allow for the transcription of thousands of genes in a single experiment[1]. In DNA microarrays, thousands of single strands of DNA or gene fragments (called probes) are attached in discrete, addressable and microscopic patterns to a solid substrate[2]. The complementary strand (called target) interact specifically to the immobilized probes by means of H bonding when exposed to the array surface under definite conditions (Figure 1). This probe-target interaction (called hybridization) is usually determined and quantified by the detection of fluorescence- [3], nanoparticle- [4], or chemiluminescence-[5] of labeled targets and allows not only for gene screening and target identification analysis[6], but also for the analysis of mRNA transcript levels expressed under various conditions.

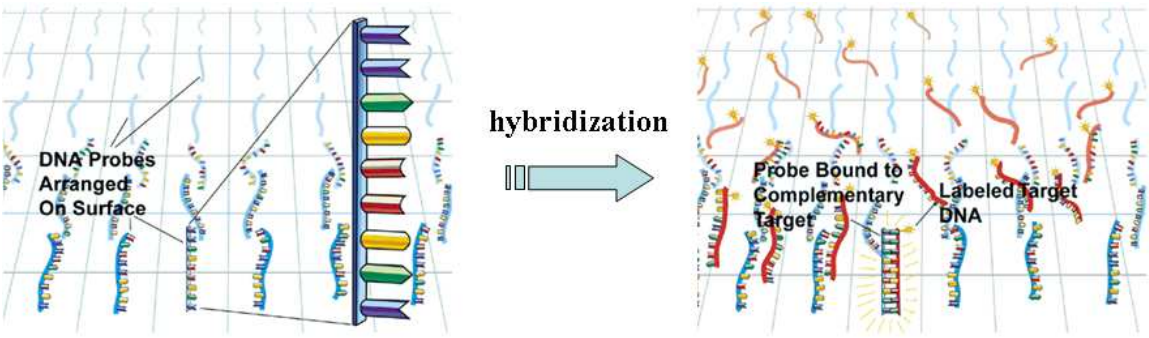

Figure 1: DNA-microarrays.
Origin: http://google.com

Gene expression profiling of cells that belong to diseased organs is crucial in clinical research for understanding disease pathology at the molecular level, and to identifying new therapies[7, 8] and perhaps in the future to monitor the progress of healing. In cancer research, for instance, microarrays are largely used to determine the population of transcribed genes (commonly known as transcriptome, and expressed as mRNA population). Although the cancer phenotype depends on protein expression regulation, which occurs both at the transcriptional and translational level, the transcriptome can be efficiently used to describe the physiological state of the cell. One severe limitation of microarrays in this field is the amount of RNA available for the analysis. RNA extracted from tissues or from a restricted group of cells in tumors at their early stages of development, amounts to few picograms, which is insufficient for a microarray analysis. To overcome this limitation, the DNA obtained from the RNA is amplified through PCR (polymerase chain reaction), which is known to alter the abundance of genes that are poorly expressed, thus affecting the performance of the device[9].

Nanotechnology research is expected to produce significant advancements in this direction, reducing the size of the array, while controlling the density and the conformation of the spotted material, and introducing detection techniques more sensitive with respect to standard optical detection. If and when we will be able to reach single cell sensitivity with a fast and inexpensive device, then the mapping of neuronal distribution in the brain, or the detection and mapping of tumors at their early stages of development will be possible[10-12].

Since mRNA expression level and the corresponding protein cellular abundances do not always correlate because of variations at the translation stage,

protein analysis and quantification is becoming more and more crucial for clinical applications[13]. Furthermore, the complexity of proteins when compared to DNA or RNA in terms of structural and biochemical diversity requires a higher degree of assay design and data analysis for complete understanding of various cellular functions[14].After all, proteins are the functional product of most genes and the target of clinical interventions[15]. Therefore, there is a clear need for developing innovative technologies to analyze the proteome activity of a biological sample for screening protein-protein or protein-ligand (DNA, lipid, drugs) interactions, which can be applied to obtain a higher level of understanding of the many functions of highly complex cellular networks[16]. Furthermore, for evaluating and diagnosing disease, vulnerability and evolution, and discovering potential therapeutic targets, more rapidly and accurately[17] efficient and low cost proteomics tools could prove very useful.

In the past years, various technologies have been developed for global analysis of protein abundance, structure and function. Existing methods, such as mass spectrometer in combination with separation techniques like two-dimensional gel electrophoresis appeared over a decade ago and are able to detect hundreds of proteins and peptides[18]. These methods have good resolution to screen proteins, however, are hindered by several limitations, such as difficulties in the detection of low levels of proteins in complex biological samples[19], and the need of relatively large amounts of sample[20]. Although these two technologies theoretically offer complete coverage of the proteome, they still lack the qualities necessary for multiplexing and miniaturization that are required for high-throughput screening of proteins. Protein array technology has been evolved to complement these traditional methods and found its way into quantitative proteomics through the construction of what is called "protein microarray" [14, 21, 22].

In general, a protein microarray comprises numerous capturing agents e.g. antibodies, peptides and other organic molecules that selectively bind to the protein of interest arrayed at high spatial density on solid substrates (Figure 2)[20]. The captured proteins are then detected and quantified by several techniques, such as fluorescent[23, 24], SPR[25, 26] and electrochemical detection[27].

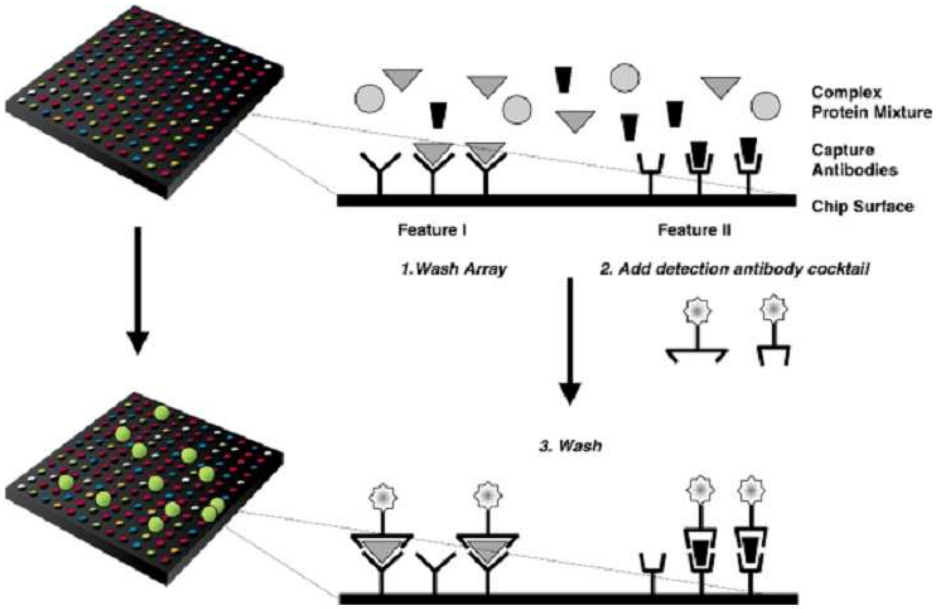

Figure 2: The use of protein microarrays in protein expression profiling. A schematic representation of antibody array is shown top left. Each feature is derivatized by a distinct antibody specifically (top right), making it possible to measure the concentrations of up to 168 proteins simultaneously. First, a complex protein mixture (biological sample) is brought into contact with the antibody array. Each feature on the array captures a single protein species from the complex mixture. After equilibration, the array is washed to remove unbound proteins. At this point, the bound proteins on the array can be directly measured in cases where the analyte proteins have been labeled by fluorescent compounds, for example (this is not explicitly shown). Alternatively, a cocktail of labeled detection antibodies can be added to the array, thus forming sandwich complexes on the features that have captured analyte protein (bottom right). After washing, the signal on the array can be quantified. The Figure adopted from (Wilson, D. S and Nock, S. **2003)**[20]

Despite rapid progress in immobilizing proteins, challenges remain before protein arrays can achieve its full potential for proteomics. For instance, immobilizing a large number of different proteins in as many different spots is still a problem because of the relative vulnerability of these biopolymers. In order to overcome these issues, a versatile method for immobilization of proteins has been introduced by He and co-workers[28]. Using “Protein In Situ Array (PISA)”procedure, they reported on the fabrication of protein arrays directly from PCR-generated DNA with cell free synthesis (Cell-free protein synthesis (also called in-vitro protein synthesis), is the

production of protein without the use of living cells (Origin: Wikipedia)) of $(His)_6$-tagged proteins and simultaneous immobilization on a suitably treated surface. A similar approach to PISA was demonstrated by Ramachandran and coworkers in 2004[29]. Using standard DNA microarray technology, they printed complementary DNAs onto glass slides to translate target proteins with mammalian reticulocyte lysate. The presence of tags on the proteins made them immobilized in situ by a capture molecules arrayed parallel to cDNAs on the surface (Figure 3). They named this methodology nucleic acid programmable protein array (NAPPA) and were able to map pair-wise interactions among 29 human DNA replication initiation proteins.

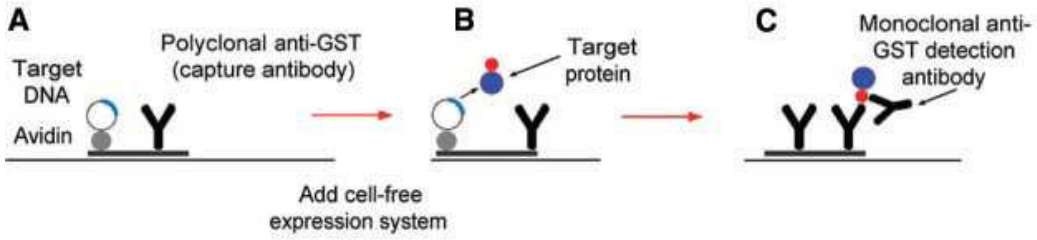

Figure 3: NAPPA approach. Biotinylation of DNA: Plasmid DNA is cross-linked to a psoralen-biotin conjugate with the use of ultraviolet light (*17*). (**A**) Printing the array. Avidin (1.5 mg/ml, Cortex), polyclonal GST antibody (50 _g/ml, Amersham), and Bis (sulfosuccinimidyl) suberate (2 mM, Pierce) are added to the biotinylated plasmid DNA. Samples are arrayed onto glass slides treated with 2% 3-aminopropyltriethoxysilane (Pierce) and 2 mM dimethyl suberimidate.2HCl (Pierce). (**B**) In situ expression and immobilization. Microarrays were incubated with 100 _l per slide rabbit reticulocyte lysate with T7 polymerase (Promega) at 30°C for 1.5 hours then 15°C for 2 hours in a programmable chilling incubator (Torrey Pines). (**C**) Detection. Target proteins are expressed with a C-terminal GST tag and immobilized by the polyclonal GST antibody. All target proteins are detected using a monoclonal antibody to GST (Cell Signaling Technology) against the C-terminal tag confirming expression of fulllength protein. Figure adopted from (Ramachandran, 2004)[29].

Despite addressing successfully those main concerns, there are still technical challenges for this method[30]. For instance, sterically blocking either the N- or C-terminus and requiring the addition of fusion tags to all target proteins, are one of the

most critical factor in producing and purifying many proteins needed for protein microarrays.

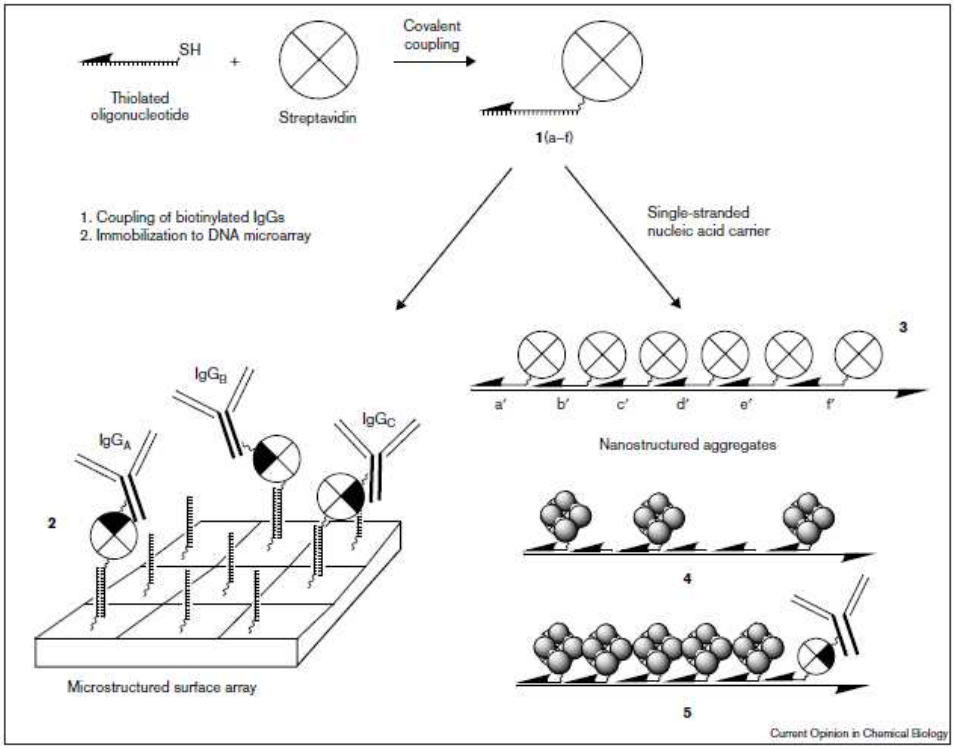

Synthesis and applications of covalent DNA–streptavidin conjugates **1** consisting of 5′-thiol-modified oligonucleotides and STV. A set of conjugates **1** containing individual nucleotide sequences (e.g. **1**a–f), self-assemble in the presence of a single-stranded nucleic acid carrier molecule, containing the complementary sequence stretches (a′–f′), to form supramolecular aggregates **3**. This strategy was used for the spatially controlled positioning of proteins [9,11] and was later applied to the fabrication of 'nanocrystal molecules' from gold nanoclusters [23]. Note that the DNA–STV conjugates **1** can be functionalized with any biotinyl-derivatized molecular compound to obtain oligofunctional aggregates. Following this strategy, biometallic aggregate **4** has been fabricated from 1.4 nm gold-cluster-labeled **1**, and an antibody-containing, functional biometallic construct **5** was obtained from gold-labeled **1**, as well as a conjugate of **1** and a biotinylated immunoglobulin, previously coupled in separate reactions [11]. The conjugates **1** can also be applied as an auxilliary in the DNA-directed immobilization (DDI) of biotinylated macromolecules [9,10]. In this example, various STV conjugates **1** are coupled with individual biotinylated antibodies by mixing of the two compounds. A DNA microarray containing complementary capture oligonucleotides is used as a matrix for immobilization (**2**). Note that because of the specificity of DNA base pairing, many compounds can be site-specifically immobilized simultaneously in a single step (see also Update). The 3′-ends of the oligonucleotides are indicated by an arrowhead, the spacer-chains between DNA and protein are represented by wavy lines. Biotin is indicated by shaded quadrants of the streptavidin.

Figure 4: Concept and use of DDI. Figure adopted from (Niemeyer, 2000)[31]

The use of DNA microarrays technology for proteomics has also been demonstrated by Niemeyer and co-workers. It was first introduced in 1994[32] and known as DNA-Directed Immobilization (DDI)[33, 34]. In this method, highly parallel attachment of multiple proteins each to a different predetermined spot onto a solid support was carried out by generating semisynthetic DNA-protein conjugates. These conjugates, produced by combining the unique properties of DNA with the almost unlimited variety of protein components (Figure 4)[31] made it possible to fabricate a multiple spot array in a single operation, provided a suitable micro or nano array of DNA oligomers is available. To date, DDI has been used in a variety of applications

ranging from the fabrication of functional bio-metallic nanoarrays from gold nanoparticles[35] and the production of mixed arrays containing both nucleic acids and proteins for genome and proteome research[31, 36, 37], to the generation of artificial multiplexed complexes with enhanced bio-catalytic activity[38, 39].

However, as the intricacy of these devices and the corresponding number of features increase, the ability to miniaturize the array and their feature size, becomes of fundamental importance, especially with regard to sensitivity maximization. In addition, if such features are generated having sizes of few ten of nanometers rather than micrometers, one can also overcome the large sample volume requirement and start to access important biochemical information with sample quantities that are hardly accessible with microarrays[16].

1.2 Nanoscale Protein Arrays: Fabrication Tools

The discussion presented in the first part of the chapter has clarified the reasons why many researchers in the field of nanotechnology are aiming to develop innovative tools for opening up possibilities to move in that direction. Several techniques have been introduced for generating biological arrays with feature size ranging from few hundreds to few tens of nanometers in order to achieve higher spot density and consequently, sensitivity than that with microarrays. These techniques include Atomic Force Microscopy (AFM) based nano-lithographic methods[40-43], BioNEMS, such as nano-mechanical cantilever array[44-46] and micro contact printing (μCP)[47]. In particular, nano-mechanical cantilever arrays are sensitive mass-measuring devices that can be considered modern derivatives of the quartz microbalance. This approach has been employed to observe molecular recognition events in real time, both in air and aqueous solution[48]. The captured molecules are immobilized on a cantilever surface and unlabelled target molecules are added. The change in cantilever deflection indicates the amount of captured molecules on them. Cantilever arrays have lots of potential but require still further miniaturization to be able to achieve high sensitivity under water conditions and have the intrinsic limitation of needing a relatively large volume of solution to wet the cantilevers that is equivalent to an intrinsic limit to their sensitivity.

AFM based lithography methods are attractive nano-arraying techniques and have shown the potential in generating arrays with significantly reduced amount of

capture materials (e.g. DNA, peptides, antibodies or proteins). Further, these methods utilized AFM tip (radius of curvature < 10nm) to selectively pattern complex structures on the surface and can offer high sensitivity and resolution. The great advantage of AFM patterning is that the same tip is used for both patterning and reading (i.e. detection). By using AFM molecular height for detection, several physical and mechanical properties can be measured.

There are two major approaches in AFM based lithography methods. One of these is known as Dip Pen Nanolithography (DPN)[41, 42]. It was originally demonstrated by Mirkin in 1999. In DPN, a capturing material is transferred from the tip to the substrate patterning nano-structures. Subsequently, the substrate is exposed to bio-resist molecules to cover the rest of substrate and finally, it is brought in contact with the solution of target molecules[49-52]. The resolution of fabricated spot depends on the tip-surface contact time, relative humidity and surface roughness[42]. Although DPN is commonly used for parallel fabrication of molecules, the main limitation of this method is the lack of control on the molecular packing due to the lack of control on the adsorption properties of the “ink” molecules on the tip.

An, in our opinion, more powerful method that has about an order of magnitude better resolution than DPN was introduced by Liu in 1997[43], and is known as nanografting. This method employs an AFM tip to exchange the molecules that belong to a pre-existing SAM layer (i.e. bio-resist molecules) in a selected area with the molecules that, coming from a solution that is in contact with the first SAM, form another SAM that is sometimes called a NAM or Nanografting Assembled Monolayer. Among several advantages, the exclusive feature of this method is the improved molecular packing densities and molecular order of the NAMs over their corresponding spontaneously adsorbed SAMs. Other advantages of this method include: 1) the possible identification of molecular orientation by measuring the molecular height with high precision (of order of ~ 1Å) with respect to a supporting substrate ; 2) the well defined patterning of homogeneously oriented molecules, which allows the investigation of several phenomena, including fundamental biophysics at nanometer scale; 3) last but not the least, the possibility that is shared by DPN of printing multiple features in array format, where different molecules are placed selectively at different sites.

In pioneering work by Liu and coworkers[53], nanografting was employed to create DNA nanostructures with feature sizes of few tens of nanometers as illustrated in Scheme1.

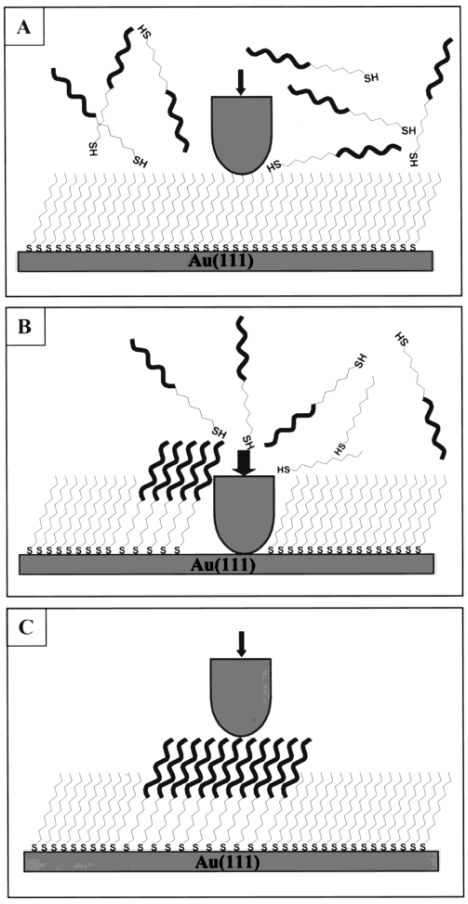

Scheme 1: Schematic diagram illustrating the basic steps to produce ssDNA nanostructures using nanografting. Figure adopted from (Liu, 2002) [54].

In the first step, an alkanethiol SAM is imaged in a liquid medium containing thiolated ssDNA under a low load (A). After a fabrication site is selected, the thiol molecules are removed by the tip with a higher force while thiolated ssDNA molecules in solution adsorb by exchange with the freshly desorbing alkanethiol molecules following the scanning track of the AFM tip (B). The desorbed alkanethiol molecules solubilized at extreme dilution cannot return to the surface making the operation irreversible. The DNA pattern can then be characterized by using the same AFM tip at a reduced imaging force (C)[54, 55]. It was not until 2005- when the feasibility of nanografting was well recognized, that this method was utilized on controlling the packing density of ssDNA molecules inside the nanostructures. In this

report, Liu and coworkers have provided the fundamental information on creating ssDNA nanostructures with controllable packing densities[53]. They then used these structures to monitor the hybridization process with complementary sequence as a function of the packing density of ssDNA. Though this study has established the optimizing condition for producing ssDNA nanostructures, the full potential of the method was not utilized to show its usefulness in making practical biosensors.

In this thesis we aim at combining two well established techniques, i.e. nanografting and DDI, in order to create multiple protein arrays, and artificial multi-enzyme complexes, at the nanometer scale. Additionally, it will be shown that the generated features by nanografting are biologically active and capable of performing multiplexed protein profiling in the presence of human serum, a complex biological mixture.

In the chapter 2, the use of nanografting as a method to create ssDNA patterns with controlled densities and its application to the measurement of the degree of hybridization are described. An overview of our recent studies is reported in the part A of this chapter. In this work, we have demonstrated extremely sensitive and precise detection of hybridization of unlabeled DNA through AFM relative height measurements, specifically on gold surfaces[56]. We have found, contrary to evidence published by others[57, 58] that the decrease in hybridization efficiency found in high density DNA Self Assembled Monolayers (SAMs) was due to the lack of inherent molecular order in SAMs and not the density of the probe molecules. Part B of this chapter deals with the detection of hybridization of non-fully matched complementary strands. Specifically, the hybridization between a probe and two half strands, which are complementary to upper half and lower half of a probe, is investigated and results are compared with fully matched strands. Using AFM relative height and compressibility measurements, we are able to discriminate full sequence hybridization from half sequence (upper and lower half strands) hybridization.

Chapter 3 introduces the combination of nanografting and DDI methods, toward multi-proteins nanoarrays. Using DDI, we are able to immobilize multiple proteins onto nanografted patterns of ssDNA of variable packing densities. Subsequently, the biological activities of proteins on the nanografted patterns are probed by specific binding of corresponding antibodies also in the presence of complex mixture (human serum). The molecular interaction is investigated and quantified by determining equilibrium binding parameters.

As a consequence of its tremendous use in genomics and proteomics research areas, DNA can be used as generic material in the construction of three dimensional spatial arrangements of bio- molecules with molecular binding sites at defined positions for the design of multifunctional assemblies in novel devices[59, 60]. In one of earliest attempts to construct artificial multienzyme architectures, Niemeyer and coworkers suggested the use DNA-directed assembly[39]. Two enzymes, NAD(P)H:FMN Oxidoreductase (NFOR), which reduces flavin mononucleotide (FMN) to FMNH2 by using nicotinamide adenine dinucleotide (NADH) as an electron donor, and Luciferase (Luc), which catalyze two consecutive reaction steps, were used in their work. In the first step, NFOR reduces flavin mononucleotide (FMN) to FMNH2 by using nicotinamide adenine dinucleotide (NADH) as an electron donor. FMNH2 dissociates from NFOR and binds to Luc. In a second step, dodecanal is oxidized by Luc with the aid of molecular oxygen and emits blue-green light. They demonstrated the overall activity of two enzymes to be significantly increased when arranged in close proximity on DNA carrier strands. More recently, Willner and coworkers have attached glucose oxidase and horseradish peroxidase enzymes on DNA templates[61] by using self-assembly of the two enzymes, which were first covalently coupled to a unique anchoring strand of DNA that bound to the templates at specific positions. The oxidation-reduction cascade reaction for the synthesis of Au nanowires on the DNA templates was reported to be effectively activated. Although these studies provide useful tools for the construction of multifunctional molecular assemblies, the design of novel biosensors from these mix assemblies remains a future challenge in nano- biotechnology.

Following these pioneering works, we combine nanografting and DDI to create novel arrangements of bienzyme complexes, in which both lateral and vertical spacing can be tuned. Chapter 4 depicts preliminary results on the construction and characterization of these bienzyme systems. Both AFM relative height and friction measurements are utilized to characterize the activation of the two enzymes within ordered DNA nanostructures. This study suggests that, due to different sizes and position of the two enzymes on the probe strand, it is possible to enhance the reactivity of bienzyme complexes. Although the resulting complexes are shown to be effective platforms in the detection of low concentration of glucose, a number of challenges need to be face to achieve highly sensitive glucose sensors.

Chapter 5 summarizes the results, lists some conclusions and provides an outlook on possible future developments.

1.3 References

1. DeRisi, J.L., Iyer, V.R. & Brown, P.O. Exploring the metabolic and genetic control of gene expression on a genomic scale. *Science* **278**, 680-6 (1997).
2. Schena, M., Shalon, D., Davis, R.W. & Brown, P.O. Quantitative monitoring of gene expression patterns with a complementary DNA microarray. *Science* **270**, 467-70 (1995).
3. Shalon, D., Smith, S.J. & Brown, P.O. A DNA microarray system for analyzing complex DNA samples using two-color fluorescent probe hybridization. *Genome Res* **6**, 639-45 (1996).
4. Park, S.J., Taton, T.A. & Mirkin, C.A. Array-based electrical detection of DNA with nanoparticle probes. *Science* **295**, 1503-6 (2002).
5. Karger, A.E., Weiss, R. & Gesteland, R.F. Digital chemiluminescence imaging of DNA sequencing blots using a charge-coupled device camera. *Nucleic Acids Res* **20**, 6657-65 (1992).
6. Wang, J. From DNA biosensors to gene chips. *Nucleic Acids Res* **28**, 3011-6 (2000).
7. Cobb, J.P. et al. Application of genome-wide expression analysis to human health and disease. *Proc Natl Acad Sci U S A* **102**, 4801-6 (2005).
8. Trevino, V., Falciani, F. & Barrera-Saldana, H.A. DNA microarrays: a powerful genomic tool for biomedical and clinical research. *Mol Med* **13**, 527-41 (2007).
9. Woolley, A.T. et al. Functional integration of PCR amplification and capillary electrophoresis in a microfabricated DNA analysis device. *Anal Chem* **68**, 4081-6 (1996).
10. Coppola, G. & Geschwind, D.H. Technology Insight: querying the genome with microarrays--progress and hope for neurological disease. *Nat Clin Pract Neurol* **2**, 147-58 (2006).

11. Johnston, M.V. Gene expression profiling: a new tool for pediatric neurology? *Curr Opin Neurol* **18**, 89-90 (2005).
12. Mischel, P.S., Cloughesy, T.F. & Nelson, S.F. DNA-microarray analysis of brain cancer: molecular classification for therapy. *Nat Rev Neurosci* **5**, 782-92 (2004).
13. Griffin, T.J. et al. Complementary profiling of gene expression at the transcriptome and proteome levels in Saccharomyces cerevisiae. *Mol Cell Proteomics* **1**, 323-33 (2002).
14. Kumble, K.D. Protein microarrays: new tools for pharmaceutical development. *Anal Bioanal Chem* **377**, 812-9 (2003).
15. Sydor, J.R. & Nock, S. Protein expression profiling arrays: tools for the multiplexed high-throughput analysis of proteins. *Proteome Sci* **1**, 3 (2003).
16. Templin, M.F. et al. Protein microarray technology. *Trends Biotechnol* **20**, 160-6 (2002).
17. Martinsky, T. Protein Microarray Manufacturing. *PharmaGenomics* **2**, 42-46 (2004).
18. Aebersold, R. & Mann, M. Mass spectrometry-based proteomics. *Nature* **422**, 198-207 (2003).
19. Espina, V. et al. Protein microarrays: molecular profiling technologies for clinical specimens. *Proteomics* **3**, 2091-100 (2003).
20. Wilson, D.S. & Nock, S. Recent developments in protein microarray technology. *Angew Chem Int Ed Engl* **42**, 494-500 (2003).
21. Kambhampati, D. Protein microarray technology (ed. Kambhampati, D.) (Weinheim: Wiley-VCH 2004).
22. Zhu, H. & Snyder, M. Protein chip technology. *Curr Opin Chem Biol* **7**, 55-63 (2003).
23. Haab, B.B., Dunham, M.J. & Brown, P.O. Protein microarrays for highly parallel detection and quantitation of specific proteins and antibodies in complex solutions. *Genome Biol* **2**, RESEARCH0004 (2001).
24. Zhu, H. et al. Global analysis of protein activities using proteome chips. *Science* **293**, 2101-5 (2001).
25. Campbell, C.T. & Kim, G. SPR microscopy and its applications to high-throughput analyses of biomolecular binding events and their kinetics. *Biomaterials* **28**, 2380-92 (2007).

26. McDonnell, J.M. Surface plasmon resonance: towards an understanding of the mechanisms of biological molecular recognition. *Curr Opin Chem Biol* **5**, 572-7 (2001).
27. Warsinke, A. Electrochemical biochips for protein analysis. *Adv Biochem Eng Biotechnol* **109**, 155-93 (2008).
28. He, M. & Taussig, M.J. Single step generation of protein arrays from DNA by cell-free expression and in situ immobilisation (PISA method). *Nucleic Acids Res* **29**, E73-3 (2001).
29. Ramachandran, N. et al. Self-assembling protein microarrays. *Science* **305**, 86-90 (2004).
30. LaBaer, J. & Ramachandran, N. Protein microarrays as tools for functional proteomics. *Curr Opin Chem Biol* **9**, 14-9 (2005).
31. Niemeyer, C.M. Self-assembled nanostructures based on DNA: towards the development of nanobiotechnology. *Curr Opin Chem Biol* **4**, 609-18 (2000).
32. Niemeyer, C.M., Sano, T., Smith, C.L. & Cantor, C.R. Oligonucleotide-directed self-assembly of proteins: semisynthetic DNA--streptavidin hybrid molecules as connectors for the generation of macroscopic arrays and the construction of supramolecular bioconjugates. *Nucleic Acids Res* **22**, 5530-9 (1994).
33. Niemeyer, C.M. Bioorganic applications of semisynthetic DNA-protein conjugates. *Chemistry* **7**, 3188-95 (2001).
34. Niemeyer, C.M. in Nanobiotechnology (eds. Niemeyer, C.M. & Mirkin, C.A.) (Weinheim: Wiley-VCH 2004).
35. Niemeyer, C.M. & Ceyhan, B. DNA-Directed Functionalization of Colloidal Gold with Proteins *Angew Chem Int Ed Engl* **40**, 3685-3688 (2001).
36. Lovrinovic, M. & Niemeyer, C.M. Rapid synthesis of DNA-cysteine conjugates for expressed protein ligation. *Biochem Biophys Res Commun* **335**, 943-8 (2005).
37. Niemeyer, C.M. & Blohm, D. DNA Microarrays. *Angew Chem Int Ed Engl* **38**, 2865-2869 (1999).
38. Muller, J. & Niemeyer, C.M. DNA-directed assembly of artificial multienzyme complexes. *Biochem Biophys Res Commun* **377**, 62-7 (2008).

39. Niemeyer, C.M., Koehler, J. & Wuerdemann, C. DNA-directed assembly of bienzymic complexes from in vivo biotinylated NAD(P)H:FMN oxidoreductase and luciferase. *Chembiochem* **3**, 242-5 (2002).
40. Liu, G.Y., Xu, S. & Qain, Y. Nanofabrication of Self-Assembled Monolayers Using Scanning Probe Lithography. *Acc. Chem. Res.* **33**, 457-466 (2000).
41. Mirkin, C.A., Hong, S. & Demers, L. Dip-Pen Nanolithography: Controlling Surface Architecture on the Sub-100 Nanometer Length Scale. *ChemPhysChem* **2**, 37-39 (2001).
42. Piner, R.D., Zhu, J., Xu, F., Hong, S. & Mirkin, C.A. "Dip-Pen" nanolithography. *Science* **283**, 661-3 (1999).
43. Xu, S. & Liu, G.Y. Nanometer-Scale Fabrication by Simultaneous Nanoshaving and Molecular Self-Assembly. *Langmuir* **13**, 127-129 (1997).
44. Arntz, Y. et al. Label-free protein assay based on a nanomechanical cantilever array *Nanotechnology* **14**, 86-90 (2003).
45. Craighead, H.G. Nanoelectromechanical systems. *Science* **290**, 1532-6 (2000).
46. Roukes, M.L.P., CA, US), Fraser, Scott E. (LaCanada, CA, US), Solomon, Jerry E. (Glendale, CA, US), Cross, Michael C. (Claremont, CA, US). (California Institute of Technology (Pasadena, CA, US), United States, 2008).
47. Delamarche, E. in Nanobiotechnology (eds. Niemeyer, C.M. & Mirkin, C.A.) (Weinheim: Wiley-VCH 2004).
48. Burg, T.P. et al. Weighing of biomolecules, single cells and single nanoparticles in fluid. *Nature* **446**, 1066-9 (2007).
49. Demers, L.M. et al. Direct patterning of modified oligonucleotides on metals and insulators by dip-pen nanolithography. *Science* **296**, 1836-8 (2002).
50. Demers, L.M. & Mirkin, C.A. Combinatorial Templates Generated by Dip-Pen Nanolithography for the Formation of Two-Dimensional Particle Arrays. *Angew Chem Int Ed Engl* **40**, 3069-3071 (2001).
51. Lee, K.B., Park, S.J., Mirkin, C.A., Smith, J.C. & Mrksich, M. Protein nanoarrays generated by dip-pen nanolithography. *Science* **295**, 1702-5 (2002).
52. Su, M., Liu, X., Li, S.Y., Dravid, V.P. & Mirkin, C.A. Moving beyond molecules: patterning solid-state features via dip-pen nanolithography with sol-based inks. *J Am Chem Soc* **124**, 1560-1 (2002).
53. Liu, M. & Liu, G.Y. Hybridization with Nanostructures of Single-Stranded DNA. *Langmuir* **21**, 1972-1978 (2005).

54. Liu, M., Amro, N.A., Chow, C.S. & Liu, G.Y. Production of Nanostructures of DNA on Surfaces. *Nano Lett* **2**, 863-867 (2002).
55. Zhou, D., Sinniah, K., Abell, C. & Rayment, T. Label-free detection of DNA hybridization at the nanoscale: a highly sensitive and selective approach using atomic-force microscopy. *Angew Chem Int Ed Engl* **42**, 4934-7 (2003).
56. Mirmomtaz, E. et al. Quantitative Study of the Effect of Coverage on the Hybridization Efficiency of Surface-Bound DNA Nanostructures. *Nano Lett* **8**, 4134-4139 (2008).
57. Peterson, A.W., Heaton, R.J. & Georgiadis, R.M. The effect of surface probe density on DNA hybridization. *Nucleic Acids Res* **29**, 5163-8 (2001).
58. Petrovykh, D.Y., Kimura-Suda, H., Whitman, L.J. & Tarlov, M.J. Quantitative analysis and characterization of DNA immobilized on gold. *J Am Chem Soc* **125**, 5219-26 (2003).
59. Seeman, N.C. Nucleic acid junctions and lattices. *J Theor Biol* **99**, 237-47 (1982).
60. Wilner, O.I. et al. Enzyme cascades activated on topologically programmed DNA scaffolds. *Nat Nanotechnol* **4**, 249-54 (2009).
61. Wilner, O.I., Shimron, S., Weizmann, Y., Wang, Z.G. & Willner, I. Self-assembly of enzymes on DNA scaffolds: en route to biocatalytic cascades and the synthesis of metallic nanowires. *Nano Lett* **9**, 2040-3 (2009).

Chapter 2

Using molecular height to detect hybridization on surfaces

Introduction

The ability to anchor DNA molecules on surfaces is crucial to a wide range of research fields including fundamental biophysics and next generation DNA array technology. Only a few studies have, however, determined the impact of molecular order and/or packing densities of surface tethered DNA on the hybridization efficiency. In this chapter, we show that the degree of molecular order is not only relevant to the hybridization of fully matched DNA complementary strands, but also affects the hybridization efficiency of partly/half matched complementary strands with respect to the surface. This is to mean that the molecular order affects in a different way the hybridization when the half-matched strands hybridize the top or the bottom half of the ssDNA oligomer that is tethered to the surface.

We divided this chapter into two parts. The effect of packing densities of DNA nanostructures on hybridization is studied in part A. The results of this part were described in the article: "Quantitative Study of the Effect of Coverage on the Hybridization Efficiency of Surface-Bound DNA Nanostructures", published in "NanoLetters" 2008; 8, 4134-4139 journal.

In part B, the hybridization of DNA nanostructues with fully matched complementary strand is compared with non-fully matched, specifically with half length complementary strands.

PART A

Quantitative Study of the Effect of Coverage on the Hybridization Efficiency of Surface-Bound DNA Nanostructures*

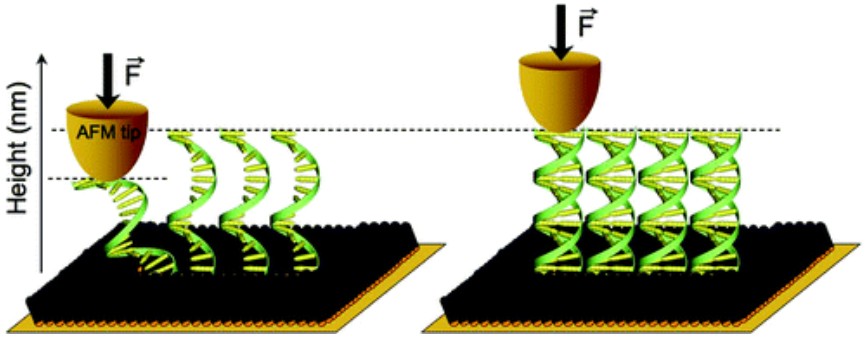

* This chapter has been published in part in: Mirmomtaz, E., Castronovo, M., Grunwald, C., Bano, F., Scaini, D., Ensafi, A. A., Scoles, G., Casalis, L. *Nano Lett.***2008**, *8*, 4134. Part A of this chapter has been done in collaboration with Elham Mirmomtaz and Matteo Castronovo.

2.1 Abstract

We demonstrate that, contrary to current understanding, the density of probe molecules is not responsible for the lack of hybridization in high density single-stranded DNA (ss DNA) self-assembled monolayers (SAMs). To this end, we use nanografting to fabricate well packed ss-DNA nanopatches within a "carpet matrix" SAM of inert thiols on gold surfaces. The DNA surface density is varied by changing the "writing" parameters, for example, tip speed, and number of scan lines. Since ss-DNA is 50 times more flexible than ds-DNA, hybridization leads to a transition to a "standing up" phase. Therefore, accurate height and compressibility measurements of the nanopatches before and after hybridization allow reliable, sensitive, and label-free detection of hybridization. Side-by side comparison of self-assembled and nanografted DNA-monolayers shows that the latter, while denser than the former, display higher hybridization efficiencies.

2.2 Introduction

Two are the main challenges in the development of new analytical methods for the detection of DNA hybridization. The first lies in reducing the minimum amount of DNA that can be directly (label- and PCR-free), detected. In this context, nano-patterned detection devices are to be preferred because when signal levels do not depend on the pattern' size they require a smaller number of molecules to reach "saturation". If reliable detection of a small number of hybridizations could be achieved it would allow for the rapid detection of single cell RNA pools and would be quite useful in forensic, neuron classification and other applications.[1-3] The second challenge is represented by the need of quantitative analysis for gene expression profiles that, using current technology, is limited by our partial knowledge of the hybridization efficiency in all surface-based detection schemes.[1, 4-8]

Many PCR-dependent methods based on, for instance, electrochemical [9, 10], surface plasmon resonance [11] and fluorescence detection have been proposed.[4, 12, 13] Among these, the most common are microarrays in which labelling target molecules and feature sizes larger than 10 microns are necessary. It is important to realize that a 10 micron spot provides space for up to 25 million DNA molecules, which, in addition to the problem of quantitatively introducing fluorescence labels, makes it

clear why PCR-free detection of low copy number (e.g. <1000) RNA sequences is a difficult task.[4, 11]

Furthermore, the detection of small amounts of non coding RNAs is especially interesting since often these molecules are involved in gene expression regulation e.g. in the cell division cycle.[14, 15] Abnormal regulation of the cell division process results in cancer and can be biochemically tracked down to malfunction (mutation) of individual proteins. Therefore capturing and quantifying of low amounts of RNAs from a few or even a single cell is not only desirable for biological basic research, but also for cancer diagnostics and, possibly, therapeutics.[1, 3, 5, 6]

Self-Assembled Monolayers (SAMs) of DNA chemisorbed, typically, on gold (111) surfaces, have been intensively studied as model systems as they allow investigation of hybridization reactions in surface tethered, spatially constrained DNA films. Although different DNA surface densities are easily accessible by changing concentrations and incubation times, inconsistent values have been reported for the saturation density of surface tethered DNA molecules.[16-20]

In this work (in the first part of this chapter), we aim at advancing the state of the art in this area in two ways. First, building on the nanografting work of G.Y. Liu and co-workers[21, 22], we demonstrate that a very low number of target DNA molecules can be reliably detected using height and/or compressibility measurements of DNA nanostructures. Second, by varying the number of scanning lines during nanografting over the area in which desired DNA nanostructure is being assembled, we show that we can control the nanoscale DNA surface density. This, coupled to in situ side-by-side comparison of hybridization of self-assembled and nano-grafted DNA-monolayers, has allowed us to prove that the probe density alone is not responsible for the lack of hybridization in high density ss-DNA SAMs as reported in the literature by at least two groups.[16, 18] Since we have independent evidence that a nanografted monolayer patch is better ordered than a spontaneously adsorbed monolayer made with the same molecules, we are led to the conclusion that it is the intrinsic lack of order (instead of the density) that is the determining factor in strongly hindering the hybridization of maximum density SAMs. Our findings provide valuable biophysical insight on the organization and hybridization of short DNA fragments tethered on surfaces, with clear implications for the fabrication and operation of DNA nano-arrays. To simplify the rest of the paper we would like to introduce a new term that would

identify an adsorbed monolayer the assembly of which has been assisted by an external agent as a Nanografting Assembled Monolayers (NAM).

2.3 Results and Discussion

Nanografting, first introduced by Gang-Yu Liu in 1997[23], is today a well established technique for nano-patterning of SAMs ([24], for a review see [25], for a theoretical modeling study see [26]). Our starting point is a flat gold (111) surface covered by a protective SAM of oligo-ethylene-glycol (OEG) modified thiols (HS-$(CH_2)_{11}$-$(OCH_2CH_2)_3$-OH). During DNA nanografting an AFM tip is scanned in a solution containing thiolated DNA at a relatively high load (few tens of nN) over the desired nanopatch area. Due to tip-induced mechanical perturbations, the OEG molecules in the protective SAM locally exchange with thiolated DNA molecules present in solution and the so fabricated nanopatch can be imaged after resetting the value of the perpendicular force load to the smallest possible, still detectable, value. In their pioneering work about DNA nanografting, G.-Y. Liu and coworkers have varied DNA concentration, scan-speed of the AFM tip, loading force and scan-line density during nanografting, to show that nanografted DNA patches of standing-up molecules could be fabricated.[22]

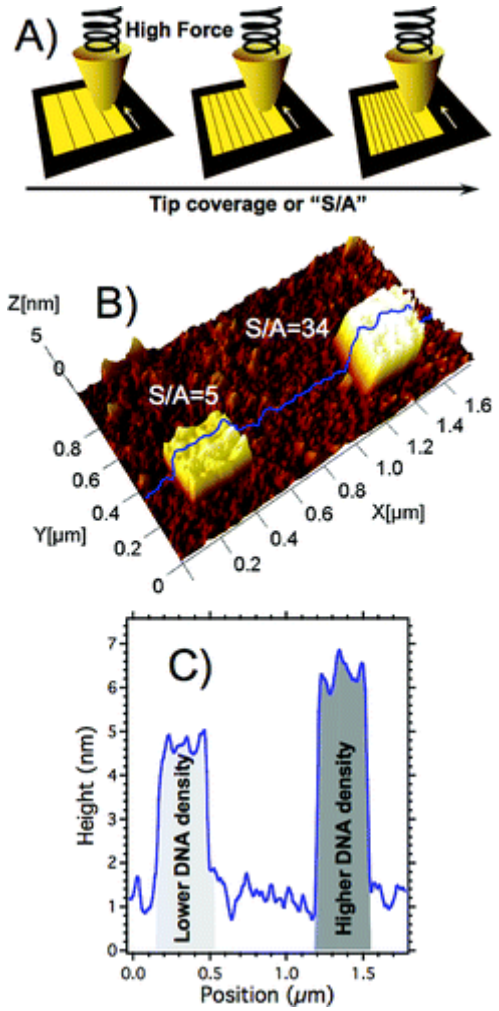

Figure 1. A) Illustration of the definition of the nanografted line density (S/A parameter, see text). **B)** AFM topographic image of two ssDNA nanopatches (NAM) obtained with S/A=5 (left) and S/A=34 (right) written into a bioresistant OEG-SAM before the hybridization. **C)** A profile of the NAM in B (see the blue line) indicates that the conformation of ssDNA molecules inside NAMs significantly depends upon S/A parameter.

We have systematically studied the increased height, by using the height of the OEG SAM as a reference (i.e. about 1.5nm from the gold(111) surface[27]), of the ss-DNA nanopatches at constant scan area, loading force and DNA concentration, but varying the number of scanning lines during the nanografting process. I.e., by grafting over the same area more than once, we find increasing heights for ss-DNA-nanopatches written at higher line overlap (see fig. 1).

In order to compare DNA-nanopatches of different sizes and to learn about the density of DNA as a function of the number of times any given area is nanografted

over, it is useful to introduce a line density parameter "S/A" where S is the scanned area and A is the actual area of the final patch. S/A = R•N/L in which R is the width of the tip at the point of contact with the surface, and N/L is the number of scan lines (in the slow scan direction) divided by the length of the patch L (in the same direction). E.g. for S/A=1 the nanografted lines do not overlap with each other, while for S/A=3 each spot in the nanopatch has been nanografted 3 times over, as shown in the cartoon in fig. 1A.

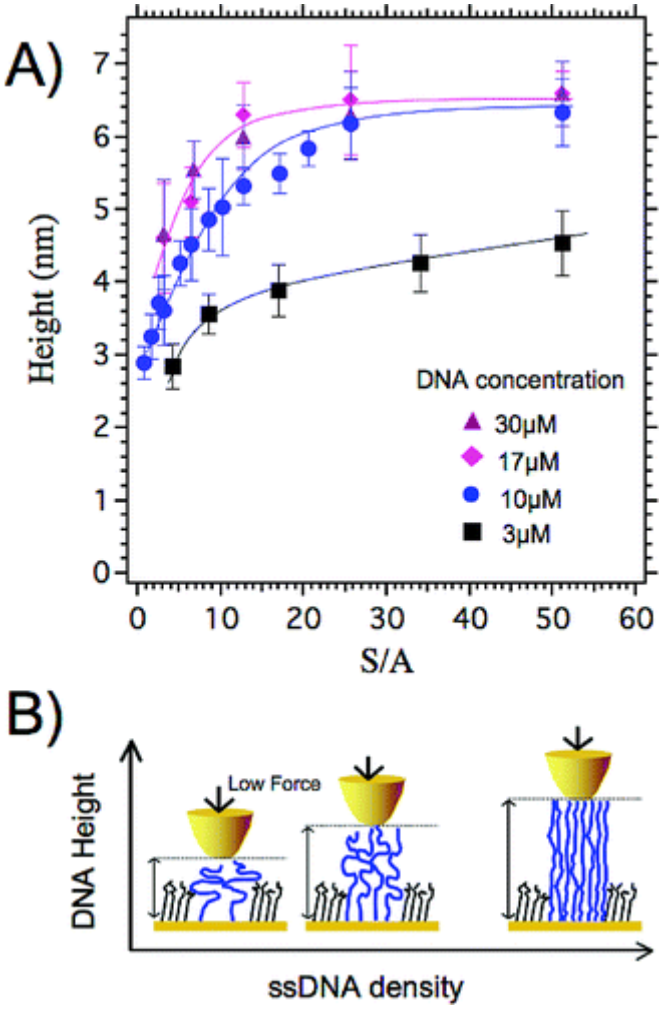

Figure 2. A) Height of ss-DNA NAM nanografted within an OEG SAM as a function of the S/A line density. During grafting ss-DNA concentration of 3.0 (black squares), 10.0 (blue dots), 17.0 (violet triangles) and 30.0 (pink rhombuses) μM have been tested (solid lines were drawn to guide the eyes through the data points). Here coloured lines are shown only just to drive the eyes along the curves. **B)** A scheme depicts our interpretation for which the increase of NAMs height is due to an increase of the density of DNA molecules.

In fig. 1B we show two ss-DNA nanopatches fabricated at low and high S/A number, respectively. The associated topography profiles (fig. 1C) show that with increased S/A numbers the height of the nanopatch increases, to indicate that more DNA-molecules are grafted into the same nano-area. These findings are extended in fig. 2A, where ss-DNA nanopatches heights are plotted, for a wide range of S/A values, at different DNA concentrations in a buffer solution. With the exception of the lowest concentration (that needs higher values of S/A to saturate) in fig. 2A we can see that all height plots reach the same saturation value, between 6 and 7 nm, which is close to to the length of the fully extended conformation of an 18-mer sequence such as the one used here. In the S/A range between 1 and 15 the height of the DNA-nanopatches is highly sensitive to the chosen S/A number provided the probe concentration during nanografting is high enough (e.g. greater than 10 μM).

The fact that when grafting additional ss-DNA molecules into the patch the height of the latter increases is certainly not surprising because the height of a ss-DNA NAM, made of standing-up, thiolated, molecules, is in fact affected by the repulsive van der Waals overlap forces and/or the electrostatic repulsion between the DNA oligomers which make them to stretch in the vertical (unconstrained) direction at higher densities (see scheme in fig. 2B). What is interesting, and somewhat of a surprise to us, is the fact that our results clearly establish that the maximum height reached by NAMs is much larger than that reached by a maximum density SAM (see below). We can only speculate at this point that during nanografting the structures that we create are undergoing a sort of tip induced local annealing (or perhaps combing) getting more dense and much less entangled at the same time, up to the limit that can be calculated for a structure with the same height of fully stretched ss-DNA molecules. This result is to be contrasted with the (likely correct) observations reported in the literature for ss-DNA SAMs, according to which spontaneous self-assembly is associated with a certain degree of molecular entanglement.[20] If disorder/entanglement would be present in our flexible ss-DNA nanostructures, we should expect that full utilization of space would be hindered and that sizable portions of the molecule would not be vertical, resulting in a patch height lower then the nominal and fully stretched, molecular height. We will come back to the crucial issue

of molecular order in nanografted DNA structures later in this paper, giving more direct evidences for our hypothesis.

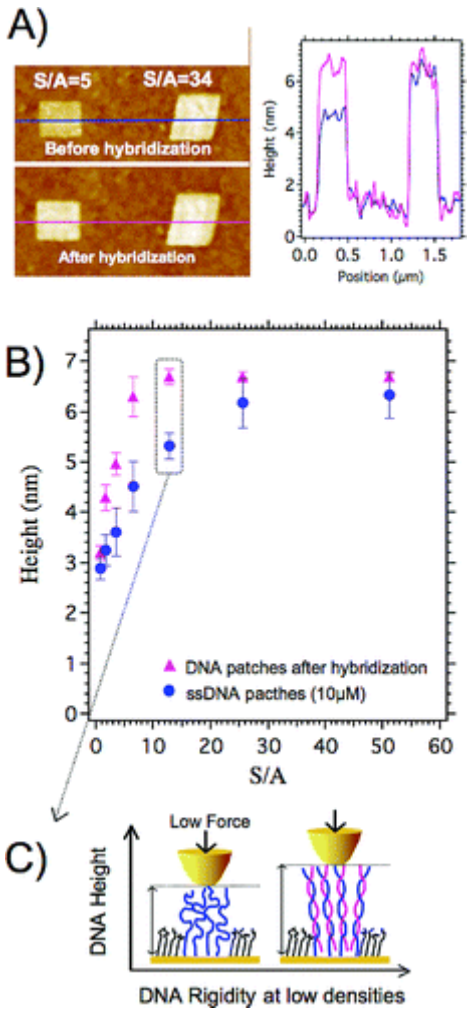

Figure 3. A) On the left DNA NAMs (S/A=5 and S/A=34) relative to fig 1A and 1B, before and after hybridization. On the right height profiles show the height change due to hybridization. The height increase only for NAM at S/A=5. **B)** Relative height of NAM in the 10μM case relative to fig. 2A. The relative height of DNA NAM within an OEG SAM is measured before (blue dots) and after hybridization (pink triangles). The plots indicate that in the low packing regime (SN ≤ 20) the height of the NAMs increases sensitively upon hybridization. **C)** A scheme depicts our interpretation of the height increase of the DNA patch in the low S/A range (e.g. S/A=10) upon hybridization.

After establishing the correspondence between the height of the nanopatches and the S/A density parameter, we investigated how the system behaves upon

hybridization. We found that, in the low S/A regime, after hybridization, the height of the DNA-nanopatches increases significantly due to the much higher stiffness of ds-DNA with respect to ss-DNA (see fig.3). Measurements of cross-reactivity of a DNA target molecule to non-complementary ss-DNA nanostructures (data not shown) confirmed that the height increase in the low density regime is selectively associated with a matching complementary ss-DNA target molecule. Indeed, when exposing the DNA nanostructures of a few different sequences to DNA molecules complementary only to one of them, no changes in height of ss-DNA-nanopatches were observed for all the non-complementary cases.

As expected, in the high S/A regime, in which the height of the nanopatches has already reached saturation, no change in height is recognized upon hybridization (see fig. 3). It follows that, in the high S/A regime it is not possible to know whether or not hybridization occurs using height measurements, because no further change in height can be expected once the ss-DNA inside the nanopatches is organized in its fully extended conformation. Compressibility measurements (e.g. height measurements vs. up to moderately elevated loading forces) offer, however, a reliable way for checking if hybridization also occurs in the high S/A regime.

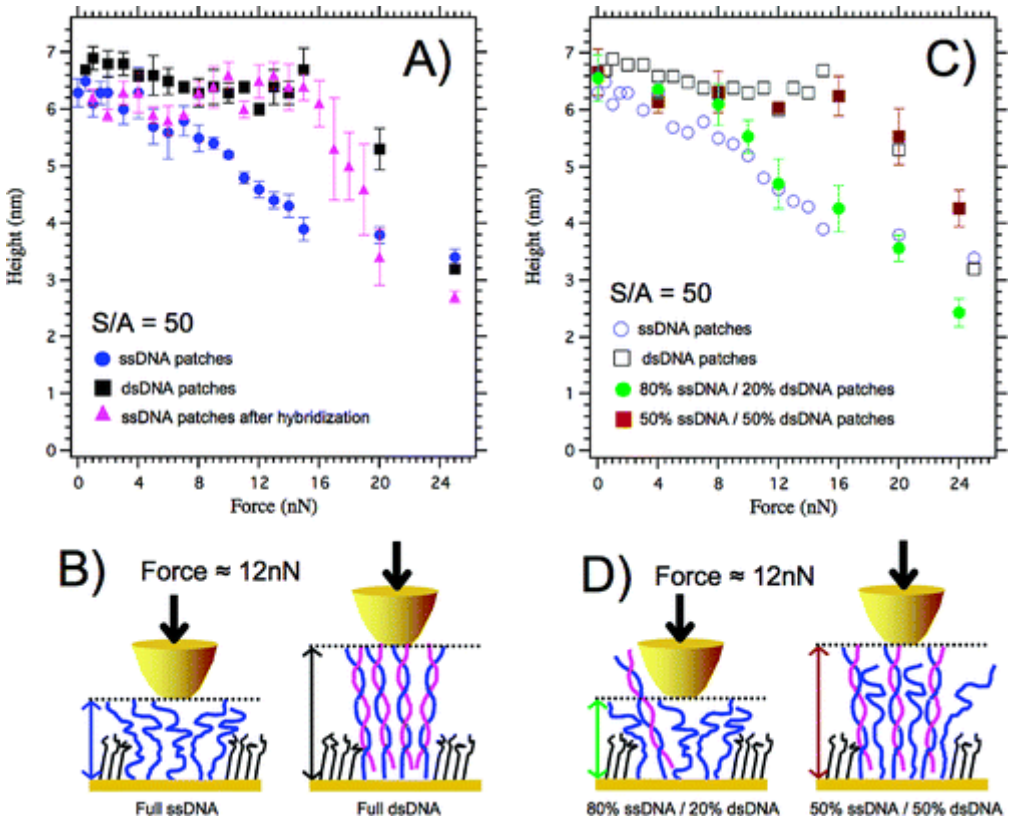

Figure 4. A). Relative height of high density DNA NAMs (S/A=50) measured as a function of the load applied by the AFM tip (compressibility curves). The mechanical resistance of a DNA NAM hybridized in-situ (pink triangles) is well distinguishable from the one relative to the same NAM before hybridization (blue dots), but is very similar to the behaviour of a NAM of ds-DNA, i.e. nanografted after hybridization in solution (black squares). **B)** A scheme depicts the result shown in fig. 4A for ssDNA NAMs and dsDNA NAMs under an applied force of 12nN. **C)** Compressibility curves of high density DNA NAMs (S/A=50) with mixed composition, i.e. 80% ssDNA / 20% dsDNA (filled green circles) and 50% ssDNA / 50% dsDNA (filled brown squares), are compared to the compressibility curves of fig. 4A relative to fully ssDNA NAMs (now reported with open blue circles) and fully dsDNA NAMs (now reported with open black squares). This observation indicates that the hybridization efficiency within highly dense ss-DNA NAM is certainly higher than the value, i.e. about 10%, reported in the literature for high density ss-DNA SAM. **D)** A scheme depicts the result shown in fig. 4B for mixed DNA NAMs under an applied force of 12nN.

The height-to-load response of 3 NAMs made respectively with ss-DNA, ds-DNA and ds-DNA produced by in-situ full hybridization of ss-DNA-nanopatches, was investigated at S/A = 50. The results are summarized in fig. 4A revealing three important findings: 1) the elastic response of DNA-nanopatches before (in blue) and after hybridization (in pink) differs sufficiently to allow for easy identification. 2) ds-DNA is almost incompressible with forces below 16 nN which is consistent with the fact that the persistence length of ds-DNA is 50 times larger that that of ss-DNA 3) the stiff mechanical response of the in-situ hybridized DNA nanostructure (in pink) is almost identical to that of the nanografted ds-DNA-nanopatch (in black). These results are schematized in the cartoon of fig. 4B.

From the changes in compressibility we conclude that, in nanografted patches also in the high S/A (density) regime hybridization occurs even if the heights before and after hybridization are, of course, the same. However, a quantitative determination of the hybridization efficiency of our highly dense patches is not yet possible from the presented data. Towards this end, we studied the compressibility behavior of nanopatches of mixed ss-DNA and ds-DNA composition. In particular, we grafted a mixture containing 50% ss-DNA and 50% ds-DNA (brown filled squares

in fig. 4C) and a mixture with 20% ds-DNA and 80% ss-DNA (green filled circles in fig. 4C). While in the latter case data points are in between the compressibility plots of ss-DNA and ds-DNA of fig. 4A, the former series of data were almost indistinguishable from the 100% grafted ds-DNA, proving that the hybridization efficiency in our nanografted patches is at least 50%, i.e. much higher than the value of 10% reported in the literature for the high-density DNA SAMs.[18]

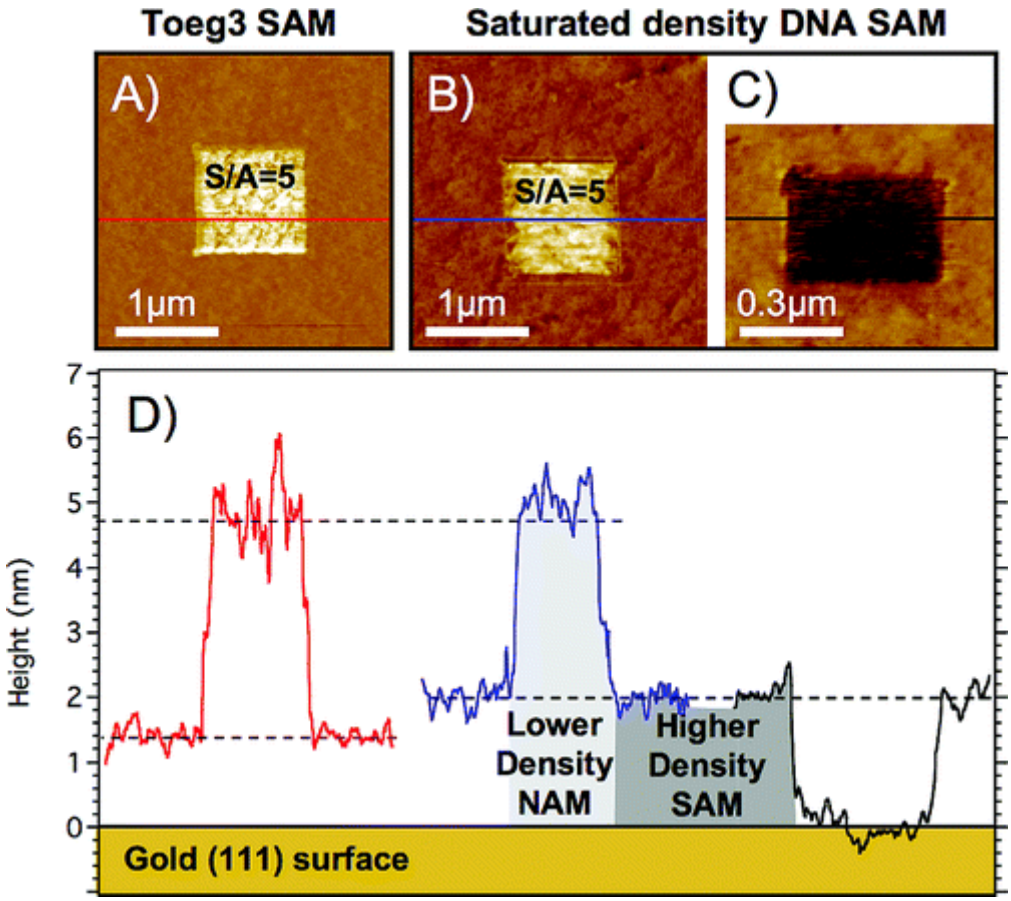

Figure 5: A) A ssDNA NAM is grafted in low density range (S/A=5) within an OEG terminated bioresistant SAM. **B)** A ssDNA NAM is grafted in low density range (S/A=5) within a high density ssDNA SAM of the same molecule of the NAM. C) A shaving of the high density DNA SAM relative to fig. 5B is used to measure the absolute height of the DNA molecules in the SAM. **D)** The red graph on the left is the height profile of the DNA NAM relative to fig. 5A (see red lines). The absolute height of the OEG SAM is about 1.5nm (see ref to the Ying PhD thesis). The blue graph in the center is the height profile of the DNA NAM relative to fig. 5B (see blue line). The absolute height of the DNA NAM is given by the sum of the relative height between the DNA NAM and the DNA SAM in fig 5B (see blue line) and the absolute

height of the DNA SAM relative to fig. 5C that is reported with the green graph on the right (see green line). Reasonably, the height of the low density NAMs grafted in the OEG terminated SAM (see fig. 5A) and in the high density DNA SAM (see fig. 5B) are the same while, surprisingly, although the molecular density of the NAM has to be lower than in the SAM, the height of a "low" density NAM is found to be about three times higher than the one of the high density SAM.

To give a direct proof that it is the sterical hindrance due to the disorder in the film that inhibits hybridization in DNA SAMs, and that our NAM patches are more ordered, following what done previously by other groups we directly compared our nanopatches with the DNA SAM. Since both Tarlov and Georgiadis groups, who extensively studied DNA SAMs, found the hybridization reaction to be very inefficient at high monolayer coverage, we used their protocols[16, 18] to produce a high density SAM, into which we created DNA patches by nanografting. In this way we use the same detection technique, i.e. topography height, to compare DNA SAMs and NAM patches excluding any possible influence of the detection technique on the contrasting results. Therefore, we nanografted a DNA sequence into a SAM of the same DNA sequence, obtained, according to the Tarlov protocol, from prolonged immersion (more than 24 hours) of the gold substrate into a highly concentrated (microMolar) solution of ssDNA molecules. In fig 5 an AFM topography image and relative profiles of this "autografted" ssDNA patch is shown (fig. 5B), together with an image and profile of a patch of the same density (S/A = 5) nanografted into a TOEG SAM (fig. 5A). To establish the absolute height of all four systems compare here, the height of the high density SAM surrounding the patch of fig. 5B is then measured by creating a squared "hole" in the SAM by nanoshaving, as shown in fig. 5C. While the height of the ssDNA NAM patch does not change whether it is embedded into a TOEG SAM or into a DNA carpet (fig. 5A and 5B), the height of a NAM patch, not even saturated, is found to be more than twice the height of a maximum density ssDNA SAM. This result is clearly suggesting that in our DNA nanopatches not only the density but also the degree of order is larger than in SAMs. Moreover, we verified that the height of the high density ssDNA SAM does not change upon hybridization: detailed studies on the hybridization of DNA SAMs of different densities will be shown in a separate paper.[28]

We have demonstrated that combining height and elastic compressibility measurements it is possible to detect hybridization of nanostructured DNA. In particular, we have used nanografting to control the density and improve the molecular packing in ss-DNA nano-assemblies, demonstrating that even in very dense NAMs the efficiency of hybridization is larger than 50% hereby demonstrating that molecular density cannot be the sole source for the inefficient (<10%) hybridization in high coverage SAMs.

Very recently the group of A. Belcher reported on hybridization detection of ss-DNA nanofeatures produced by dip-pen nanolithography by means of kelvin-probe-microscopy.[29] While the detection method was shown to work efficiently on the nanoscale, the proposed nano-devices lack a detailed knowledge of the conformational state of the molecules in the patches. By using nanografting in combination with height profile measurements, we have provided for the first time a method to control systematically the surface coverage of DNA on the nanoscale, and at the same time to detect quantitatively the hybridization efficiency of ss-DNA nanostructures.

Nanografted DNA monolayers hybridize differently than DNA SAMs. First of all NAMs can achieve heights not achievable by SAMs made using the same oligonucleotides. Furthermore, their asymptotic high density height corresponds to the fully extended conformation of their DNA molecules which likely reflects the lack of entanglement for the densely packed surface tethered DNA molecules. Finally at all coverage values explored (far inside the height saturation regime), we could not identify a range of densities in which hybridization would not steadily increase.

Hybridization induced rearrangement of DNA probe molecules tethered to a solid interface was previously described by M.J. Tarlov and coworkers using spectroscopic tools like FTIR and XPS. These rearrangements where rationalized with changes in the persistence length of DNA upon hybridization (persistence length of ss-DNA ~ 1nm and for ds-DNA ~ 50nm). In order to compare directly our results on DNA NAMs patches with those on DNA SAMs, we have performed experiments comparing self-assembled, high-density DNA monolayers produced following M.J. Tarlov's protocols, with AFM tip induced nano-assemblies of the same DNA sequence, on the same surface. From our height measurements we can show that a low density (S/A = 5) patch is 3 times higher than a maximum density SAM. Since a high density NAM is about one and half time as high as these lower density samples

(see fig. 2) it follows that a maximum density SAM is about four and half time lower than a high density NAM. It is also pertinent and interesting to note that, due to molecular entanglement, i.e. the existence of empty space at the interior of the SAM, the latter system is much more compressible than a non-entangled NAM.

2.4 Conclusions

Looking at the future, we can be, with G.Y. Liu and coworkers, confident about the possibility of fabricating DNA nano-arrays of unprecedented sensitivity but by controlling probe molecule packing and/or non-entanglement, we can be confident about the quantitative aspects of the analysis of gene expression profiling including, eventually, PCR free single cell analysis. Our method being based on height and elasticity measurements before and after hybridization, requires no labeling of the target molecules, this being no minor advantage if we are thinking about its widespread use for instance for screening purposes.

2.5 Experimental section

Materials. All oligonucleotides were purchased from Sigma-genosys Ltd. or Biomers and were used without further purification. Absolute ethanol used e.g. for growing SAMs was coming from Fluka. The buffer referred from now on as TE-buffer was composed of the following compounds: 1M NaCl (Baker), 10mM Tris (Fluka), 1mM EDTA (Fluka) with the pH adjusted to 7.2. Only Milli-Q water (resistance > 18 MΩ/cm) was used for buffer preparation. After buffer preparation the solution was additionally purified by filtering through 0.22 µm pore size filters (syringe filters, Carl Roth, Germany).

Preparation of ultra flat gold surfaces. Ultra flat gold films substrates were prepared using a modified Ulman procedure.[30] Briefly, freshly cleaved mica sheets (Mica New York Corp., clear ruby muscovite) were mounted in an electron beam gold evaporator about 50 cm above the gold source and were kept at room temperature. Gold films were deposited at a rate of ~ 0.1 nm/s and a chamber pressure of about 10^{-6} mbar until a thickness of 100 nm was reached. Cleaned glass slides (BK7, Menzel, 76 mm x 26 mm x 1 mm) were cut into pieces of 5mm x 5mm and

glued to the gold surface using a solvent resistant epoxy glue (Epo-tek 377 - Epoxy Technology) that was cured a few hours at 150 ^{0}C.

After curing the glue the gold-MICA interface was opened mechanically and the Ulman surface was immediately dipped into a freshly prepared 100 μM solution of an ethylene-glycol terminated alkylthiol (OEG-thiol, HS-$(CH_2)_{11}$-OEG_3-OH, Prochimia) in absolute ethanol (Fluka, purity ≥ 99.8%). The Substrates were kept in the thiol solution overnight in the dark at room temperature. In this way an ultra flat surface covered with OEG-thiols was obtained. AFM test measurements confirmed a roughness in the range of only a few Å.

Nanografting of the DNA nano patches. All AFM experiments were carried out with conventional AFMs using a XE-100 (Park System, former PSIA) working in contact mode with commercially available "hard" silicon cantilevers (NS36C, MikroMasch, nominal spring constant 0.6 Nm^{-1}, tip radius <10 nm). In all the experiments the process of nanografting was performed in the following steps: (a) A freshly prepared SAM substrate was mounted in a closed liquid cell. Prior to grafting a worn out cantilever (e.g. a cantilever with blunted tip) was used to scratch a sign into the gold surface. This sign allows aligning the cantilever optically to an origin which facilitates finding back the nano patterns. (b) The liquid cell was filled with the nanografting solution. DNA was grafted in a 1:1 mixture (v/v) of TE-buffer and absolute ethanol. For nanografting ssDNA patches the concentration of the DNA in the liquid cell ranged from 3 to 30 μM, while, when dsDNA was nanografted, the duplex was prepared by incubating a 1:2 solution of SH-$(CH_2)_6$-5'-ATC TCA CCT GTG CAC TGC-3' (18-mer) and its complemetary sequence (not thiolated 18-mer) in the TE buffer at 37°C for 2 hours to produce a final 10 μM duplex concentration. The SAM was imaged in liquid at low load to select the area where to fabricate the DNA nanostructures. (c) The desired patterns were obtained within the SAM by scanning the AFM tip at approximately 80-100 nN and with a scan rate of about 500 nm/s. In this way the alkylthiol SAM phase was locally disrupted and immediately exchanged with the DNA monolayer phase. As demonstrated above the DNA density inside the nano patches depends critically on the parameters chosen during the nanografting procedure, namely on the number of scan lines and the loading force. The "right" loading force for DNA nanografting has to be determined in pre-experiments for each cantilever to be used. This is due to the slight differing of individual tip shapes and/or

sizes among the cantilevers used. The S/A parameter was defined by estimating the size of the tip-surface contact area during nanografting to be about 10nm. After the nano-fabrication process the surface was copiously washed with Ethanol and TE-buffer.

AFM measurements over DNA nanostructures: relative height and mechanical compressibility. The relative height of the DNA patches with respect to the surrounding TOEG SAM was measured by scanning side by side the patches within the SAM at the minimum force (the pull-off force is interpreted as 0 nN) and at constant speed. In the case of the mechanical compressibility measurements, the relative height of the DNA assemblies was measured as a function of the applied force. The force exerted over the DNA assemblies was increased from low (0 nN) to high loads (~ 50 nN). In the low force regime (<15 nN) the compressibility is found to be fully reversible while at high forces (>20 nN) significant damage was induced. For hybridizing DNA structures we incubated the ss-DNA nano patches with 1 µM solutions of complementary perfectly matching sequences in TE-buffer. Then we again washed the surface intensively before imaging the DNA nano patches.

Preparation of highly dense DNA self-assembled monolayers. Immediately after opening the gold-MICA interface the glass-supported gold surface is dipped into TE-buffer solution containing 1 µM thiolated DNA (same of ref [18]). The preparation of ss-DNA-SAMs was done as previously described by M.J. Tarlov and co-workers. Briefly, highly dense ss-DNA-SAMs were prepared by allowing the contact time for thiolated ss-DNA solutions towards the gold surfaces for more that 24 hours. Subsequently these substrates were incubated for 1h in 1mM solutions of mercaptohexanol ($HS-(CH_2)_6-OH$, Fluka). The mercaptohexanol solution was prepared by fresh dilution of a pure mercaptohexanol solution into TE-buffer. Incubating with mercaptohexanol molecules helps preventing unspecific interaction between ssDNA and gold.[16] Under these conditions according to the literature, with the used DNA molecules, a density in the range of $1.1x10^{13}$ molecules per cm^2 is achieved.[16, 18]

PART B

Hybridization efficiency of surface bound DNA nanostructures: A case study of fully matched (24 bases) vs. half matched (upper 12 or lower 12 bases) targets.*

* Unpublished observations

In the previous section, we intensively studied how the density of probe ssDNA can be varied on gold surfaces by changing the NG parameters, and how this influences the efficiency of hybridization of unlabeled DNA targets to the immobilized surface DNA. Results of compressibility measurements obtained using AFM imaging showed that hybridization of high probe density DNA nanografted patches (NAMs) is quite different from that of spontaneously (or self-) adsorbed DNA monolayers (SAMs).

In order to advance our general understanding of these phenomena and, for instance, of the behavior of mismatched DNA, (which is important for various applications including the detection of single nucleotides polymorphisms in gene expression) [31, 32] we examine here the hybridization of ssDNA with non-fully matching targets. Particularly, we aimed at investigating the hybridization of immobilized DNA with half length complementary strands, namely upper half and lower half complementary strands. To discriminate between upper and lower hybridization by height measurements, we decided to approach the problem systematically. Specifically, we used three target DNA sequences (two half and one full complementary targets, see experimental section for details), interacting with the same 24-mer tethered probe DNA, as shown in Scheme 1. The two 12-mer strands that bind to different positions on the 24-mer probe strand were chosen to be thermodynamically equivalent. We investigate these probe-target interactions at different probe densities via height and compressibility measurements. An important feature of this study is that the resulting array shows enhanced distinction between full versus upper or lower duplexes. Furthermore, it provides valuable information that is important for numerous applications of immobilized DNA on solid support in life science studies, including single cell RNA characterization, gene expression profile and genetic variability.

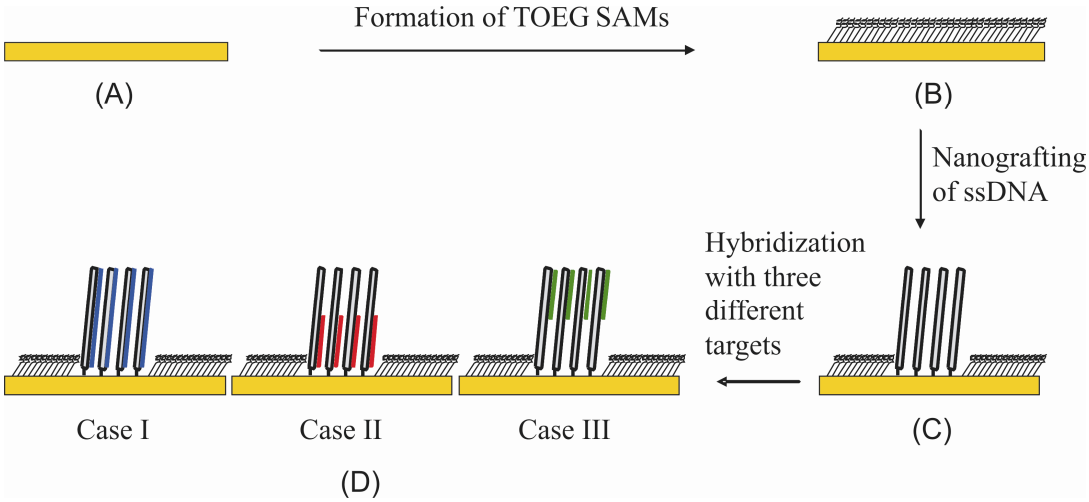

Scheme 1: Schematic layout of the current studies. (A) Bare gold surface (B) gold surface covered with TOEG molecules (C) Nanografting of ssDNA nano-patches (NAMs) within TOEG3 SAMs. (D) Hybridization reactions with three different targets. Explicitly, Case I dealt with full length target strands (Tfull24, in blue) while Case II with lower part of half-target strand (Tdown12, in red) and Case III with upper part of half-target (Tup12, in green).

For the preparation of ssDNA nanostructures, patches of ssDNA, 24 bases long, were fabricated within oligo-ethylene-glycol terminated alkylthiol SAMs on a flat gold surface via nanografting. As shown in Fig. 6, 250 x 250 nm^2 patches of ssDNA were grafted into 1 x 1 μm^2 area of a TOEG SAM with three different values of S/A (for the definition of S/A see section 2.3). Briefly S/A can be thought as the density of scanning lines multiplied by the tip size at the point of contact with the surface. Therefore, the higher is the number of sweeps or lines "painted" in a given area by AFM tip, the higher is the S/A. We stress here that only far from saturation S/A may be proportional to the surface density of DNA probe and that we do not claim that proportionality exists even at low values of S/A. What we claim is that we do have an easy and reproducible way to change the surface coverage of probe DNA.

Fig. 6 shows the resulting height profiles of ssDNA measured by AFM after washing the surface with TE buffer. As shown, the height of ssDNA nano-patches is increasing with increasing S/A number (see schematic representation in fig. 6), to exhibit higher packing densities of ssDNA into the same area, which is in good agreement with our previous studies (see part A).

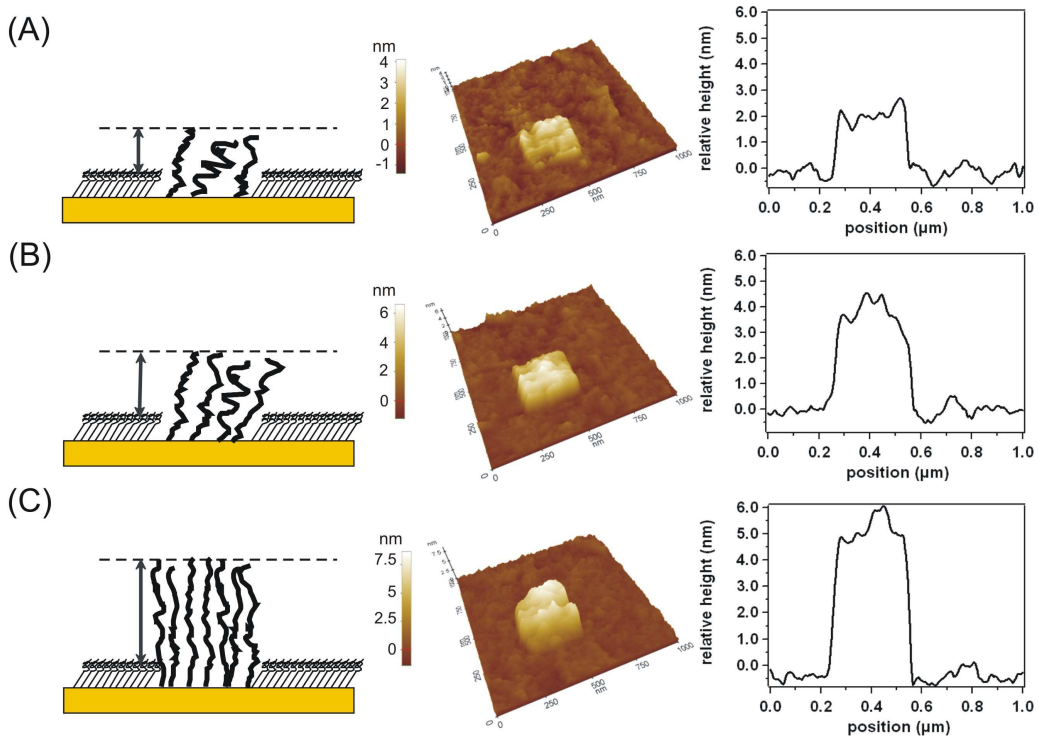

Figure 6: Contact-mode AFM topographic image of 250 x 250 nm^2 nano-patch of ssDNA fabricated into a TOEG SAM with (A) S/A = 1, (B) S/A = 5 and (C) S/A = 10. The corresponding average line profiles are shown, with schematic representation of increasing DNA density by increasing the S/A. All the scan sizes are 1 x 1 μm^2 and the scale bars represent 300nm.

We followed the hybridization of ssDNA nano-patches with full and half length (upper and lower) targets created at different values of S/A. Figure 7 A, B and C show AFM topographic images and corresponding height profiles of DNA nano-patches after reacting with target DNA, Tfull24, Tdown12 and Tup12, respectively. The nano-patches were carefully washed with TE buffer after hybridization and imaged by AFM in a (1:1) solution of TE buffer and Ethanol. As can be seen in fig. 7, the height profile of ssDNA grafted at S/A =1 (average height ~ 2.2 ± 0.4 nm, fig. 6A) shows an increase in height of 3.2 ± 0.4 nm, 1.9 ± 0.4 nm and 0.7 ± 0.5 nm after hybridization with Tfull24 (average height ~ 5.4 ± 0.3 nm, fig. 7A), Tdown12 (average height ~ 4.1 ± 0.4 nm, fig. 7B) and Tup12 (average height ~ 2.9 ± 0.5 nm, fig. 7C), respectively.

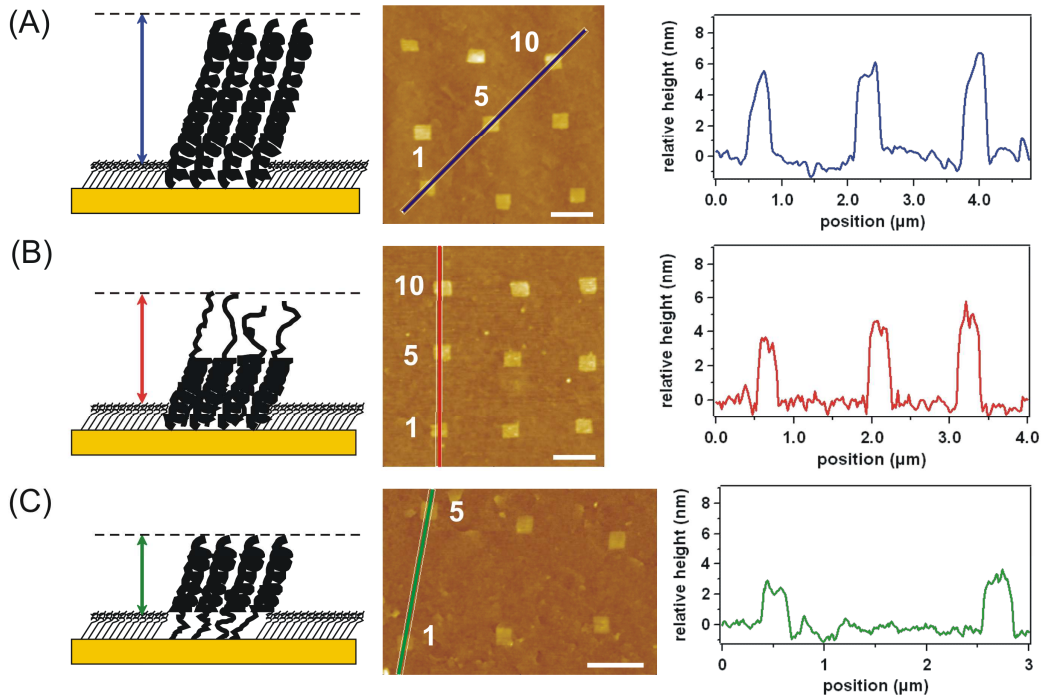

Figure 7: Three hybridization cases: Schematic representation and 4 x 4 μm^2 AFM topographic image containing nine nano-patches of 24-mer ssDNA incubated with 1µM solution of (A) Tfull24 and (B) Tdown12 targets. Nano-patches were fabricated with S/A = 10 (first row from the top), 5 (second row) and 1 (third row) within a TOEG SAM. Corresponding average line profiles are shown; (C) Schematic representation and 4.5 x 3 μm^2 AFM topographic image with the corresponding average line profile of six nano-patches produced with S/A = 5 (top row) and 1 (bottom row) and subsequently incubated with 1µM solution of Tup12 target. All the scale bars represent 500nm.

The relative heights of ssDNA nano-patches before and after hybridization with the three target strands for a wide range of S/A are summarized in fig. 8A. As can be seen in the plot, in the low packing regime (S/A $\leq$ 20), we observe a height increase only upon hybridization with Tfull24 (blue squares) and Tdown12 (red down triangles), while for Tup12 targets (green up triangles), which hybridize to the top part of the ssDNA strand, only little changes in height are observed. More in general, we can stress the fact that from this set of measurements, we can already discriminate between full and partial hybridization of the grafted nano-patches. One possible explanation for the different behavior of Tdown12 and Tup12 can be found on the different rigidity of the two systems [33]: the duplexes formed at the top of the probes, upon hybridization with Tup12 targets, are sitting on top of a flexible, 12 bases long

ssDNA tail (see schematic representation in fig. 7), while the duplexes formed upon hybridization with Tdown12 are located at the bottom, so conferring more rigidity to the system. This result suggests that the upper duplexes, sitting on the flexible tail behaves more like a flexible polymer than the lower duplexes.

When the packing density is increased to S/A > 20, the height values of DNA nano-patches for lower half target (Tdown12) vs. upper half target (Tup12), were hardly distinguishable. This is due to the fact that ssDNA molecules in high density nano-assemblies adopt a fully extended conformation (see the previous section), which corresponds to a saturated height of the patches, that cannot increase further upon hybridization (fig. 8). We performed height-S/A measurements also in the case of grafted dsDNA nano-patches (the complementary strands were first let to hybridize in solution). Results are reported in fig. 8B-D. As shown, the height-S/A response of hybridized ssDNA nano-patches is very similar to the one of grafted dsDNA nano-patches, for all the three target strands, in low and high S/A regimes, meaning that there are no restrictions for in-situ hybridization in the nano-structures. It should be noticed that the relative height of grafted dsDNA nano-patches is initiating from a lower value (~4 nm) as compared to fully hybridized ssDNA nano-patches (~5.4 nm), and that the asymptotic height is hardly reached in the case of grafted dsDNA. We ascribe this difference to the different thermodynamics behavior of ssDNA and dsDNA molecules: the latter are less mobile in the solution and tend to form aggregates. As a consequence, grafting of dsDNA is more critical.

In order to distinguish between upper and lower hybridization, we have performed compressibility measurements for low and high S/A values. The concept of compressibility measurements has been already introduced in the previous section: the height response versus applied load of AFM tip that can provide useful information on the mechanical behavior of the system.

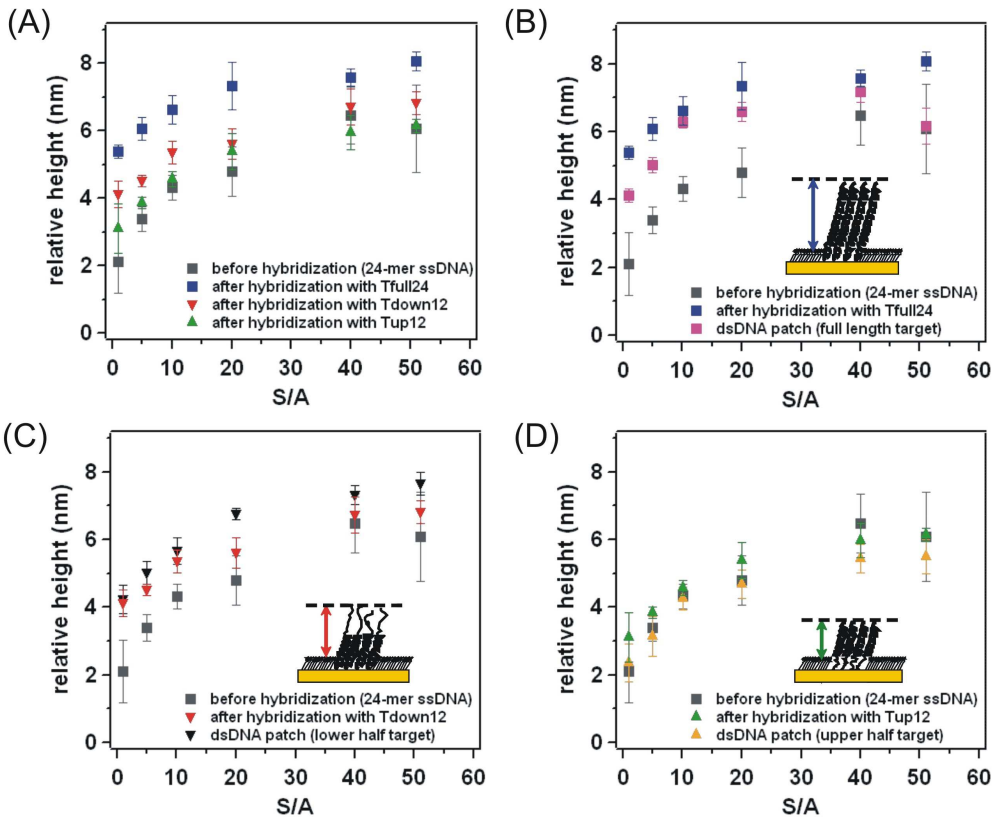

Figure 8: (A) Relative heights of DNA nano-patches within TOEG3 SAMs as a function of S/A. The relative heights are shown for ssDNA nano-patches, before (grey squares) and after hybridization with Tfull24 (blue squares), Tdown12 (red down triangles) and Tup12 (green up triangles). Comparison between hybridized ssDNA nano-patches and grafted dsDNA nano-patches is shown for; (B) Tfull24 (blue vs. purple squares), (C) Tdown12 (red vs. black down triangles) and (D) Tup12 (green vs. orange triangles). Error bars reflect the averaged over the heights of three nano-patches and are related to the variations, expected from sample to sample and AFM tips used in each experiment.

The height vs. applied load responses were measured for ssDNA, fully hybridized and partly hybridized nano-patches (for the Tup12 and Tdown12 targets) and compared for S/A = 5 (fig 9A) and S/A = 40 (fig. 9C). All the results for the three different target strands can be explained keeping in mind that dsDNA is much more rigid than ssDNA due to persistence length which is 50 times larger [33, 34].

In the low density regime, or S/A = 5 (fig. 9A), there is a slight difference in the compression of ssDNA before (grey squares, fig 9A) and after hybridization with full length target (Tfull24, blue squares, fig. 9A), which can be explained by the large

DNA-DNA distance between molecules at this density (see a scheme in fig. 9B). Presumably, at low densities, ssDNA is in a “mushroom-like” configuration, resulting in a low initial height. This height changes a little upon increased load, since the “mushroom” configuration is covering the bottom of the patch uniformly. When hybridizes with full length targets, the ssDNA molecules become more rigid and stand-up (initial height increases from 4 to 7 nm), but their relatively large lateral distance makes the AFM tip easily penetrating the nano-structures: compressibility data show therefore, higher slope for dsDNA than for ssDNA. Interestingly, the compressibility curves of Tdown12 (red down triangles, fig. 9A) and Tfull24 (blue squares, fig. 9A) - hybridized strands are similar. The two curves, although starting from different initial heights, have the same slope. On the other hand, upper half target (Tup12, green up triangles, fig. 9A) hybridized strands and ssDNA show the same compressibility behavior, which reflects a reduced resistance to the AFM tip due to the lower rigidity of the system.

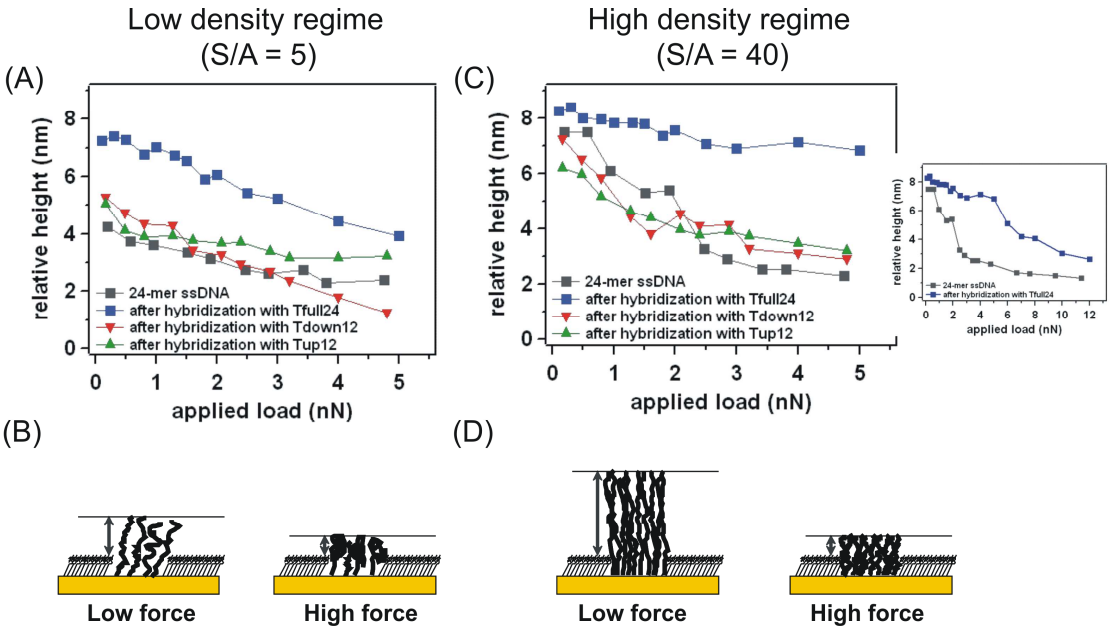

Figure 9: Comparison of low and high S/A regime: relative heights as a function of applied load are shown for ssDNA nano-patches of 24-mer before (grey squares) and after hybridization with Tfull24 (blue squares), Tdown12 (red down triangles) and Tup12 (green up triangles) in (A) low density regime, S/A = 5 with a scheme (B) to depict low density DNA patches and (C) high density regime, S/A = 40 with a scheme (D) to depict high density DNA patches. The increase in relative height of DNA

patches by increasing values of S/A is due to increase of density, and vertical orientation toward the surface normal, of DNA molecules (see previous section).

When the S/A value is increased to 40, or in high density regime, the results are significantly different. Clearly, the decreased compressibility of fully hybridized ssDNA (Tfull24, blue squares, fig 9C) reflects the increased stiffness of this system, in agreement with previous data (see fig. 4A in the previous section). Here, we need to specify that the data reported in fig. 9 were taken with a cantilever which was 20 times less stiff of the one used to collect the data showed in the previous paragraph in order to be more sensitive to the initial region of compressibility (fig. 4A). Therefore, the plots shown in fig. 9B are not directly comparable with the ones in fig. 4A, since the applied load values reported in the x-axis are not in the same scale. As a calibration point, we will take the force load at which the high density dsDNA patch undergoes the non-reversible transition, in correspondence of which the tip starts removing the molecules and liberating the Au surface underneath. Such transition occurs at 15 nN for the hard cantilever (spring constant = 0.63 Nm^{-1}), and at 5 nN for the soft one (spring constant = 0.03 Nm^{-1}). With such rescaling in mind, we can see that the compressibility of ssDNA showed in fig. 4A is equivalent to the one shown in fig. 9B (See inset in fig. 9B).

In the case of half-target hybridizations, we cannot discriminate between upper and lower hybridization, and barely even between half-hybridized and not hybridized targets (i.e. probe strands). Since we proved in the previous section, that hybridization efficiency is still high (>50%) in highly dense DNA nano-structures, it is reasonable to assume that also half-hybridization should occur in a similar structures. It is possible therefore, that in the case of lower-half hybridization a large incubation time is required in order to let the half-target strands diffusing through the non-matching upper part of the probe strands. We can clearly distinguish, however, between fully and partially hybridized patches. More measurements and a careful comparison with theoretical studies are needed to investigate the distinctive behavior of half length targets from low to high density regimes.

In summary, we have investigated the selective response of ssDNA nano-structures on hybridization with three different target strands for a wide range of probe densities. We have demonstrated that by changing the value of density parameter (S/A), we can control the density of DNA inside the nano-structures. From

our compressibility measurements, even at very high probe density, we are able to distinguish between various hybridization reactions that mostly take place with the same immobilized DNA on the surface. In particular, we have studied half matching target strands (12-mer), which are complementary to the lower and upper part of ssDNA and the results have been compared with full length target (24-mer). Since our approach is sensitive enough to detect un-labeled hybridization reactions at the nano-scale, it can be applied to wide range of applications in genomics. In particular, due to reduced dimensions of the spotted areas, our DNA nano-arrays are expected to work with very small quantities of generic material. However, in order to use these devices in a more quantitative manners, it is imperative to measure the surface coverage (or packing densities) of DNA nano-structures (NAMs) in the absolute terms.

Materials and Methods

Sample preparation: Ultra flat gold films were prepared as described in the part A. In the present work, Epoxy SU-8 100 (MicroChem) was used as a glue as well as a solid support in order to produce ultra flat gold films. The approach involved the following steps. 1) SU-8 100 was first placed on gold surfaces in the form of tiny drops and cured at 95° C for at least 5 hours. 2) SU-8 100/gold/mica sandwiches were exposed to UV light (at the power ~70 $\mu W/cm^2$) for 15 minutes. 3) The samples were cured again at 95°C for another 2 hours. The buried gold-mica interface was disclosed with a pair of tweezers and immediately soaked into freshly prepared 100µM solution of top oligo-ethylene-glycol (in short TOEG3) terminated alkythiols ($OH\text{-}(OEG)_3\text{-}(CH_2)_{11}\text{-}SH$, (Prochimia)) in absolute ethanol (Fluka, purity ≥ 99.8 %) at room temperature for at least 24 hours. The resulting ultra flat surface assembled with TOEG3 terminated alkythiols was then rinsed with ethanol and dried with soft spurt of nitrogen.

Reagents: The modified 5'-thiol DNA (24-mer) oligomers and all the non-thiolated complementary strands (see table 1) were purchased from Sigma-genosys Ltd and used without further purification. All the oligomers solutions (final concentration ~100µM) and TE buffer were made in MilliQ water (resistance > 18 MΩ cm). The composition of TE buffer was 1M NaCl, 10mM Tris, 1mM EDTA with pH 6.9 and

filtered through a Millipore filter (GP Express PLUS Membrane, 0.22 µm pore size) before use.

Table 1: Oligomer sequences and their nomenclatures.

Name	**Sequence**
24-mer (probe)	SH-(CH_2)6-5'- TAATCGGCTCATACTCTGACTGTA
Tfull24 (target)	5'- TACAGTCAGAGTATGAGCCGATTA
Tdown12 (target)	5'- ATGAGCCGATTA
Tup12 (target)	5'- TACAGTCAGAGT

Immobilization and Hybridization Conditions: All the AFM experiments were accomplished using a XE-100 microscope (Park Scientific Instruments Advanced Corp. – PSIA) with a custom liquid cell with a capacity of 350µL at room temperature. Standard silicon rectangular cantilevers, (NSC19, MikroMasch, 0.63 Nm^{-1}) and (CSC38/B, MikroMash, 0.03 Nm^{-1}) were utilized for nanografting and imaging, respectively. In all the experiments, the images were taken in contact mode and in liquid medium with scan speed of 2Hz. The protocol of nanografting has been reported earlier. Briefly, AFM tip scanned the selected area at relatively large forces (usually in the range of 90-200 nN at 2Hz) in the presence of thiolated ssDNA dissolved in TE buffer/ethanol 1:1 solution with the final concentration of 10µM. This caused TOEG3 molecules from the surface to be replaced locally with thiolated ssDNA molecules present in the solution. The forces for nanografting varied from sample to sample and are also influenced by the tip's sharpness and cantilever's spring constant. The resulted ssDNA patterns were then imaged at minimum force (typically in the range of 0.5 nN -1nN).

All the hybridization reactions were carried out immediately after patterning the ssDNA nano-patches within an AFM liquid cell by following a substantial step of washing with TE buffer in order to expunge loosely bound ssDNA probe molecules. The concentration of each complementary strand was 4µM in TE buffer and the incubation time for all the hybridization reactions was 1 hour at room temperature in each experiment. The relative heights of ssDNA nano-patches were accumulated after the completion of hybridization reactions with an AFM imaging at low imaging force

(below 1nN). Afterwards, compressibility measurements were performed on the same DNA nano-patches. In this case, the relative heights as a function of the applied load were collected by increasing the imaging forces from pull-off force (~ 0nN) to 5nN.

Preparation of dsDNA: To prepare the double-stranded DNA (dsDNA) probes through the hybridization, the ssDNA probes were incubated for 10 minutes in a complementary strands solution (1:3/2 of probe and each target in TE buffer). Incubation temperature was different for each sequence (65° for Tfull24 and 37° for Tdown12 and Tup12). After the incubation the temperature was allowed to cool down to room temperature. The final concentration of each dsDNA was 10µM.

References

1. Todd, R. & Margolin, D.H. Challenges of single-cell diagnostics: analysis of gene expression. *Trends in Molecular Medicine* **8**, 254-257 (2002).
2. Nygaard, V. & Hovig, E. Options available for profiling small samples: a review of sample amplification technology when combined with microarray profiling. *Nucl. Acids Res.* **34**, 996-1014 (2006).
3. Mischel, P.S., Cloughesy, T.F. & Nelson, S.F. DNA-microarray analysis of brain cancer: molecular classification for therapy. *Nat Rev Neurosci* **5**, 782-792 (2004).
4. Hesse, J. et al. RNA expression profiling at the single molecule level. *Genome Res.* **16**, 1041-1045 (2006).
5. Galvin, J.E. & Ginsberg, S.D. Expression profiling in the aging brain: A perspective. *Ageing Research Reviews* **4**, 529-547 (2005).
6. Evans, S.J., Watson, S.J. & Akil, H. Evaluation of Sensitivity, Performance and Reproducibility of Microarray Technology in Neuronal Tissue. *Integr. Comp. Biol.* **43**, 780-785 (2003).
7. Draghici, S., Khatri, P., Eklund, A.C. & Szallasi, Z. Reliability and reproducibility issues in DNA microarray measurements. *Trends in Genetics* **22**, 101-109 (2006).

8. Jason Reed, B.M. & Gimzewski, J.K. Single molecule transcription profiling with AFM. *Nanotechnology* **18**, 044032 (044015pp)-044032 (044015pp) (2007).
9. Drummond, T.G., Hill, M.G. & Barton, J.K. Electrochemical DNA sensors. *Nat Biotech* **21**, 1192-1199 (2003).
10. Wang, J. & Bard, A.J. Monitoring DNA Immobilization and Hybridization on Surfaces by Atomic Force Microscopy Force Measurements. *Anal. Chem.* **73**, 2207-2212 (2001).
11. Fang, S., Lee, H.J., Wark, A.W. & Corn, R.M. Attomole Microarray Detection of MicroRNAs by Nanoparticle-Amplified SPR Imaging Measurements of Surface Polyadenylation Reactions. *Journal of the American Chemical Society* **128**, 14044-14046 (2006).
12. Marta Bally, M.H. Optical microarray biosensing technique. *SURFACE AND INTERFACE ANALYSIS* **38**, 1442-1458 (2006).
13. Wang, J. From DNA biosensors to gene chips. *Nucl. Acids Res.* **28**, 3011-3016 (2000).
14. Ambros, V. The functions of animal microRNAs. *Nature* **431**, 350-355 (2004).
15. Barad, O. et al. MicroRNA expression detected by oligonucleotide microarrays: System establishment and expression profiling in human tissues. *Genome Res.* **14**, 2486-2494 (2004).
16. Herne, T.M. & Tarlov, M.J. Characterization of DNA Probes Immobilized on Gold Surfaces. *J. Am. Chem. Soc.* **119**, 8916-8920 (1997).
17. Peterlinz, K.A., Georgiadis, R.M., Herne, T.M. & Tarlov, M.J. Observation of Hybridization and Dehybridization of Thiol-Tethered DNA Using Two-Color Surface Plasmon Resonance Spectroscopy. *J. Am. Chem. Soc.* **119**, 3401-3402 (1997).
18. Peterson, A.W., Heaton, R.J. & Georgiadis, R.M. The effect of surface probe density on DNA hybridization. *Nucl. Acids Res.* **29**, 5163-5168 (2001).
19. Petrovykh, D.Y., Kimura-Suda, H., Whitman, L.J. & Tarlov, M.J. Quantitative Analysis and Characterization of DNA Immobilized on Gold. *J. Am. Chem. Soc.* **125**, 5219-5226 (2003).
20. Steel, A.B., Levicky, R.L., Herne, T.M. & Tarlov, M.J. Immobilization of Nucleic Acids at Solid Surfaces: Effect of Oligonucleotide Length on Layer Assembly. *Biophys. J.* **79**, 975-981 (2000).

21. Liu, M., Amro, N.A., Chow, C.S. & Liu, G.y. Production of Nanostructures of DNA on Surfaces. *Nano Letters* **2**, 863-867 (2002).
22. Liu, M. & Liu, G.Y. Hybridization with Nanostructures of Single-Stranded DNA. *Langmuir* **21**, 1972-1978 (2005).
23. Xu, S. & Liu, G.y. Nanometer-Scale Fabrication by Simultaneous Nanoshaving and Molecular Self-Assembly. *Langmuir* **13**, 127-129 (1997).
24. Liu, G.Y., Xu, S. & Qian, Y. Nanofabrication of Self-Assembled Monolayers Using Scanning Probe Lithography. *Acc. Chem. Res.* **33**, 457-466 (2000).
25. Kramer, S., Fuierer, R.R. & Gorman, C.B. Scanning Probe Lithography Using Self-Assembled Monolayers. *Chem. Rev.* **103**, 4367-4418 (2003).
26. Ryu, S. & Schatz, G.C. Nanografting: Modeling and Simulation. *J. Am. Chem. Soc.* **128**, 11563-11573 (2006).
27. Hu, Y. Towards Nanobiosensors: Positioning of De novo Proteins on Gold with a Predictable Orientation and the Study of Protein Resistant Layers. *PhD thesis, Princeton University* (2005).
28. Grunwald, C.*et al*., *in preparation* (2008).
29. Sinensky, A.K. & Belcher, A.M. Label-free and high-resolution protein//DNA nanoarray analysis using Kelvin probe force microscopy. *Nat Nano* **2**, 653-659 (2007).
30. Pooja Gupta, K.L. Facile Route to Ultraflat SAM-Protected Gold Surfaces by ldquoAmphiphile Splittingrdquo13. *Angewandte Chemie International Edition* **43**, 520-523 (2004).
31. Thoeni, S., Kressierer, C.J. & Giese, B. Site-specific DNA cleavage on a solid support: a method for mismatch detection. *Angew Chem Int Ed Engl* **46**, 2112-4 (2007).
32. Kelley, S.O., Boon, E.M., Barton, J.K., Jackson, N.M. & Hill, M.G. Single-base mismatch detection based on charge transduction through DNA. *Nucleic Acids Res* **27**, 4830-7 (1999).
33. Mearns, Freya J., Wong, Elicia L.S., Short, K., Hibbert, D.B. & Gooding, J.J. DNA Biosensor Concepts Based on a Change in the DNA Persistence Length upon Hybridization. *Electroanalysis* **18**, 1971-1981 (2006).
34. Bustamante, C., Smith, S.B., Liphardt, J. & Smith, D. Single-molecule studies of DNA mechanics. *Curr Opin Struct Biol* **10**, 279-85 (2000).

Chapter 3

Towards Multiprotein Nanoarrays Using Nanografting and DNA Directed Immobilization of Proteins*

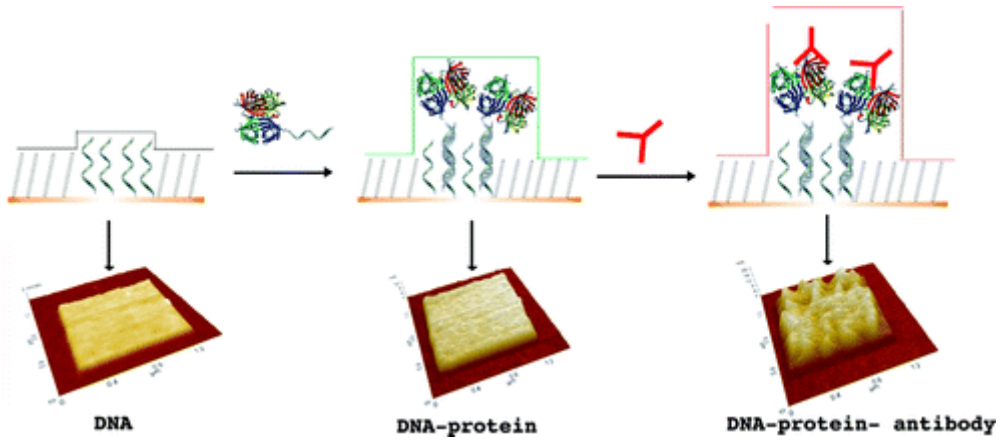

* This chapter has been published in: Bano, F., Fruk, L., Sanavio, B., Glettenberg, M., Casalis, L., Niemeyer, C. M., Scoles, G. *Nano Lett.***2009**, *9*, 2614. This work has been done in collaboration with Prof. Ch. Niemeyer (University of Dortmund) and Dr. Ljiljana Fruk (University of Karlsruhe)

Abstract

AFM nanografting was utilized to prepare DNA nanopatches of different size (200x200 to 1000x1000 nm^2) onto which DNA-protein conjugates can be anchored through DNA-directed immobilization. Height measurements were used to assess the binding of the proteins as well as their subsequent interaction with other components, such as antibodies. The results indicate that nanografted patch arrays are well suited for application in biosensing and could enable the fabrication of multi feature protein nanoarrays.

The development of protein arrays with feature sizes at the micrometer length scale is currently of great interest for biomedical diagnostics and life sciences because these devices promise to evolve into a powerful technological platform for high-throughput analysis of biomolecular interactions with low requirements on the sample amount and hands-on processing time.[1,2,3,4]. An important area in the developments of protein and small molecule arrays concerns their further miniaturization to the nanometer regime. Although various methods have been developed based on e.g., dip-pen nanolithography,[5-7] SNOM lithography,[8] or micro contact printing,[9] it is currently still very difficult to fabricate nanoarrays containing multiple features, such as a range of different proteins or small-molecule ligands. We here report a novel approach for the fabrication of protein nanoarrays, which takes advantage of Atomic Force Microscopy (AFM)-based nanografting, previously developed and applied for hybridization studies of DNA and other nucleic acids,[10-14] and DNA-directed immobilization (DDI) of semisynthetic protein-DNA conjugates. The latter method, which takes advantage of the specific Watson-Crick hybridization of oligonucleotide-modified proteins to surface-bound complementary oligomers, has previously been developed[15] and largely applied for the generation of self-assembled protein arrays at the micrometer length scale.[16] Although both AFM-based nanografting[17] and DDI[18] are by now considered established methods, it has not yet been shown that these two methods can indeed be combined and used to synergistically enable fabrication of protein nanoarrays with high control over lateral dimensions as well as options for reliable read-out, based on topographic AFM measurements. As depicted in Figure 1, DDI is used here to decorate nanometer-sized patches of single-stranded DNA

(ssDNA), previously prepared by AFM-based nanografting of alkylthiol-modified gold surfaces,[14] with complementary DNA-protein conjugates. The integrity and biochemical functionality of the resulting protein arrays are demonstrated by AFM topography measurements and immunological assays, respectively.

To demonstrate the feasibility of our fabrication method (Fig. 1), we initially generated nanografted patches of ssDNA within a monolayer of protein-repellent ethylene-glycol-terminated alkylthiols (HS-$(CH_2)_{11}$-$(OCH_2CH_2)_3$-OH) on a flat (111) gold substrate, using the previously published method.[10,13,14] Subsequently, proteins covalently modified with complementary DNA sequences were immobilized onto the nanopatch by means of DDI, thus producing a ready-to-use detector for protein interaction studies.

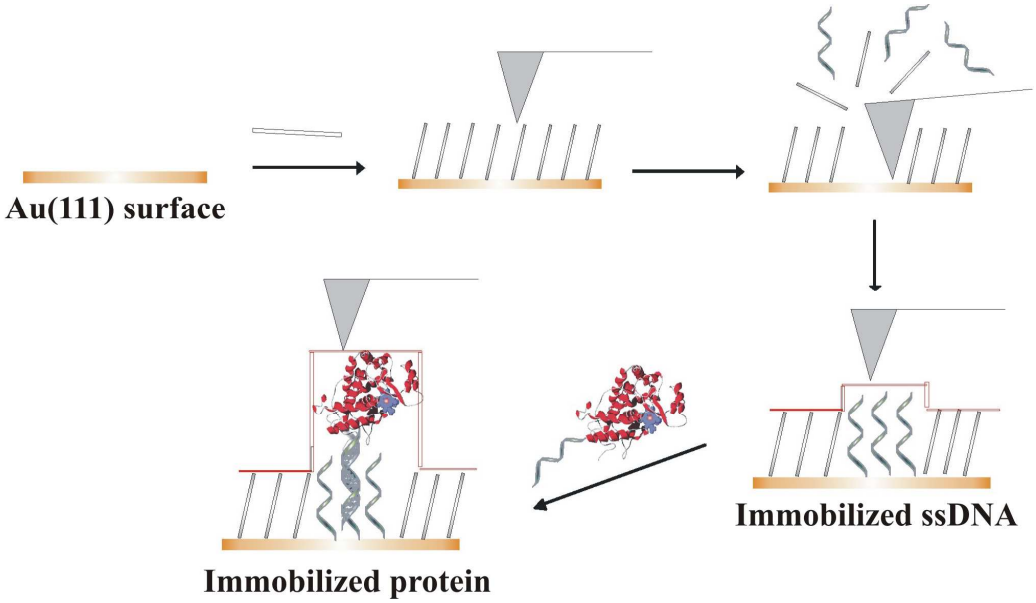

Figure 1: Schematic representation of the nanografting of ssDNA patches into a monolayer of ethylenglycol-modified thiols (top) and their subsequent functionalization with DNA-protein conjugates (bottom).

As shown in Figure 2, the substrate flatness allowed us to monitor both nanografting and subsequent protein decoration steps by means of AFM topographic height measurements. In particular, a 1μm x 1μm patch of alkylthiol-modified ssDNA **cD1** (for oligonucleotide sequences, see Supporting Information) was grafted within the monolayer of ethylene glycol alkylthiols. Subsequently, a covalent conjugate of streptavidin tethered with oligomer **D1** (**D1-STV**) was allowed to bind to the patch by sequence-specific DNA hybridization. The gold surface was carefully washed with phosphate buffer (PBS, phosphate buffered saline) to remove any physically adsorbed

molecules and imaged by AFM; all experiments were performed at least in triplicates and the given values and errors correspond to the mean values and standard deviation of height obtained from at least three independent patches. The resulting height profile of the initial ssDNA patch (average height ≈ 6.5 ± 0.5 nm) and the STV-modified patch (≈10.5 ± 0.5 nm) indicated an increase in height of 4 ± 0.5 nm, which is in good agreement with the size of native streptavidin (approximately 4.2 x 4.2 x 5.6 nm^3), as determined by X-ray crystallography.[19] To independently identify STV and to demonstrate that the protein patches are suitable for protein-protein interaction studies, an anti-STV immunoglobulin G (**anti-STV IgG**) was allowed to bind to the surface. As shown in Fig. 2a, the successful binding of IgG was clearly indicated by an increase in height from about 10.8 nm (STV patch histogram) to about 14.9 nm of the IgG-containing patch. It is known that IgG molecules have typical dimensions of 14.5 x 8.5 x 4.0 nm^3,[20] and thus, the increase of about 4 nm suggested that either incomplete coverage of the patch occurred or that IgG molecules are immobilized to the patch in a horizontally oriented layer.

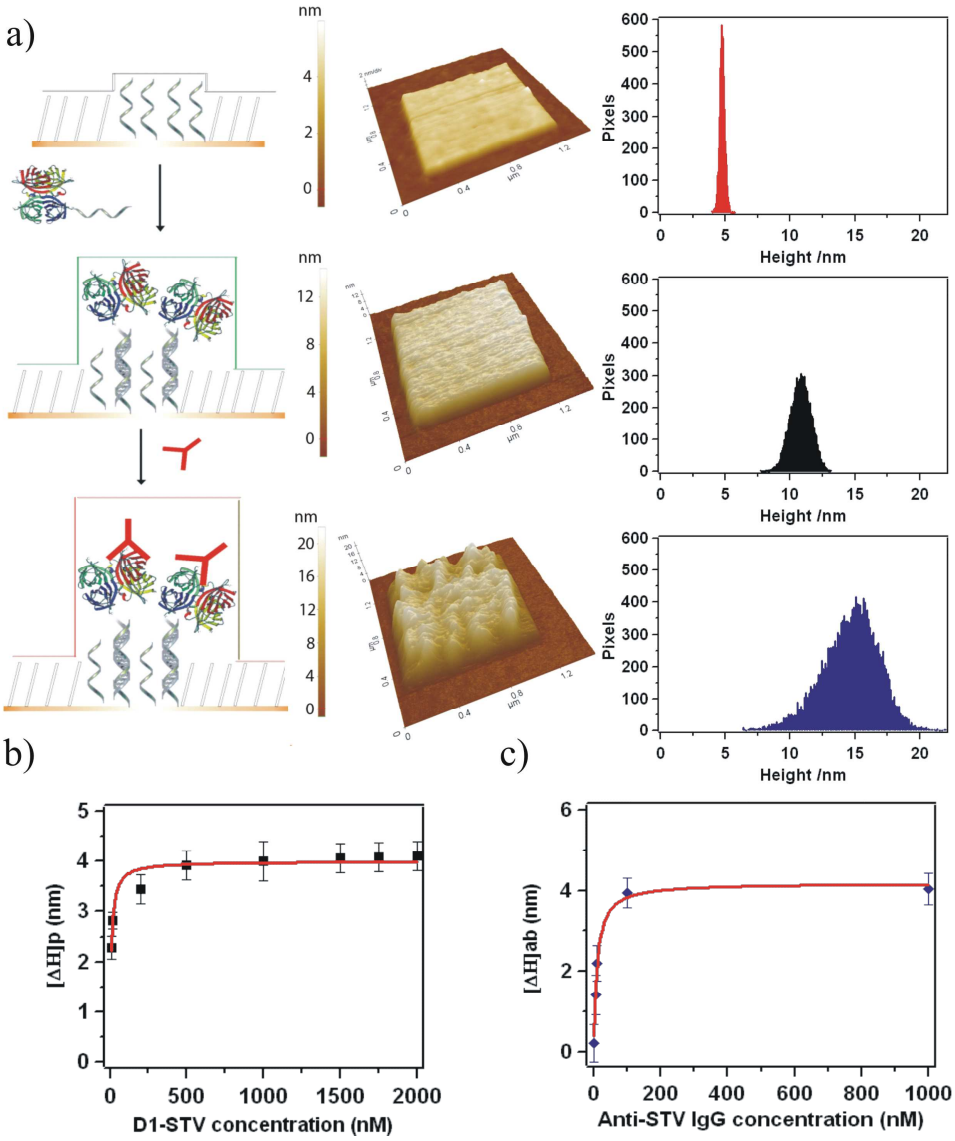

Figure 2: Nanografting-based preparation of protein arrays; a) schematic representation and resulting height histograms obtained for a single-patch DNA-directed sensor, generated from a covalent DNA-streptavidin conjugate (**D1-STV**), which was then used for the binding of the corresponding **anti-STV IgG** antibody. The curves in b) and c) show the changes in height as a consequence of variable protein concentrations. Note that the concentration of **D1-STV** used in all the experiments of antibody (**anti-STV IgG**) immobilization on STV modified patches was 1µM.

To further investigate the molecular interactions occurring on the nanografted DNA patch and to demonstrate that our method is well suited to the design of devices useful for biosensing , we determined quantitative affinity constants by using the differential

height values, that is the height difference between the relevant and a reference patch (for definition see Fig. S1 in SI). To this end, differential height values were plotted as a function of the target molecule concentration and data were fitted to the Langmuir equation with h and K_D as free parameters (for details, see SI) to yield the respective dissociation constants K_D. The resulting plots and K_D values, obtained for both the binding of the ssDNA-STV conjugate (**D1-STV**) and the **anti-STV IgG** are shown in Fig. 2b, c and Table 1, respectively. The K_D value obtained for the hybridization of the ssDNA-STV conjugate (8.1 ± 1.3 nM) is in good agreement with data obtained from BIAcore studies of similar DNA-STV conjugates (approximately 11 - 35 nM, depending on the oligonucleotide sequence).[21] Moreover, the K_D value obtained for the binding of **anti-STV IgG** (9.5 ± 1.1 nM) is consistent with data reported in the literature for this interaction.[22]

Table 1. Summary of binding parameters obtained from the increase of the height observed on AFM nanografted patches upon hybridisation of DNA-STV conjugate and subsequent binding of anti-STV IgG to this patch.

	K_D (nM)	h (nm)
D1-STV	8.1 ± 1.3	4.0 ± 0.1
anti-STV IgG	9.5 ± 1.1	4.2 ± 0.1

To further prove intactness and functionality of patch-immobilized STV molecules, we also investigated whether the STV can still bind biotinylated molecules. As shown in Fig. S2 (SI), the patches decorated with **D1-STV** specifically bound biotinylated goat anti-mouse IgG, thus leading to an increase in patch height of 4.8±0.5 nm. This result therefore not only demonstrates preserved functionality of patch-immobilized STV but, being in full agreement with height values mentioned previously for binding of the antibody directed against STV, it also validates both our result and the method of detection used here, i.e. relative height measurements on a very flat surface.

To verify scalability to the nanometer regime of the combined nanografting/DDI approach, we also carried out a set of experiments, in which the size of the ssDNA patch was varied from 200 x 200 nm^2 to 1000 x 1000 nm^2 (SI, Figure S3). We

observed a consistent increase in patch height of about 4 ± 0.5nm upon hybridization of the ssDNA patches with the **D1-STV** conjugate, regardless of patch dimensions. In contrast, control experiments with STV lacking the covalently tethered oligomer revealed no increase in patch heights.

To further illustrate the applicability of our method to fabricate multiple-feature protein nanoarrays, a three patch device was generated (Fig. 3), using three different DNA oligonucleotides (**cD0**, **cD1** and **cD2**, sequences are listed in the Supporting Information). Oligomers **cD1** and **cD2** are complementary to conjugate **D1-STV** and a covalent DNA conjugate of horseradish peroxidase (**D2-HRP**), respectively, while **cD0** is a non-complementary control sequence. After the grafting of ssDNA patches A, B and C (Fig. 3a) and wash with PBS buffer to remove physically adsorbed molecules, the gold substrate was immersed in a solution of **D1-STV** conjugate (1000nM, PBS, pH 7.3). As shown in Fig. 3b, AFM measurements revealed an increase in height (4.5 ± 0.5 nm) only at patch B, which bears the complementary capture oligonucleotide. The same sample was then immersed in a solution containing the **D2-HRP** conjugate (500nM, PBS, pH 7.3). Again, AFM imaging revealed an increase in height of 3.8 ± 0.5nm (Fig. 3c) only for patch C, thereby clearly indicating specific surface immobilization of the **D2-HRP** conjugate. The dimension of HRP molecules are known from X-ray crystallography (4.0 x 6.7 x 11.7 nm^3)[23] and the observed increase in height of patch C is in good agreement with previous studies on HRP immobilization.[24]

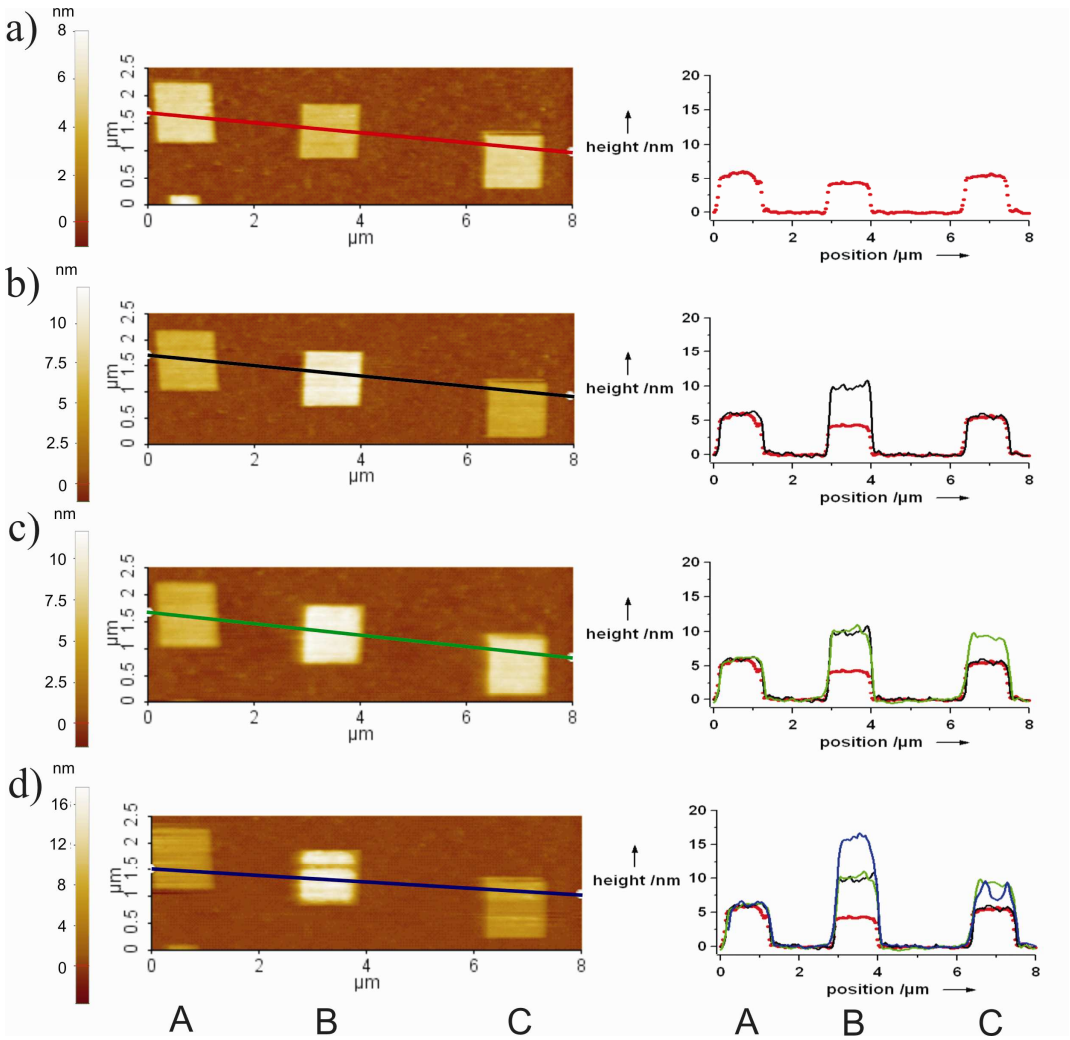

Figure 3: AFM topographic images (8 x 2.5 µm^2) and corresponding height profiles of a three-patch device, fabricated from DNA oligonucleotides **cD0** (patch A, left), **cD1** (patch B, middle), and **cD2** (patch C, right); a) pattern after nanografting of ssDNA (red line), b) pattern after hybridization of **D1-STV** conjugate (black line), c) pattern obtained after further hybridization of **D2-HRP** conjugate (green line) and d) pattern obtained after further binding of **anti-STV IgG** (blue line in height profile).

The patch array was then probed with a solution of **anti-STV IgG** (1000nM, PBS, pH 7.3). As expected, only the height of patch B, which contained **D1-STV** conjugate was increased (Fig. 3d). In contrast, no significant changes were observed for patches A and C, and also, the background heights remained entirely unchanged in the course of this multi-step experiment (Fig. 3).

Similar results were obtained in a set of experiments concerning the simultaneous DNA-directed immobilization of DNA-HRP and DNA-GOx (GOx = glucose oxidase) conjugates on nanografted patches and the subsequent probing with an HRP specific

antibody (Fig. S4). A patch array was prepared by nanografting patches (1 x 1 μm^2) of **cD0** (control patch A), **cD2** (patch B) and **cD1** (patch C). After grafting, solutions containing **D2-HRP** or **D1-GOx** were allowed to bind to the patch array by means of DDI. From the increase in height it was clearly evident that the immobilization occurred in a sequence specific manner and no cross reactivity was apparent. Subsequent antibody binding experiments showed the presence of HRP on patch B (cD2), while the control patch showed no increase in height both after the hybridization of protein conjugates and antibody binding. This result clearly indicated specificity of DNA directed immobilization of HRP conjugate as well as the anti-HRP antibody-antigen interaction.

Given the successful demonstration of multiplex immunoassays on the nanografted patches, we then challenged our system with the biomedically relevant matrix of human serum. In particular, we investigated whether the nanografting/topography platform is suitable to detect a target protein in the complex matrix of standardized human serum (BISEKO). To this end, a patch array was grafted, containing **cD0** (control patch A), **cD2** (patch B) and **cD1** (patch C), and **D2-STV** and **D1-GOx** were allowed to bind to this array (Fig. 4). Following, two specific antibodies, **anti-STV IgG** and **anti-GOx IgG** dissolved in BISEKO matrix, were allowed to bind to this array, and each binding was monitored sequentially by topography measurements. It is clear from the results shown in Fig. 4c and 4d, respectively that both antibodies could be detected and no indication of non-specific binding of either matrix components or target proteins disturbed these analyses. The high specificity of both DDI and IgG binding was also confirmed for our samples by standard microarray analyses (Fig. S5), which also clearly indicated the absence of any non-specific binding and cross-reactivity.

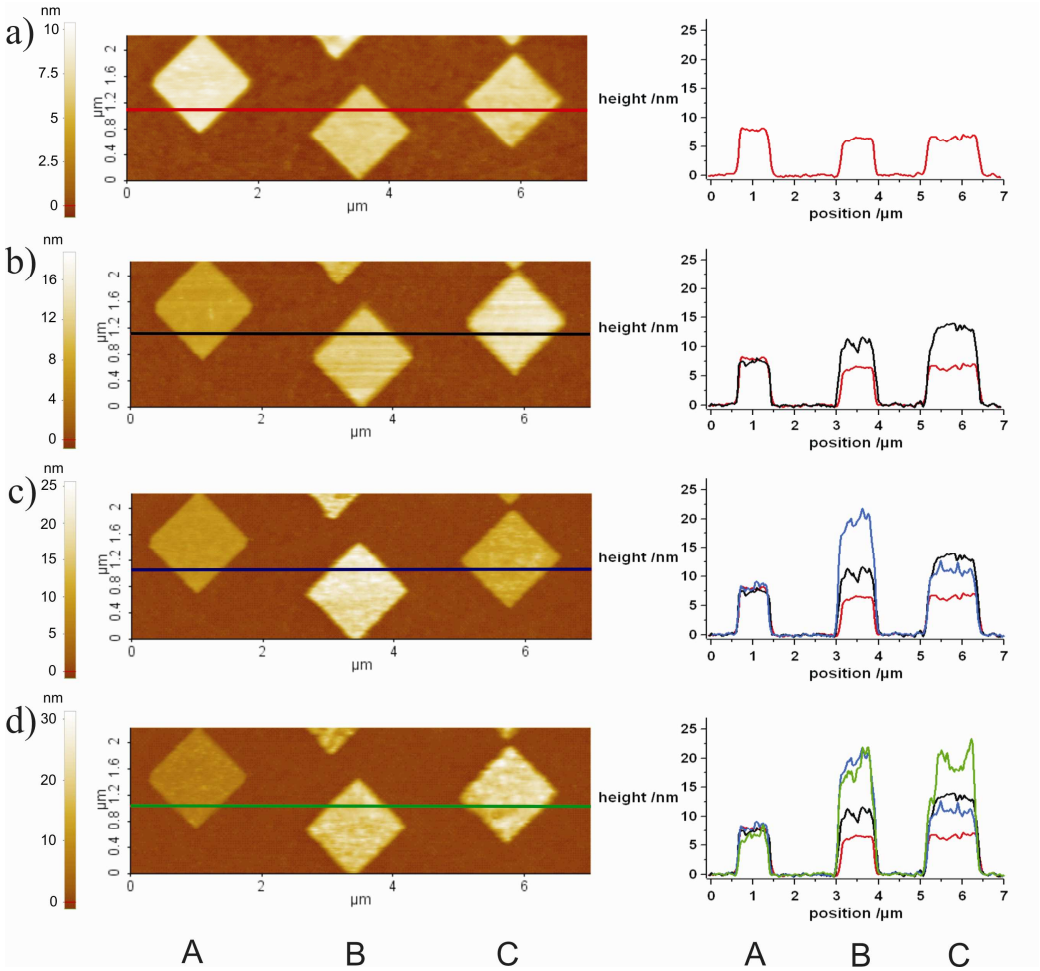

Figure 4: AFM topographic images (7 × 2.2 µm^2) and corresponding height profiles of antibody interaction with immobilized proteins. a) fabrication of ssDNA nanopatches, **cD0** (control patch A), **cD2** (patch B) and **cD1** (patch C), red line profile; b) patches after incubation with a solution containing **D2-STV** and **D1-GOx**. Note that the increase in height indicates successful immobilization of both conjugates, **D2-STV** (B) and **D1-GOx** (C), black line profile; c) patches after incubation with **anti-STV IgG** , dissolved in standardized human serum (BISEKO), blue line profile, and d) patches after incubation with the **anti-GOx IgG** in BISEKO, green line profile.

In conclusion, we reported here on the use of nanografted oligonucleotide patches for specific immobilization of proteins and on their subsequent use for label-free detection of protein binding interactions. In particular, the observed specificity of biomolecular recognition and the lack of non-specific binding, clearly illustrate that nanografted patch arrays are well suited for applications in biosensing. Since this

platform can be conveniently scaled down to the nanometer regime, it should prove useful for the fabrication of multi-feature protein nanoarrays, useful for multiplexed analysis of biomolecular recognition events and other applications in nanobiotechnology, such as single-cell proteomics.

Acknowledgment. This work was supported in part by the Zentrum für Angewandte Chemische Genomik (ZACG), a joint research initiative founded by the European Union and the Ministry of Innovation and Research of the state Northrhine Westfalia. CMN thanks Max-Planck Society for financial support of a Max-Planck Fellow research group at the Max Planck Institute of Molecular Physiology, Dortmund. LF was supported by Marie Curie International Incoming Fellowship (project 514582). The nanografting work was carried out in the SISSA-IIT/Elettra Laboratory at Synchrotron in Trieste, Italy (Elettra) and supported by Ministro della Ricerca PRIN 2006020543. GS would like to acknowledge partial financial support by CBM and useful discussion with colleagues in this medicinal oriented institution. The highly interdisciplinary environment of CBM was essential to the shaping of several of the ideas contained in this paper.

Supporting information available: Experimental procedures, the details on the nanopatch stability and specific, on patches, STV-biotinylated antibody binding are available.

References

(1) Phizicky, E.; Bastiaens, P. I.; Zhu, H.; Snyder, M.; Fields, S. *Nature* **2003**, *422*, 208-215.

(2) Tomizaki, K. Y.; Usui, K.; Mihara, H. *ChemBioChem* **2005**, *6*, 782-799.

(3) Sobek, J.; Bartscherer, K.; Jacob, A.; Hoheisel, J. D.; Angenendt, P. *Comb Chem High Throughput Screen* **2006**, *9*, 365-380.

(4) Jonkheijm, P.; Weinrich, D.; Schroeder, H.; Niemeyer, C. M.; Waldmann, H. *Angew. Chem. Int. Ed.* **2008**, *47*, 9618-9647.

(5) Demers, L. M.; Ginger, D. S.; Park, S. J.; Li, Z.; Chung, S. W.; Mirkin, C. A. *Science* **2002**, *296*, 1836-1838.

(6) Lim, J. H.; Ginger, D. S.; Lee, K. B.; Heo, J.; Nam, J. M.; Mirkin, C. A. *Angew Chem Int Ed Engl* **2003**, *42*, 2309-2312.

(7) Salaita, K.; Wang, Y.; Mirkin, C. A. *Nat. Nanotechnol.* **2007**, *2*, 145-155.

(8) Leggett, G. J. *Analyst* **2005**, *130*, 259-264.

(9) Coyer, S. R.; Garcia, A. J.; Delamarche, E. *Angew Chem Int Ed Engl* **2007**, *46*, 6837-6840.

(10) Xu, S.; Miller, S.; Laibinis, P. E.; Liu, G.-Y. *Langmuir* **1999**, *15*, 7244–7251.

(11) Liu, M. X.; Amro, N. A.; Chow, C. S.; Liu, G. Y. *Nano. Lett.* **2002**, *2*, 863-867.

(12) Liu, M.; Liu, G. Y. *Langmuir* **2005**, *21*, 1972-1978.

(13) Castronovo, M.; Radovic, S.; Grunwald, C.; Casalis, L.; Morgante, M.; Scoles, G. *Nano Lett* **2008**.

(14) Mirmomtaz, E.; Castronovo, M.; Grunwald, C.; Bano, F.; Scaini, D.; Ensafi, A. A.; Scoles, G.; Casalis, L. *Nano Lett* **2008**.

(15) Niemeyer, C. M.; Sano, T.; Smith, C. L.; Cantor, C. R. *Nucl. Acids Res.* **1994**, *22*, 5530-5539.

(16) For examples, see: (a) Wacker, R.; Niemeyer, C. M. *ChemBioChem* **2004**, *5*, 453–459; (b) Wacker, R.; Schroeder, H.; Niemeyer, C. M. *Anal. Biochem.* **2004**, *330*, 281–287; (c) Becker, C. F. W.; Wacker,R.; Bouschen, W.; Seidel, R.; Kolaric, B.; Lang, P.; Schroeder, H.;Müller, O.; Niemeyer, C. M.; Spengler, B.; Goody, R. S.; Engelhard, M. *Angew. Chem. Int. Ed.* **2005**, *44*, 7635–7639; *Angew. Chem.* **2005**, *117*, 7808–7812; (d) Schroeder, H.; Ellinger, B.; Becker, C. F. W.; Waldmann, H.; Niemeyer, C. M. *Angew. Chem. Int. Ed.* **2007**, *46*, 4180–4183; *Angew. Chem.* **2007**, *119*, 4258–4261; (e) Fruk, L.; Müller, J.; Weber, G.; Narváez, A.; Domínguez, E.; Niemeyer, C. M. *Chem. Eur. J.* **2007**, *13*, 5223–5231; (f) Schroeder, H.; Adler, M.; Gerigk, K.; Müller-Chorus, B.; Götz, F.; Niemeyer, C. M. *Anal. Chem.* **2009**, *81*, 1275–1279.

(17) Liu, M.; Amro, N. A.; Liu, G. Y. *Annu Rev Phys Chem* **2008**, *59*, 367-386.

(18) Niemeyer, C. M. *nanotoday* **2007**, *2*, 42-52.

(19) Weber, P. C.; Ohlendorf, D. H.; Wendoloski, J. J.; Salemme, F. R. *Science* **1989**, *243*, 85-88.

(20) Silverton, E. W.; Navia, M. A.; Davies, D. R. *Proc. Natl. Acad. Sci. U S A* **1977**, *74*, 5140-5144.

(21) Niemeyer, C. M.; Bürger, W.; Hoedemakers, R. M. J. *Bioconjugate Chem.* **1998**, *9*, 168-175.

(22) Uram, J. D.; Mayer, M. *Biosens. Bioelectron.* **2007**, *22*, 1556-1560.

(23) Gajhede, M.; Schuller, D. J.; Henriksen, A.; Smith, A. T.; Poulos, T. L. *Nat Struct Biol* **1997**, *4*, 1032-1038.

(24) Hobara, D.; Uno, Y.; Kakiuchi, T. *Phys. Chem. Chem. Phys.* **2001**, *3*, 3437-3441.

Supporting Information

Materials and Methods

Chemicals: Thiol- and amino -modified oligonucleotides,

cD0 (SH or NH_2-$(CH_2)_6$-5'-TTCGGCTCATACTCTGACTGTA-3'),

cD1 (SH or NH_2-$(CH_2)_6$-5'CTTCACGATTGCCACTTTCCAC-3'),

cD2 (SH or NH_2-$(CH_2)_6$-5'-CTTATCGCTTTATGACCGGACC-3') and

non-modified oligonucleotide, **D0** (5'-TACAGTCAGAGTATGAGCCGAA-3')

were all purchased as HPLC purified grade from Biomers GmbH (Ulm, Germany). The final concentration of all oligomers was 100µM. Sodium chloride (NaCl), ethylenediaminetetraacetic acid (EDTA) and phosphate buffered saline (PBS) tablets were purchased from Sigma. The buffers, TE (1M NaCl, 10mM Tris, 1mM EDTA, pH 6.9) and PBS (10mM phosphate buffer, 2.7mM potassium chloride (KCl) and 137mM NaCl, pH 7.3) were prepared using MilliQ water (resistance > 18 MΩcm) and filtered before use. Sulfo-succinimidyl-4-(N-maleimido-methyl)-cyclohexan-1-carboxylate (sSMCC) was obtained from Pierce and dithiothreitol (DTT) from Fluka.

Proteins: Horseradish peroxidase (HRP) and glucose oxidase (GOx) were purchased from Sigma. Streptavidin (STV) was expressed as recombinant core streptavidin in *E. coli* using a published protocol and purification procedures[1] and all of the used antibodies were obtained from Abcam (Cambridge, UK).

AFM: All AFM experiments were carried out using an XE-100 PARK AFM system, equipped with a custom liquid cell. All Nanografting (NG) experiments were performed by contact-mode AFM with standard ("hard") silicon cantilevers

(MikroMasch, nominal spring constants 0.63Nm^{-1}, tip radius < 10nm) at an applied force of 80-100nN and a tip speed of 500nm/sec, in the presence of thiolated single stranded DNA (ssDNA) solution (10 µM, dissolved in a 1:1 mixture of TE buffer and ethanol). Topographic images of NG-generated ssDNA nano-patches were recorded with standard ("soft") silicon cantilevers (MikroMasch, nominal spring constants 0.03Nm^{-1}, tip radius < 10nm) in modified PBS buffer (1M PBS, 1mM EDTA, pH 7.2). The substrates were washed thoroughly with TE and PBS buffers before and after the hybridization, respectively, to remove physically adsorbed molecules.

Monolayer preparation: For preparing a protein resistant monolayer on ultra flat (111) gold substrate, a 100nm thick gold film was deposited on freshly cleaved mica sheets (Mica New York Corp., clear ruby muscovite) at a pressure of about 10^{-5} mbar in an electron-beam evaporator at a rate of 0.1nm/sec. In the present work, Epoxy SU8-100 (negative tone photoresist, MicroChem) was used as a solid support. A drop of SU-8100 was placed over small slides (few millimeters in size) of gold substrate and then cured to form SU8-100/gold/mica sandwich. The gold-mica interface was uncovered mechanically, and immediately immersed into a freshly prepared 100µM solution of top oligo-ethylene-glycol3 terminated alkylthiols (TOEG3, SH-$(CH_2)_{11}$-$(O\text{-}CH_2\text{-}CH_2)_3$-OH, Prochimia) in pure ethanol (Fluka, purity ≥ 99.8 %), and incubated for 15 hours at room temperature. The resulting SAM was then rinsed with ethanol and dried under a mild stream of nitrogen. AFM was used to measure the roughness of the SAM, which was typically in the range of a few angstroms.

DNA-protein conjugates preparation: The **D1-STV, D2-STV**, **D2-HRP** and **D1-GOx** conjugates were prepared using the bifunctional crosslinker sSMCC (sulfo-succinimidyl-4-(N-maleimido-methyl)-cyclohexan-1-carboxylte), following a previously described method.[2,3] Briefly, 100 µL of a 100 µM solution of the corresponding 5'-thiol modified oligonucleotide in TE buffer was mixed with 60 µL DTT (1M) and incubated overnight at 37°C to reduce any disulfide bonds formed upon storage of the oligonucleotide. 200 µL of 200 µM protein solution (in phosphate buffer, pH 7.2) were incubated for 1 h at 37°C with sSMCC (2 mg in 60 µL DMF). Both DNA and protein solution were purified by two consecutive gel-filtration chromatography steps using NAP5 and NAP10 size exclusion columns (Pharmacia). The purified DNA and protein solutions, each of which had a volume of 1.5 ml, were then combined and incubated in the dark at room temperature for 3 h. The reaction

mixture was concentrated to approx 300 μL by ultrafiltration (Centricon 30, Milipore) and the buffer was exchanged to Tris (20 mM, pH 8.3) during this step. The conjugates were purified by anion exchange chromatography on a MonoQ HR 5/5 column (Pharmacia) using linear gradient over 25 min (AKTA purifier, Amersham Bioscience, buffer A: 20 mM Tris A pH 8.3 and buffer B: 20mM Tris A and 1.5 M NaCl). The concentration was determined spectrophotometrically, as described previously.[2,3]

Protein immobilization: Nanografting was carried out as described earlier.[4] Briefly, the AFM tip scans the selected area at relatively large forces in the presence of thiolated ssDNA molecules in solution. Under the tip load, molecules from the liquid solution phase replace, in a localized manner, molecules removed from the TOEG3 SAM and self-assemble on the gold surface. In our previous studies, we have demonstrated that the density of DNA confined by NG within a nanosized area on the surface is proportional to the number of sweeps driven by the AFM tip in a particular area.[5,6] For quantitative studies, we have introduced a grafting parameter that is the ratio, namely S/A, between the total area (S) that is covered by the tip during nanografting and the area of the patch (A). Basically S/A can be expressed as the density of nanografted scanning lines multiplied by the tip size at the point of contact with the surface. Therefore, the higher the density of strokes applied by the tip, the higher is S/A. For instance, for S/A = 1, the nanografted scanning lines do barely touch each other, while for S/A = 5, the distance between adjacent scanning lines is 1/5 of the tip size, and in this way each area in the nano-patch has been “overwritten” five times. Nanopatches of ssDNA molecules (e.g., cD1) of various S/A were fabricated. To immobilize the protein, the sample was then incubated in a solution containing the DNA-protein conjugate (e.g., **D1-STV**, 2 μM in PBS buffer) for 2h at room temperature.

Antibody binding: To accomplish the binding of antibodies, the substrate containing immobilized protein features, such as **D1-STV** and **D2-HRP**, were incubated with a solution of polyclonal antibodies (rabbit **anti-STV IgG**, concentrations ranging from 500pM to 1000nM, and/or rat **anti-HRP IgG** (10nM to 1000nM) in PBS buffer for 3h at RT. For the set of serum experiments, the binding of antibodies were carried out by incubating the immobilized protein patterns (**D2-STV** and **D1-GOx**) with a solution of the mixture of 50% standardized human serum (BISEKO) and **anti-STV IgG**

(1000nM, PBS, pH 7.4) for 30 min. After washing, the substarte was then incubated with a solution of **anti-GOx IgG** (1000nM, PBS, pH 7.4) dissolved in 50% serum for 30 min. Subsequent to incubation; the substrates were thoroughly washed with PBS buffer to remove any non-specifically adsorbed materials prior to AFM measurements.

Determination of dissociation constants. To determine the dissociation constants for the binding of the protein conjugate **D1-STV** and the **anti-STV IgG** within the nanografted DNA patches, differential height values (Fig S1), that is the height difference between the relevant patch and a reference patch (example in Fig S1), were measured as a function of probe concentration. The average height values obtained from three independent measurements were taken into account. Differential height is defined as [ΔH]p in the case of **D1-STV**, and [ΔH]ab in the case of **anti-STV IgG**. For **anti-STV IgG,** the measured differential height was corrected by subtracting the measured size of STV i.e. [ΔH]p to reflect the binding signal of **anti-STV IgG**. Assuming that the target-probe binding events are unaffected by surface coverage (i.e. the filled fraction of target molecules binding sites), and in addition, that the differential height is proportional to the surface coverage, Langumir equation states:

$$\Delta H = h\frac{[C]}{[C]+K_D}$$

where C represents the concentration of target molecules in solution (**D1-STV**, **anti STV IgG**), and h is a proportionality constant, which represents the saturation height signal at asymptotically high values of the concentration.

Figure S1

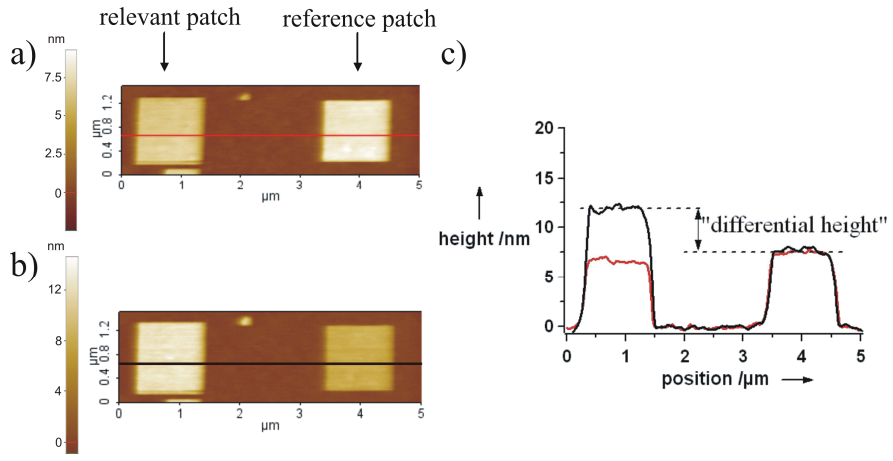

***Figure S1*:** AFM topographic images (5 × 1.5 μm^2) of two ssDNA nanopatches indicated as relevant patch (**cD1**) and reference patch (**cD2**); a) before hybridization; b) after hybridization with **D1-STV** conjugate; c) corresponding height profiles with the description of "differential height".

Investigation of specific STV-biotin interaction. Nanopatches of **D1-STV** were prepared as described above and exposed to 1μM solution of biotinylated and non-biotinylated goat anti-mouse IgG to investigate whether the nanopatch-immobilized STV has retained its specific biotin-binding capability. The results are shown in Fig. S2.

Figure S2

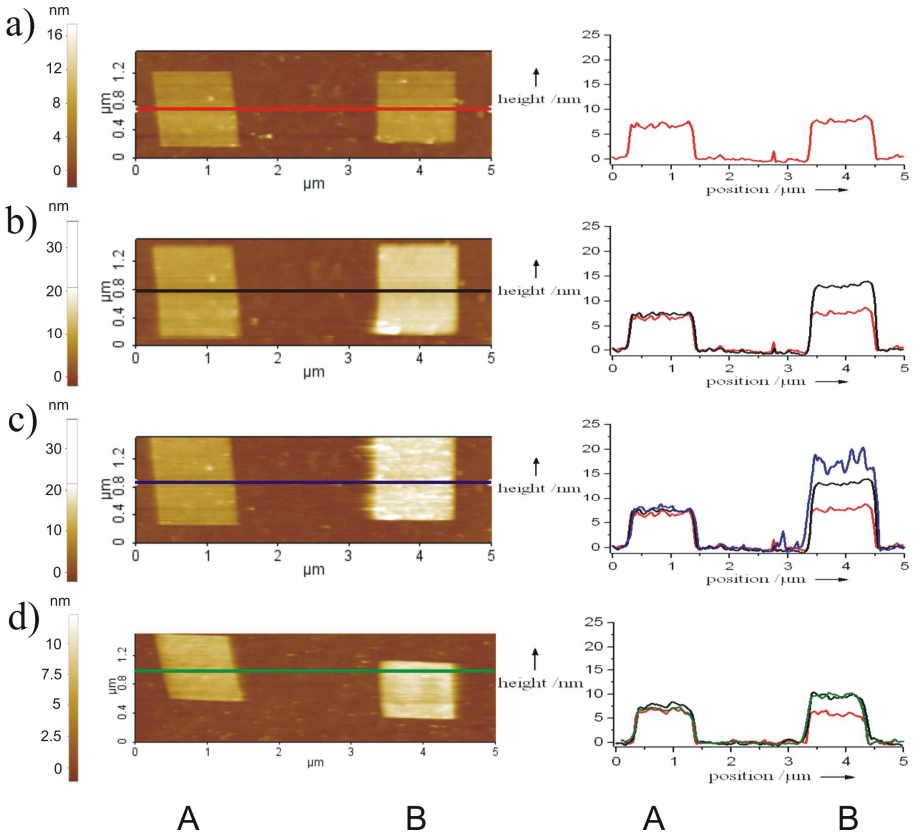

***Figure S2*:** Interaction of **D1-STV** immobilized on a DNA nanopatch with a biotinylated antibody. Patches **A** and **B** contain non-complementary (control, **cD0**) and complementary capture oligomers **(cD1)** respectively. a) grafted ssDNA. b) **D1-STV** immobilization, subsequent addition of c) biotinylated goat anti-mouse IgG and d) non-biotinylated goat anti-mouse IgG Comparison of c) and d) clearly indicates

that only biotinylated IgG binds to the STV-modified patch.

Scalability of nanografted patches. Patches of ssDNA molecules (**cD1**) of various sizes, ranging from 200 x 200 to 1000 x 1000 nm^2 were prepared. Different S/A ratios were realized, ranging from S/A = 40 to S/A = 1. As already discussed, S/A is the ratio between the total area that is covered by the tip (S) during nanografting and the area of the patch (A) and is proportional to the density of the released ssDNA molecules in the nanopatch. Resulting AFM images and height profiles are shown in Fig. S3. In the height profiles, the red dotted lines indicate S/A = 1, while the green lines indicate S/A = 40. The sample was then incubated with DNA-protein conjugate (**D1-STV**, 2 μM, PBS), and height measurements were carried out. As shown in Fig. S3b, a clear increase in height of 4 ± 0.5nm was observed after hybridization of **D1-STV** conjugate for both S/A = 1 and S/A = 40.

Figure S3:

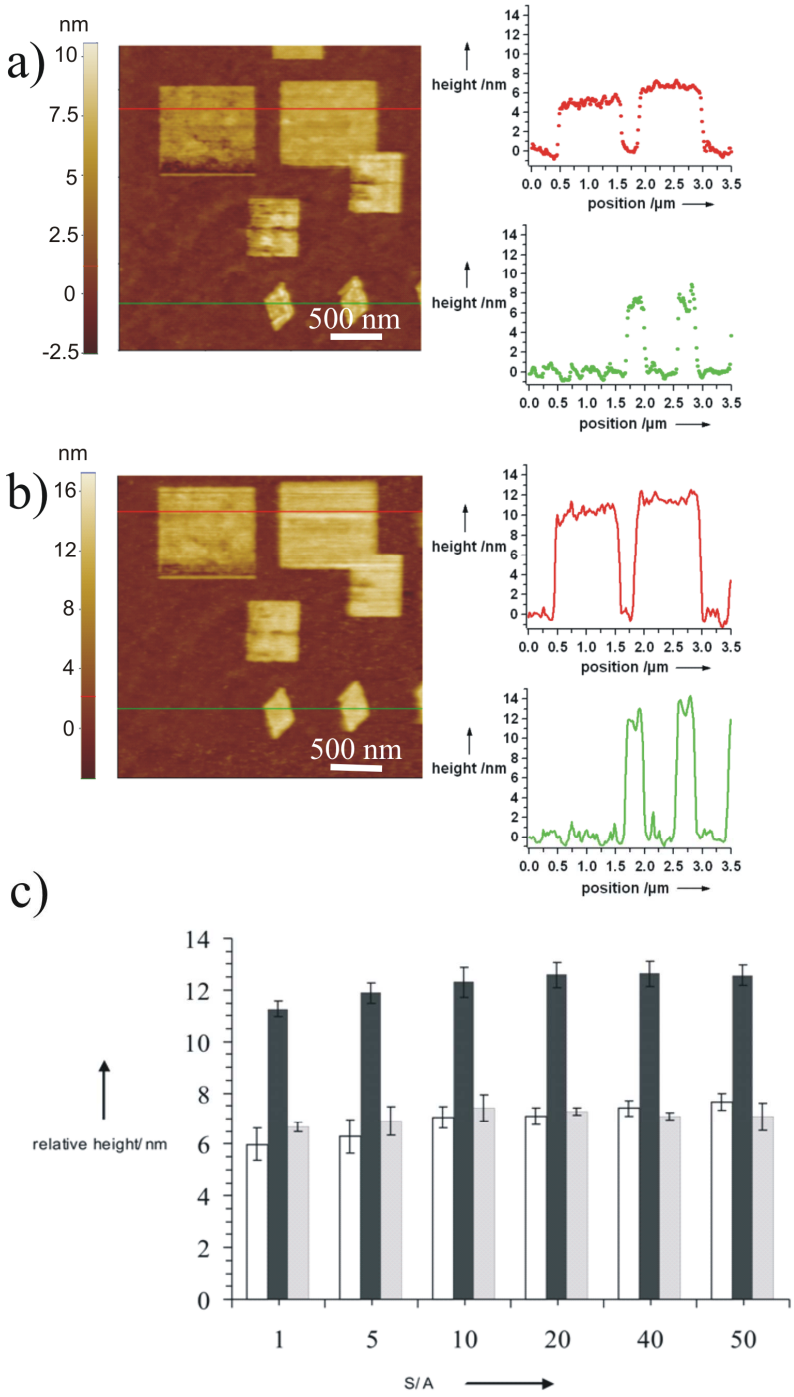

Figure S3: AFM topographic images (3.5 x 3.5 µm^2) of nano-patches of different sizes. a) the fabrication of ssDNA **cD1** nanopatches by nanografting DNA in varying S/A ratios. The red and green lines indicate S/A=1 and S/A=40, respectively; b) hybridization of **D1-STV** conjugate and c) plot of relative heights of the patches as a function of S/A before (white columns) and after hybridization with **D1-STV** conjugate (black columns). Grey column represent a control (hybridization of unmodified STV).

***Figure S4: DDI of* D2-HRP and D1-GOx conjugates on DNA nanopatches and corresponding antibody binding.**

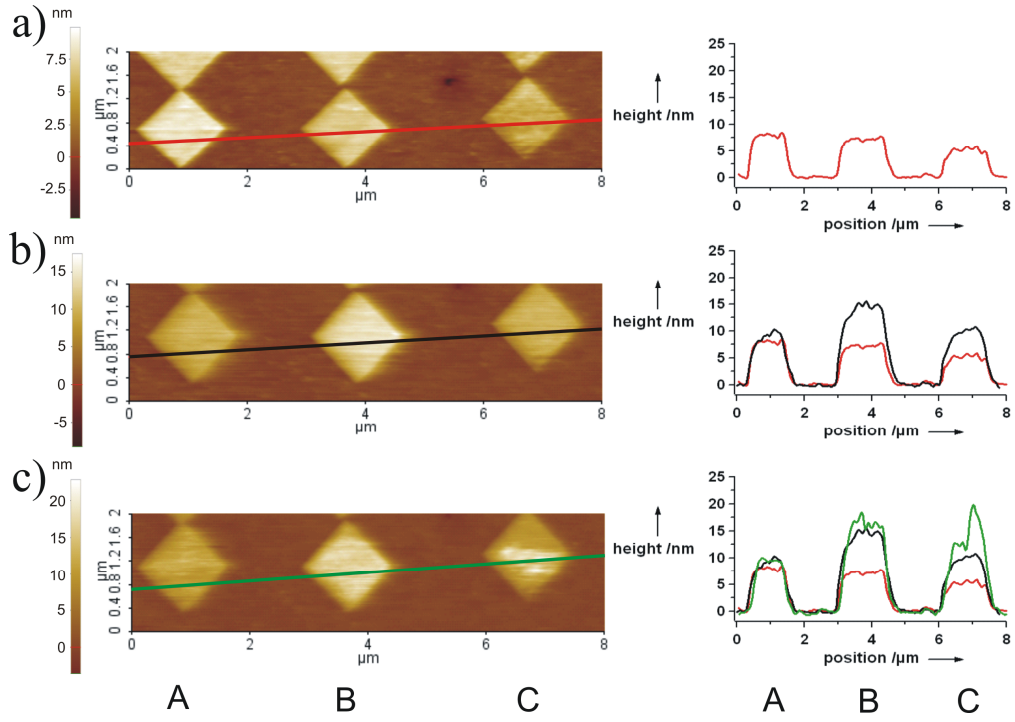

Figure S4: AFM topographic images (8 × 2 µm^2) and corresponding height profiles of antibody binding on the immobilized protein nanopatches; a) ssDNA nanopatches, **cD0** (control patch, A), **cD1** (patch B) and **cD2** (patch C), red line profile; b) patches after incubation with a solution containing DNA-protein conjugates **D1-GOx** and **D2-HRP**. Note that the increase in height indicates successful immobilization of both conjugates**, D1-GOx** (patch B) and **D2-HRP** (patch C), black line profile); c) patches after incubation with the mixture of **anti-HRP IgG** and **anti-STV IgG**. Note that only the HRP-containing patch (C) reveals an increased height (green line profile).

Figure S5: Glass microarray-based immunoassays to analyze possible cross reactions between DNA sequences, protein conjugates and antibodies.

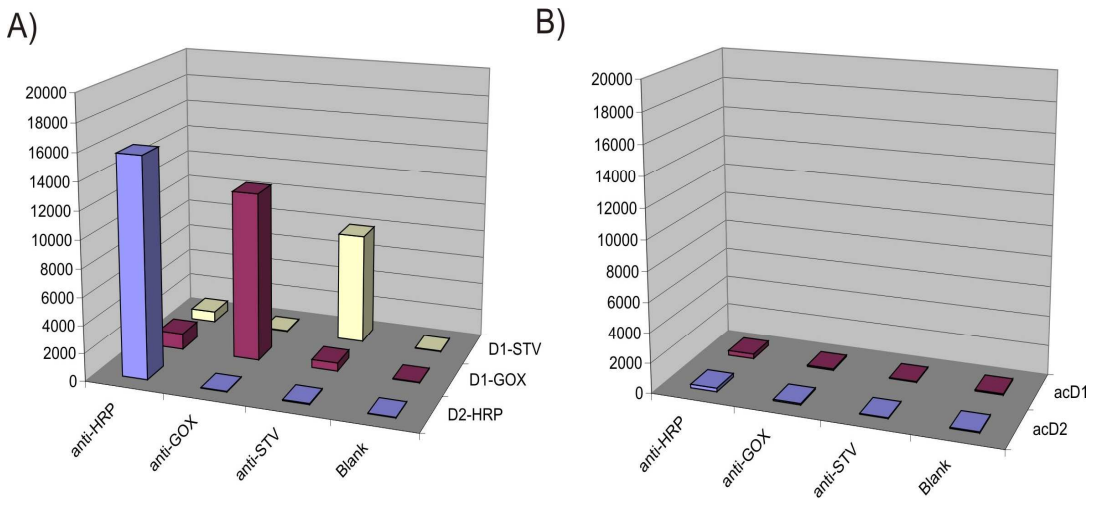

Figure S5: Immunoassay experiments performed on glass slides, using complementary DNA spotted as capture for DDI onto glass surfaces. A) DNA-protein conjugates (**D1-STV**, **D1-GOx** and **D2-HRP**) were hybridized to their complementary sequences and subsequently treated with specific fluorescently labelled antibodies (**anti-HRP IgG**, **anti-GOx IgG** and **anti-STV IgG**) B) Control slide where no proteins were hybridised.

Experimental procedure. To prepare the microarrays used for the micro-immunoassays, a solution of the desired 5'- amino-modified oligonucleotides (caD1 and caD2) was spotted onto 3DProtein Slides (Chimera Biotec, Dortmund, Germany) using a piezo-driven spotting device. The slides were incubated overnight and subsequently stored at 4 °C until use. The following incubation steps were carried out in a humidity chamber, under mild orbital shaking (100 rpm) at room temperature. Each incubation step was followed by washing with 60 μL TETBS (2 x 30 s, 2 x 5 min). Prior to the first binding step, the spotted glass substrates were rinsed with TETBS, followed by blocking with MESTBS buffer for 30 min. Subsequently, the slides were washed, shacked dry and incubated with the specific DNA-Enzyme conjugates (D1-STV, D2-HRP, and D1-GOx) for 90 min. After washing, the substrates were incubated with 100 nM solutions of the primary antibodies (anti-STV, anti-HRP and anti-GOx all from rabbit) dissolved in standardized human serum (BISEKO). In the final incubation step, DyLight^{TM} 549 conjugated anti-Rabbit IgG from goat was allowed to bind for 30 min (100 nM in TETBS). Final washing with TETBS and once with ddH_2O was followed by centrifugation of the substrates at

1500 rpm for 3 min. Fluorescent signals on the glass slide was then analyzed using a GenePix 4100B Microarray Reader (Laser Power 100, PMTGain 330).

Buffers used:

TETBS 20 mM Tris-Cl, 150 mM NaCl, 5 mM EDTA, 0.05% Tween-20, pH 7.5

MESTBS 20 mM Tris-Cl, 150 mM NaCl, 4.5 % milk powder, 5 mM EDTA, 0.2% NaN_3, 1 mg/ml DNA, pH 7.35

References:

1. T. G. M. Schmidt, A. Skerra, *J. Chrom. A* **1994**, 676, 337-345.
2. C. M. Niemeyer, T. Sano, C. L. Smith, C.R.Cantor, Nucleic Acids Res. 1994, 22, 5530-5539.
3. L. Fruk, J. Mueller, G. Weber, A.Narvaez, E. Dominguez, C. M. Niemeyer, *Chemistry* **2007**, 13(18), 5223-5231.
4. S. Xu, S. Miller, P. E. Laibinis, G.-Y. Liu, *Langmuir* **1999**, *15*, 7244–7251.
5. E. Mirmomtaz, M. Castronovo, C. Grunwald, F. Bano, D. Scaini, A. A. Ensafi, G. Scoles, L. Casalis, *Nano Lett.* **2008**, *8*, 4134-4139
6. M. Castronovo, S. Radovic, C. Grunwald, L. Casalis, M. Morgante, G. Scoles, *Nano Lett.* **2008**, *8*, 4140-4145.

Chapter 4

Biocatalyst Activity of Artificial Multienzyme Complexes Immobilized on Surfaces*

* Unpublished observations. This work has been done in collaboration with Dr. Denis. Scaini (ELETTRA Synchrotron Light Source, Italy) and Dr. Ljiljana Fruk (University of Karlsruhe, Germany).

4.1 Abstract

This study describes the immobilization of multienzyme complexes with controlled spatial positioning on surfaces, for enzyme-based biosensors. A combined approach of nanografting and DDI was utilized to immobilize glucose oxidase (GOx) and horseradish peroxidase (HRP) enzymes on the grafted ssDNA nanopatches. These bienzyme nanopatches comprising of DNA-GOx-HRP were then employed to sense glucose. The GOx catalyzed oxidation of β-D-glucose yielded D-glucono-δ-lactone and H_2O_2 and, the resulting H_2O_2 oxidized 4-Chloro-1-Naphthol (4CN) into Benzo-4-Chloro Cycloexadienone (B4CHD), a precipitated product, in the presence of HRP. Atomic Force Microscopy (AFM) relative height and friction measurements were utilized to probe this biochemical reaction with a various concentrations of glucose and have showed a significant increase in the reactivity of the complex in which HRP was more exposed to the sample solution.

4.2 Introduction

The development of advanced sensing methods for bio-molecules at small dimensions has received a rising interest. The main inspiration for this enhanced activity is the increasing demand for miniaturized biosensors, particularly for medical diagnostic applications[1, 2]. One of the main challenges to develop innovative biosensors is to couple ordered arrangement of bio-molecules to an appropriate detection method for the routine readout of analytes present in small sample volumes. Among existing methods[3, 4], scanning probe microscopy[5, 6], seems to face this challenge and has the potential to resolve many issues concerning precise positioning of biomolecules and label-free detection. Although substantial progress has been made in the label-free detection of bio-molecules, such as DNA, proteins and enzyme[7-9], precise detection of small molecules[10-12] in highly diluted environment (including various sugars, amino acids, metal ions, etc) remains a challenging goal.

Based on nanograftingy[13, 14] and DDI[15-17] described extensively in chapter 3, we studied the immobilization of bienzyme complexes comprised of DNA conjugated glucose oxidase (GOx) and horseradish peroxidase (HRP) enzymes onto previously NG-generated patterns of complementary DNA strand within an alkanethiol monolayer on gold surface. The biochemical activity of these immobilized complexes

was then probed by the activation of the GOx-HRP system with β-D-glucose, successively characterized by AFM topographic relative height measurements, which give a measurement of the height of the molecular assembly with respect to the surrounding monolayer. The GOx mediated oxidation of β-D-glucose yields D-glucono-δ-lactone and H_2O_2 and consequently, the resulting H_2O_2 oxidized 4-Chloro-1-Naphthol (4CN) into Benzo-4-Chloro Cycloexadienone (B4CHD), an insoluble product that precipitates, by HRP (Figure 1a). For the detection of low concentration of β-D-glucose, we take advantage of AFM friction measurement due to its remarkable capability of determining small morphological changes[18]. Moreover, the influence of spatial position of bienzyme complexes on biochemical reactions was observed. Our results showed a significant rise in the reactivity of the complexes, when HRP is immobilized on the top of the hosting DNA sequences forming the nanopatches.

4.3 Results and discussion

To generate complex molecular assemblies (Figure 1b), patterns of ssDNA were initially fabricated within a monolayer of top oligo-ethylene-glycol3 (HS-$(CH_2)_{11}$-$(OCH_2CH_2)_3$-OH), on an ultraflat gold surface, using nanografting. The covalently modified enzymes with cDNA sequences were then assembled onto the generated patterns by mean of DDI. To obtain the information about the bio-recognition events, we used AFM topographic relative height and friction measurements. Figure 2a shows a typical 1μm x 1μm pattern of thiolated-ssDNA HS-cD1-cD2 (for sequences, see Table 1) at S/A = 0.16, which was grafted into the monolayer of thiolated ethylene glycol from a 10 μM solution of ssDNA. The nanografting parameter S/A has been thoroughly discussed in this thesis (see chapter 2).

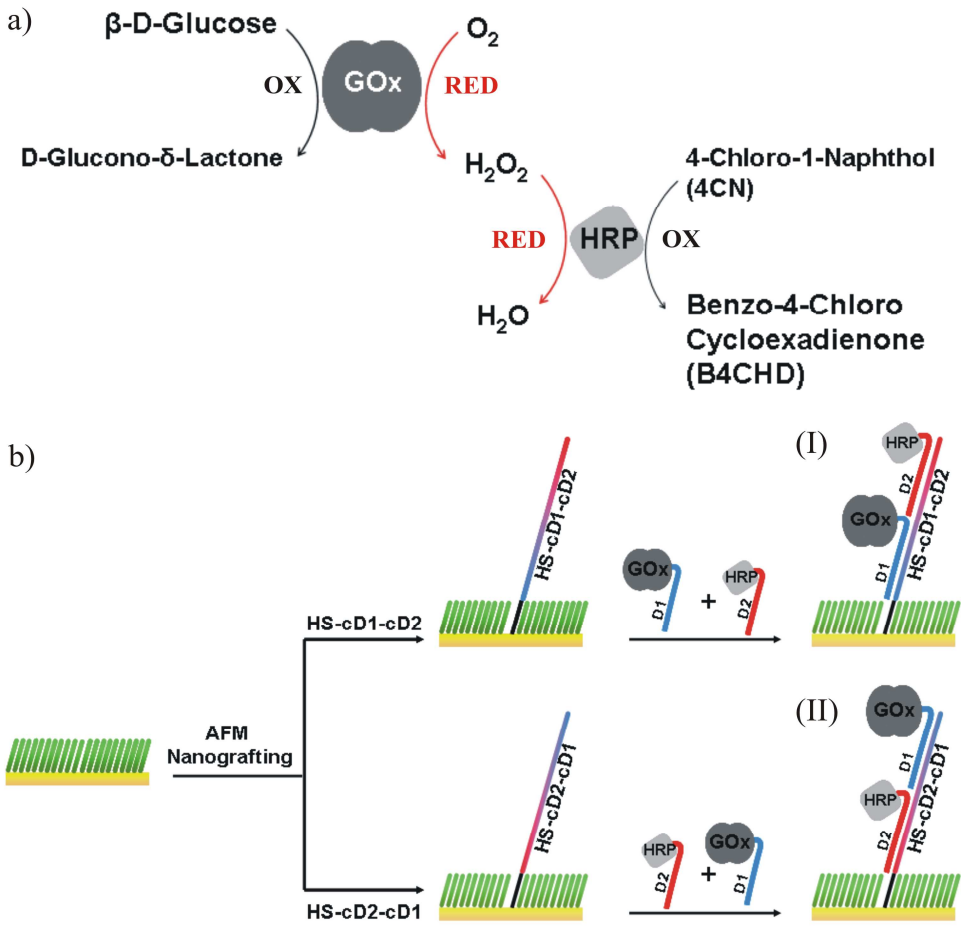

Figure 1: (a) Schematic illustration of biochemical activity of the coupled enzymes, glucose oxidase (GOx) and horseradish peroxidase (HRP). (b) Two different complexes of the enzymes were obtained by nanografting, HS-cD1-cD2 (top) and HS-cD2-cD1 (bottom) into a monolayer of ethylene glycol-terminated alkanethiols and their subsequently association with DNA-enzyme conjugates. Complex (I) and (II) depict the two enzymes in the two different configurations.

The resulting patches are then allowed to bind with a mixture of covalent conjugates of glucose oxidase (GOx) tethered with oligomer D1 (D1-T6-GOx), and horseradish peroxidase (HRP) tethered with oligomer D2 (D2-T6-HRP), by a simple hydrogen-binding interactions in sequence specific DNA hybridization (for details, see experimental section). These DNA-enzyme conjugates contain T6 spacer between the enzyme and the main sequence of DNA in order to facilitate the assembly of bienzyme within the cDNA nanostructures.

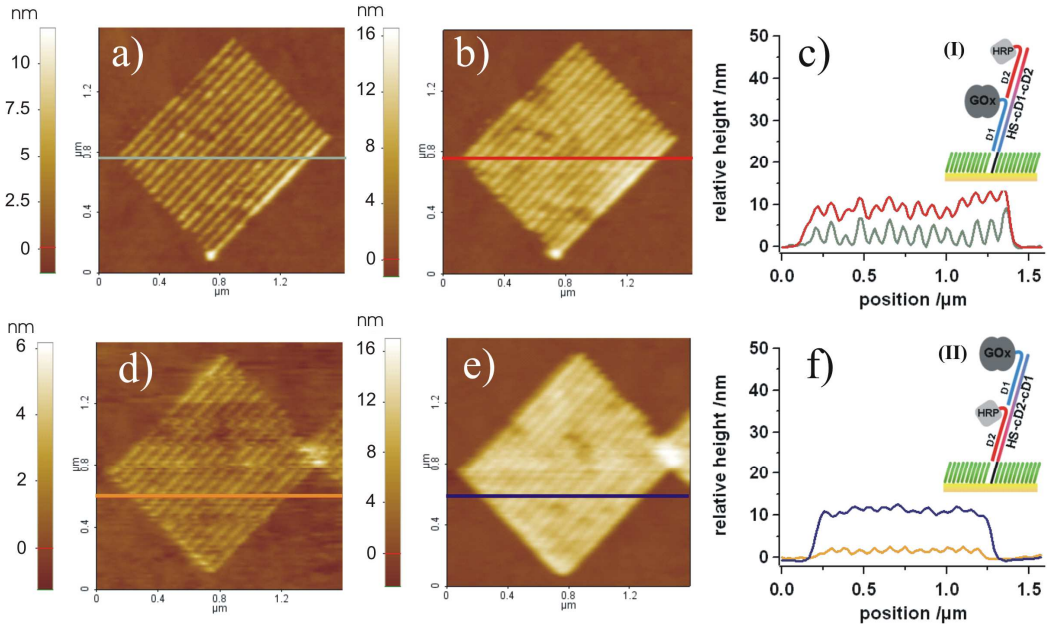

Figure 2: AFM topographic images (1.6µm x 1.6µm) of nanografted DNA (44 bps) patches containing sequences of, HS-cD1-cD2 (a) and HS cD2-cD1 (d), and their subsequent use for immobilizing the two enzymes (GOx, and HRP) in two different arrangements (b, e). The relative height profiles in (c) and (f) illustrate the change in height before (in silver and orange) and after (in red and blue) the generation of the complex I and II, respectively.

Figure 2a and 2b are AFM topographic images of ssDNA nano-patches before (in silver) and after (in red) the immobilization of two enzymes (GOx and HRP), respectively, while Figure 2c depicts the corresponding relative height profiles. The sample was thoroughly washed with Tris (TE) and phosphate (PBS) buffers to remove any physically absorbed molecules prior to AFM imaging. The resulting height increase of GOx-HRP-modified DNA patch indicates the immobilization of the two enzymes on the DNA patch (see Figure 1b, I). Similarly, an assembly of HRP-GOx has been obtained by grafting the sequence of thiolated-ssDNA upside down, (HS-cD2-cD1), subsequently hybridized with the conjugates, D1-T6-GOx and D2-T6-HRP (DNA-modified enzymes). It should be noted that the two enzymes are now immobilized in reverse order (for details, see Figure 1b, II). The resulting AFM topographic images and relative height profiles of this configuration are shown in Figure 2 d-f. Again, the height analysis reveals an increase in height above ssDNA patch (Figure 2d, orange line profile), consistent with the association of the enzymes, HRP and GOx (Figure 2e, blue line profile) on the patch. One can observe that the

final relative heights of both complexes have approximately the same value (i.e. 10 nm from the surrounding monolayer), even though initial heights of ssDNA nanopatches were different by about a factor of 2. Likely, this is due to the different bending properties of oligonucleotides, cD1 (22 bps) and cD2 (22 bps) that are arranged in reverse order in long oligonucleotides (44 bps, each).

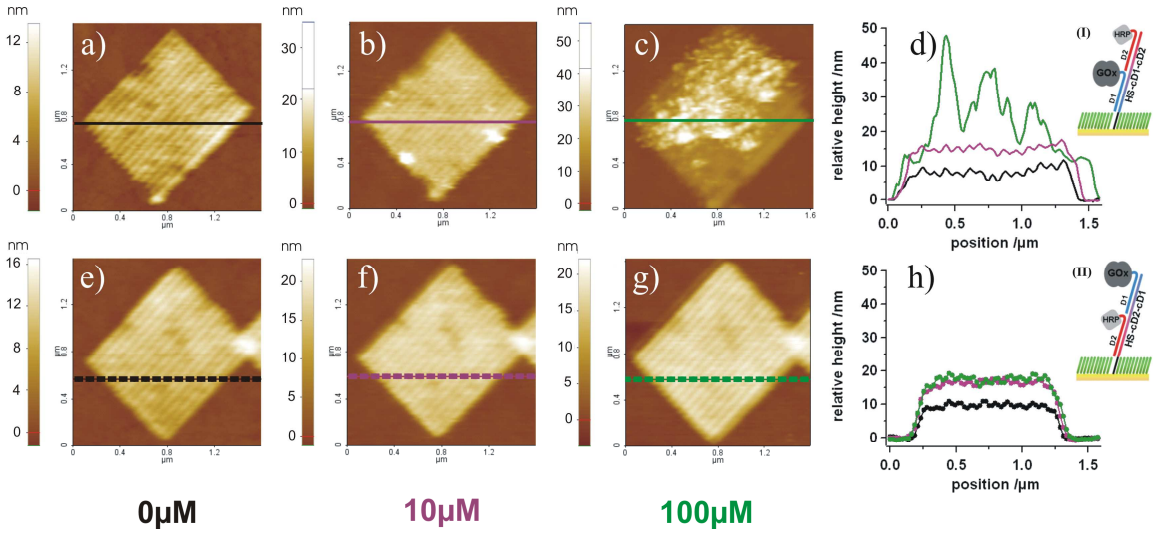

Figure 3: AFM topographic images (1.6µm x 1.6µm) and corresponding relative height profiles of the activation of bienzyme complexes on the DNA nanopatches with various concentrations of glucose: (a) and (e) show patches after the reaction with 0µM glucose (in black) for complex I (filled line) and II (dotted line), respectively. (b) and (f) show the same patches after the reaction with 10µM glucose (in purple) for complex I (filled line) and II (dotted line), respectively. (c) and (h) show the same patches after the reaction with 100µM glucose (in green) for complex I (filled line) and II (dotted line), respectively.

The biochemical activity of the two enzymes, GOx and HRP assembled on DNA nanostructures, was then examined by the activation of both complexes (I and II) with glucose, as a result of two-step reaction illustrated in Figure 1a. The activity of the coupled enzyme includes initial step of oxidizing β-D-glucose to D-glucono-δ-lactone in the presence of GOx, while generating H_2O_2. In the second step, HRP reduces H_2O_2 into H_2O and oxides the substrate 4-Chloro-1-Naphthol (4CN) to Benzo-4-Chloro Cycloexadienone (B4CHD), a precipitated product. A set of experiments was carried out, in which the concentration of glucose was varied from 0µM to 1000µM, while keeping fixed the concentration of 4CN to 1mM in kpi300

buffer (pH = 7.4). Initially, control experiment was performed to prove the intactness of our system. The sample containing enzyme modified DNA patches was incubated in the solution of 0μM glucose and 1mM 4CN (kpi300, pH = 7.4) for 20 minutes. The sample was then washed with TETBS (pH = 7.29), and PBS (pH = 7.3) buffer to remove physically adsorbed molecules and imaged by AFM. As shown in Figures 3a and 3e, the relative height profiles revealed no change in patch heights (in black, filled and dotted line profiles).

To activate bienzyme complexes, the sample was then incubated with 10 μM glucose and 1 mM 4CN in kpi300 buffer (pH = 7.4) for 20 minutes. The resulting relative height profiles of enzyme modified DNA patches indicated an increase in height of ~7.3 nm (Figure 3d, purple line profile) and ~5.6 nm (Figure 3h, purple dotted line profile) for complex I and II, respectively. The increased height is attributed to the presence of the small amount of precipitation residues on the patches. These results clearly indicate that the immobilization of the two enzymes on the DNA nanopatch allows the communication between the two enzymes or biocatalysts within the nanostructures due to the close proximity of the two enzymes on the DNA strands. The H_2O_2 produced by GOx forms a high local concentration next to the HRP, resulting in the effective activation of the second enzyme.

The same sample was then immersed in the solution of 100μM glucose for 20 minutes after regenerating the assembly of two enzymes. AFM relative height measurements revealed an irregular increase in height above the patch containing the bienzyme complex I, as illustrated in Figure 3c (green line profile in Figure 3d) and no further change in height in the case of complex II (Figure 3g and green dotted line profile in Figure 3h). We attributed this irregularity in patch height to the enhanced activity of complex I. The difference in the activity registered between complex I and II might be a result of the different size of the two enzymes and their spatial position on the DNA strands. HRP is a smaller enzyme with molecular weight of ca. 40 kDa, while GOx is known to be a large dimeric protein (molecular weight of 160 kDa[19]). Thus, the immobilization of HRP subsequent to GOx (complex I) is likely to oxidize 4CN more efficiently, with the better access to the sample solution, and thus resulting in large concentration of precipitated product on the patch.

The plots of relative heights for both complexes (I and II) at various concentrations of glucose are shown in Figure 4a. It is evident from the plot that complex I (in red) showed higher activity than II (in blue). Furthermore, in the case of

complex II, relative height response indicates that saturation is almost reached for 10µM glucose concentration. The saturation in the relative heights at these glucose levels can be attributed to a barrier effect due to the localized precipitation of B4CHD between HRP and GOx that limits the diffusion of H_2O_2, the electron mediator of the bienzyme, in complex II. In order to follow the production of precipitation residues in the range of 10µM to 1000µM glucose concentration for complex II, we decided to carry out more sensitive frictional studies.

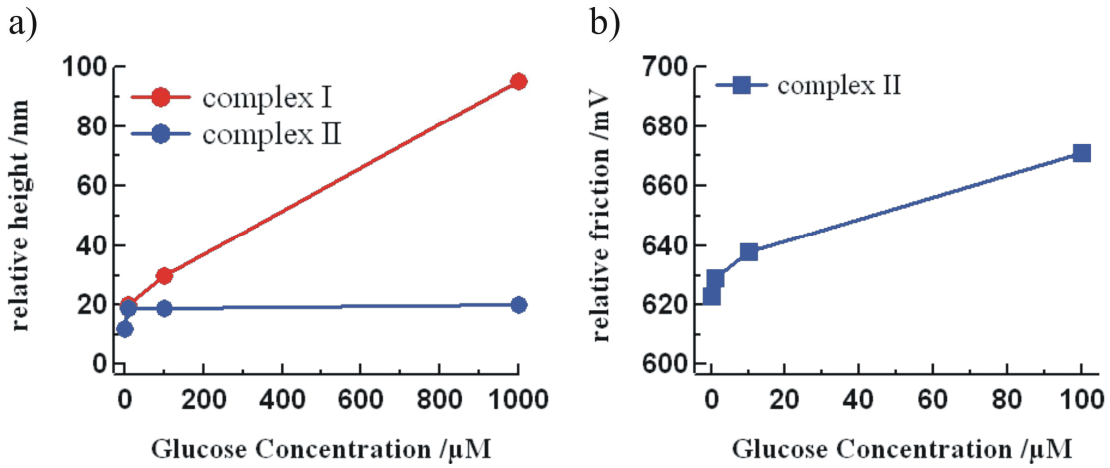

Figure 4: Comparison between relative height and friction measurements; (a) relative height versus glucose concentration after the activation of complex I (in red) and II (in blue). (b) The relative friction values are plotted for the case of complex II in a low range of glucose concentration (i.e. from 0µM to 100µM).

The use of AFM to study frictional properties of SAM of, for instance, n-alkanethiols, monolayers of methyl- or carboxyl-terminated thiols, on gold surfaces has been already demonstrated by several studies [20-22]. These studies have found that friction determined with AFM is inversely proportional to the level of order of the SAM. In other words, SAM which is highly ordered exhibits less friction than the SAM with lower degree of order[23, 24]. A similar attempt to investigate ligand-binding events by means of AFM-friction measurements has been reported by Staii, et. al. Using AFM nanografting, they have fabricated patches of maltose binding protein (MBP) within a monolayer of ethylene glycol-modified thiols on gold surface. Using friction measurements, they were able to monitor the changes in the protein

conformation due to the binding of maltose on these patches and to determine the dissociation constant of this system (kd = 1 ± 0.04μM) [25].

Figure 4b shows the data analysis of relative friction regarding to the experiments performed on complex II. In this plot, friction signal shows stronger response than height signal. This might be due to the extreme sensitivity of friction force microscopy to measure small changes in morphology and/or in the level of molecular order. From Figure 4, we also note that friction measurements (Figure 4b, blue squares) can clearly distinguish between different concentrations of glucose which was hardly seen in relative height plot/analysis (Figure 4a, blue circles). This implies that friction-based characterization can detect glucose level down to few tens of nano-molar. To determine detection limit of our system, further studies are needed.

4.4 Conclusion

In summary, we demonstrated the generation of DNA nanostructures by means of AFM nanografting, and their use for the immobilization of bienzyme complexes of GOx and HRP with controlled geometry and spatial positioning. Two different arrangements were designed to immobilize these complexes. AFM relative height and friction measurements were found to be sensitive for detecting various concentrations of glucose. Significant evidence of enhanced reactivity has been observed in the case where HRP was immobilized on the top of GOx, while a barrier to enzyme communication was found when the immobilization order was reversed. The results of this study provided a step forward for creating glucose nano-sensors; further work is however, required to optimize the sensitivity of these bi-enzyme complexes, while a proper characterization with electrochemical techniques, such as Scanning Electron Microscopy (SECM)[26, 27] is needed. SECM is a powerful electrochemical technique based on scanning probe microscopy for studying electron and/or ion transfer, patterning and other reactions in biological systems[28-33]. Among various applications, it offers the possibility to investigate the chemical reactivity at submicron and/or nanometer scale[34]. In future studies, the use of SECM to chemically image immobilized bienzyme complexes can provide valuable information about the electrochemical reaction kinetics and to differentiate between inactive and active regions of the system.

4.5 Experimental Section

Materials: Oligonucleotides were purchased from Biomers GmbH (Ulm, Germany) with HPLC purification. The sequences are listed in Table 1. Sodium chloride (NaCl), ethylenediaminetetraacetic acid (EDTA) and phosphate buffered saline (PBS) tablets, Potassiumphosphate, β-D-glucose and 4-Chloro-1-Naphthol (4CN), were purchased from Sigma. Tris was purchased from Fluka. The buffers, **TE** (1M NaCl, 10mM Tris, 1mM EDTA, pH 6.9), **PBS** (10mM phosphate buffer, 2.7mM potassium chloride (KCl) and 137mM NaCl, pH 7.3), **kpi300** (50 mM Potassiumphosphat, 300mM NaCl, pH 7.4), and **TETBS** (150mM NaCl, 20mM Tris, 5mM EDTA, 0.05% Tween 20, pH 7.29) were prepared using MilliQ water (resistance > 18 MΩcm) and filtered before use. The D1-T6-GOx and D2-T6-HRP conjugates were prepared as described earlier [Chapter 3 and references therein].

Table 1:

The list of oligonucleotides sequences used.

Name	Sequence
HS-cD1-cD2	(SH-(CH2)6-5'-CTTCACGATTGCCACTTTCCACCTTATCGCTTTATGACCGGACC-3'
HS-cD2-cD1	(SH-(CH2)6-5'-CTTATCGCTTTATGACCGGACCCTTCACGATTGCCACTTTCCAC-3'
T6-D1	5'-TTTTTTGTGGAAAGTGGCAATCGTGAAG
T6-D2	5'-TTTTTTGGTCCGGTCATAAAGCGATAAG

Substrate and preparation of monolayer: An ultra flat gold substrate was prepared as described earlier [Chapter 2 and 3, and references therein]. The monolayer of top oligo-ethylene-glycol3 terminated alkanethiols (TOEG3, SH-(CH2)11-(O-CH2-CH2)3-OH, Prochimia) was obtained using the previously reported protocol [Chapter 2 and 3 and references therein]. Briefly, gold substrate was incubated into a freshly prepared 100μM solution of TOEG3 in pure ethanol (Fluka, purity ≥ 99.8 %), for 15 hours at room temperature. The resulting SAM was then rinsed with ethanol and dried under a mild stream of nitrogen.

AFM and preparation of DNA nanostructures via nanografting: AFM imaging was performed using an XE-100 PARK AFM system, equipped with a custom liquid

cell. AFM nanografting experiments for fabricating ssDNA patterns were performed using previous described procedure. Briefly, contact mode AFM was operated in the presence of thiolated single stranded DNA (ssDNA) solution (10μM, dissolved in a 1:1 mixture of TE buffer and ethanol) at an applied force of 80-100nN with standard silicon cantilevers (MikroMasch NSC 19 tip, nominal spring constants 0.63 Nm^{-1}, tip radius < 10nm) and a tip speed of 500nm/sec. Under high applied force, molecules from the original SAM are forced to exchange with the thiolated ssDNA molecules from the solution to pattern ssDNA nanostructures. The nanografted ssDNA nanostructures were then imaged by silicon cantilevers (MikroMasch CSC38/B tip, nominal spring constants 0.03Nm^{-1}, tip radius < 10nm) in modified PBS buffer (1M PBS, 1mM EDTA, pH 7.2). The substrates were carefully washed with TE and PBS buffers before and after the hybridization, respectively, to remove physically adsorbed molecules. The relative height and friction were recorded by collecting simultaneously the topographic and lateral force images of the patches while performing AFM in contact mode at low imaging forces.

Preparation of bienzyme complexes: To prepare bienzymes complexes, the sample containing NG-generated ssDNA patches of HS-cD1-CD2 and/or HS-cD2-cD1, was incubated with the solution of equal concentration of D1-T6-GOx and D2-T6-HRP conjugates (1000nM, PBS, pH 7.3) for 2h at room temperature (~23-25°C).

4.6 References

1. Sahoo, S.K., Parveen, S. & Panda, J.J. The present and future of nanotechnology in human health care. *Nanomedicine* **3**, 20-31 (2007).
2. Meyer, J.M. & Ginsburg, G.S. The path to personalized medicine. *Curr Opin Chem Biol* **6**, 434-8 (2002).
3. Cao, G. Nanostructures & nanomaterials (ed. Cao, G.) (Imperial College Press, 2004).
4. Bernard, A. et al. Printing patterns of proteins. *Langmuir* **14**, 2225-2229 (1998).
5. Foster, A.S. & Hofer, W. Scanning probe microscopy (Springer, 2006).

6. Gutmann, O. et al. A highly parallel nanoliter dispenser for microarray fabrication. *Biomed Microdevices* **6**, 131-7 (2004).
7. Burg, T.P. et al. Weighing of biomolecules, single cells and single nanoparticles in fluid. *Nature* **446**, 1066-9 (2007).
8. Harper, J.C., Polsky, R., Wheeler, D.R., Dirk, S.M. & Brozik, S.M. Selective Immobilization of DNA and Antibody Probes on Electrode Arrays: Simultaneous Electrochemical Detection of DNA and Protein on a Single Platform. *Langmuir* **23**, 8285-8287 (2007).
9. McDonnell, J.M. Surface plasmon resonance: towards an understanding of the mechanisms of biological molecular recognition. *Curr Opin Chem Biol* **5**, 572-7 (2001).
10. Medintz, I.L. Recent progress in developing FRET-based intracellular sensors for the detection of small molecule nutrients and ligands. *Trends Biotechnol* **24**, 539-42 (2006).
11. Oliver, N.S., Toumazou, C., Cass, A.E. & Johnston, D.G. Glucose sensors: a review of current and emerging technology. *Diabet Med* **26**, 197-210 (2009).
12. Salimi, A. & Roushani, M. Non-enzymatic glucose detection free of ascorbic acid interference using nickel powder and nafion sol–gel dispersed renewable carbon ceramic electrode. *Electrochemistry Communications* **7**, 879-887 (2005).
13. Liu, M. & Liu, G.Y. Hybridization with Nanostructures of Single-Stranded DNA. *Langmuir* **21**, 1972-1978 (2005).
14. Mirmomtaz, E. et al. Quantitative Study of the Effect of Coverage on the Hybridization Efficiency of Surface-Bound DNA Nanostructures. *Nano Lett* **8**, 4134-4139 (2008).
15. Niemeyer, C.M. The developments of semisynthetic DNA-protein conjugates. *Trends Biotechnol* **20**, 395-401 (2002).
16. Niemeyer, C.M., Koehler, J. & Wuerdemann, C. DNA-directed assembly of bienzymic complexes from in vivo biotinylated NAD(P)H:FMN oxidoreductase and luciferase. *Chembiochem* **3**, 242-5 (2002).
17. Schroeder, H., Ellinger, B., Becker, C.F., Waldmann, H. & Niemeyer, C.M. Generation of live-cell microarrays by means of DNA-Directed immobilization of specific cell-surface ligands. *Angew Chem Int Ed Engl* **46**, 4180-3 (2007).

18. Staii, C., Wood, D.W. & Scoles, G. Ligand-induced structural changes in maltose binding proteins measured by atomic force microscopy. *Nano Lett* **8**, 2503-9 (2008).
19. Losic, D., Shapter, J.G. & Gooding, J.J. Scanning Tunneling Microscopy Studies of Glucose Oxidase on Gold Surfaces. *Langmuir* **18**, 5422-5428 (2001).
20. Houston, J.E. et al. Comparative study of the adhesion, friction, and mechanical properties of CF3- and CH3-terminated alkanethiol monolayers. *Langmuir* **21**, 3926-32 (2005).
21. Kim, H.I. et al. Molecularly Specific Studies of the Frictional Properties of Monolayer Films: A Systematic Comparison of CF3-, (CH3)2CH-, and CH3-Terminated Films. *Langmuir* **15**, 3179-3185 (1999).
22. Lio, A., Morant, C., Ogletree, D.F. & Salmeron, M. Atomic Force Microscopy Study of the Pressure-Dependent Structural and Frictional Properties of n-Alkanethiols on Gold. *J. Phys. Chem. B* **101**, 4767-4773 (1997).
23. Barrena, E., Kopta, S., Ogletree, D.F., Charych, D.H. & Salmeron, M. The relationship between friction and molecular structure: Alkylsilane lubricant films under pressure. *Phys. Rev. Lett.* **82**, 2880-2883 (1999).
24. Xiao, X.-D., Hu, J., Charych, D.H. & Salmeron, M. Chain Length Dependence of the Frictional Properties of Alkylsilane Molecules Self-Assembled on Mica Studied by Atomic Force Microscopy. *Langmuir* **12**, 235-237 (1996).
25. Staii, C., Wood, D.W. & Scoles, G. Verification of biochemical activity for proteins nanografted on gold surfaces. *J Am Chem Soc* **130**, 640-6 (2008).
26. Bard, A.J. et al. Chemical Imaging of Surfaces with the Scanning Electrochemical Microscope. *Science* **254**, 68-74 (1991).
27. Bard, A.J., Fan, F.R.F., Kwak, J. & Lev, O. Scanning electrochemical microscopy. Introduction and principles. *Analytical Chemistry* **61**, 132-138 (1989).
28. Bard, A.J. & Mirkin, M.V. Scanning electrochemical microscopy (CRC Press, 2001).
29. Fan, F.R. & Bard, A.J. Imaging of biological macromolecules on mica in humid air by scanning electrochemical microscopy. *Proc Natl Acad Sci U S A* **96**, 14222-7 (1999).

30. Fan, F.R. et al. Charge transport through self-assembled monolayers of compounds of interest in molecular electronics. *J Am Chem Soc* **124**, 5550-60 (2002).
31. Lee, C., Kwak, J. & Bard, A.J. Application of scanning electrochemical microscopy to biological samples. *Proc Natl Acad Sci U S A* **87**, 1740-3 (1990).
32. Mirkin, M.V., Fan, F.R. & Bard, A.J. Direct Electrochemical Measurements Inside a 2000 Angstrom Thick Polymer Film by Scanning Electrochemical Microscopy. *Science* **257**, 364-366 (1992).
33. Zhan, D., Li, X., Zhan, W., Fan, F.R. & Bard, A.J. Scanning electrochemical microscopy. 58.Application of a micropipet-supported ITIES tip to detect Ag+ and study its effect on fibroblast cells. *Anal Chem* **79**, 5225-31 (2007).
34. Zhou, J., Campbell, C., Heller, A. & Bard, A.J. Scanning electrochemical microscopy. 44. Imaging of horseradish peroxidase immobilized on insulating substrates. *Anal Chem* **74**, 4007-10 (2002).

Chapter 5

Conclusions and outlooks

The utilization of an AFM-based nanofabrication technique, namely nanografting, to generate patterns of biomolecules, such as DNA, with scalable dimensions and controlled orientation has been proven to be effective for investigating mechanical and functional properties of patterned or confined molecules at the nanoscale. In this thesis, nanografting was used to pattern nanostructures of ssDNA within a monolayer of bio-resistant molecules on gold substrates. The resulting ssDNA patterns were then allowed to bind with either complementary strands for studying hybridization mechanism, or covalent conjugates of proteins and enzymes tethered with complementary strands for monitoring bio-recognition events. AFM height measurements were utilized as detection tool to provide information about molecular composition by measuring the height of the molecular assembly with respect to the surrounding monolayer.

In the case of hybridization studies, we demonstrated that the higher molecular order induced by the nanografting process evades the cross-H-binding between ssDNA molecules, since it favor the molecules assembling in standing-up configuration and reduce the molecular entanglement, even at high molecular packing densities (chapter 2). This, in turn, is reflected by the higher efficiency of hybridization (>50%) of densely packed DNA nanopatches in comparison to dense spontaneously absorbed DNA monolayer in which the efficiency at comparable densities never exceeds 10%. Additionally, the effect of half length matching target strands, which are complementary to the lower and upper part of immobilized strand, was compared with fully matching strands. The hybridization of ssDNA with full vs-half length targets was characterized by AFM height and compressibility

measurements and shown to be consistent with previous studies. Despite this success, more studies and a proper comparison with theoretical models are needed to fully understand the structure and the mechanism of hybridization in DNA nanostructures.

In addition to DNA hybridization, we reported the use of nanografted (NG) ssDNA patches for the selective immobilization of proteins and enzymes. A combined Nanografting/DDI approach was utilized to accomplish this goal. Fabrication of three patches containing patterns of DNA (control patch), STV, GOx or HRP for multiple-feature protein arrays was shown in chapter 3. Patterned proteins were characterized by AFM topographic heights and used for protein-protein binding interaction studies. In particular, we demonstrated the functionality of immobilized proteins by studying their specific interactions with corresponding IgG antibodies dissolved in the complex mixture of human serum. Moreover, as required in standard microarray analysis, we demonstrated the lack of unspecific binding and cross recognition of antibodies.

Despite the unique property of nanografting for generating biomolecular features in a controlled manner, this technique is fundamentally a serial printing method, i.e. a slow writing process as compared to other nanofabrication techniques. One approach to circumvent this problem is to utilize multiple cantilever arrays in order to rapidly increase the number of devices that can be fabricated in parallel [1, 2].

Alternatively, it may be simpler to replicate original master (fabricated by NG) by means of Supramolecular nanostampting (SuNS), a technique introduced by Stellacci and coworker in 2005. In their study, a successful transfer of a homogeneous ssDNA monolayer from one gold substrate to another was reported [3, 4].

Clearly, several challenges remain to be faced in creating innovative devices for high throughput analysis. With respect to protein array technology, one of the major challenges has been the lack of optimal systems to interface, for instance by microfluidics a sensitive device of the type described in this thesis with a cell sampling region to allow for the sensitive, quantitative detection of the protein contents and small variations of it, in cells using a small number of cells or even a single cell sampling. Numerous efforts, based on surface chemistry, have already been taken, in the design of suitable immobilization protocols. In particular, site-specific methods via bioaffinity (i.e. NTA system)[5-7] and DNA-directed immobilization[8-11] have been extensively developed. By combining such effective immobilization techniques with efficient detection methods, based for instance on precise electric measurements, will bring to a full understanding of the molecular mechanisms

responsible, for instance, for the onset of neurodegenerative diseases, the quantification of protein contents and its constitutive variations at various stages of the disease. Moreover, the potential use of protein arrays to perform high-throughput analyses could also be realized in this way.

References:

1. Fritz, J. et al. Translating biomolecular recognition into nanomechanics. *Science* **288**, 316-8 (2000).
2. McKendry, R. et al. Multiple label-free biodetection and quantitative DNA-binding assays on a nanomechanical cantilever array. *Proc Natl Acad Sci U S A* **99**, 9783-8 (2002).
3. Akbulut, O. et al. Application of supramolecular nanostamping to the replication of DNA nanoarrays. *Nano Lett* **7**, 3493-8 (2007).
4. Yu, A.A. et al. Supramolecular nanostamping: using DNA as movable type. *Nano Lett* **5**, 1061-4 (2005).
5. Gershon, P.D. & Khilko, S. Stable chelating linkage for reversible immobilization of oligohistidine tagged proteins in the BIAcore surface plasmon resonance detector. *J Immunol Methods* **183**, 65-76 (1995).
6. Lata, S., Reichel, A., Brock, R., Tampe, R. & Piehler, J. High-affinity adaptors for switchable recognition of histidine-tagged proteins. *J Am Chem Soc* **127**, 10205-15 (2005).
7. Schmid, E.L., Keller, T.A., Dienes, Z. & Vogel, H. Reversible oriented surface immobilization of functional proteins on oxide surfaces. *Anal Chem* **69**, 1979-85 (1997).
8. Muller, J. & Niemeyer, C.M. DNA-directed assembly of artificial multienzyme complexes. *Biochem Biophys Res Commun* **377**, 62-7 (2008).
9. Niemeyer, C.M. Self-assembled nanostructures based on DNA: towards the development of nanobiotechnology. *Curr Opin Chem Biol* **4**, 609-18 (2000).
10. Niemeyer, C.M. in Nanobiotechnology (eds. Niemeyer, C.M. & Mirkin, C.A.) (Weinheim: Wiley-VCH 2004).

11. Niemeyer, C.M., Sano, T., Smith, C.L. & Cantor, C.R. Oligonucleotide-directed self-assembly of proteins: semisynthetic DNA--streptavidin hybrid molecules as connectors for the generation of macroscopic arrays and the construction of supramolecular bioconjugates. *Nucleic Acids Res* **22**, 5530-9 (1994).